Fall 2015

Impact of thorium based molten salt reactor on the closure of the nuclear fuel cycle

Safwan Qasim Mohammad Jaradat

Department: Mining and Nuclear Engineering

IMPACT OF THORIUM BASED MOLTEN SALT REACTOR ON THE CLOSURE OF THE NUCLEAR FUEL CYCLE

by

SAFWAN QASIM MOHAMMAD JARADAT

A DISSERTATION

Presented to the Faculty of the Graduate School of the

MISSOURI UNIVERSITY OF SCIENCE AND TECHNOLOGY

In Partial Fulfillment of the Requirements for the Degree

DOCTOR OF PHILOSOPHY

in

NUCLEAR ENGINEERING

2015

Approved
Ayodeji B. Alajo, Advisor
Hyoung K. Lee
Carlos H. Castano
Xin Liu
Julia E. Medvedeva

ABSTRACT

Molten salt reactor (MSR) is one of six reactors selected by the Generation IV International Forum (GIF). The liquid fluoride thorium reactor (LFTR) is a MSR concept based on thorium fuel cycle. LFTR uses liquid fluoride salts as a nuclear fuel. It uses ^{232}Th and ^{233}U as the fertile and fissile materials, respectively. Fluoride salt of these nuclides is dissolved in a mixed carrier salt of lithium and beryllium (FLiBe). The objective of this research was to complete feasibility studies of a small commercial thermal LFTR. The focus was on neutronic calculations in order to prescribe core design parameter such as core size, fuel block pitch (p), fuel channel radius, fuel path, reflector thickness, fuel salt composition, and power. In order to achieve this objective, the applicability of Monte Carlo N-Particle Transport Code (MCNP) to MSR modeling was verified. Then, a prescription for conceptual small thermal LFTR and relevant calculations were performed using MCNP to determine the main neutronic parameters of the core reactor. The MCNP code was used to study the reactor physics characteristics for the FUJI-U3 reactor. The results were then compared with the results obtained from the original FUJI-U3 using the reactor physics code SRAC95 and the burnup analysis code ORIGEN2. The results were comparable with each other. Based on the results, MCNP was found to be a reliable code to model a small thermal LFTR and study all the related reactor physics characteristics. The results of this study were promising and successful in demonstrating a prefatory small commercial LFTR design. The outcome of using a small core reactor with a diameter/height of 280/260 cm that would operate for more than five years at a power level of 150 MW_{th} was studied. The fuel system ^{7}LiF - BeF_2 - ThF_4 - UF_4 with a ($^{233}U/^{232}Th$) = 2.01 % was the candidate fuel for this reactor core.

ACKNOWLEDGMENTS

First and foremost, I would like to thank “Allah”, the one and only, who has granted countless blessing, knowledge, and opportunity to successfully accomplish my PhD in nuclear engineering.

The devoted work of this dissertation could have not been done without the encouragement and guidance of my advisor. I thank Dr. Ayodeji B. Alajo, my advisor, for his continuous support and trust to achieve my goal. In addition, I would like to express my deep thankfulness to Drs. Hyoung K. Lee, Carlos H. Castano, Xin Liu, and Julia E. Medvedeva, for their direction, dedication, and invaluable contribution as committee members on this project.

I cannot forget to thank my wonderful parents who always kept me in their prayers and surrounded me with their never-ending love and encouragement. Thanks to my brothers and sisters who always believed in me and motivated me to pursue my dream in achieving my goals.

I also would like to thank my best friends: Muhammad Wardeh, Ibrahim Ahmed Said, Mahmoud Taha, Mohamed Wiem Mkaouer, who gave me a high degree of morale to do this work.

To These People and All Those Who Never Stopped To Provide Me With Their Generous Support…….

My Love and Appreciation

TABLE OF CONTENTS

Page

LIST OF FIGURES

Page

LIST OF TABLES

Page

NOMENCLATURE

Symbol	Description
MSR	Molten Salt Reactor
ORNL	Oak Ridge National Laboratory
ARE	Aircraft Reactor Experiment
MSRE	Molten Salt Reactor Experiment
MSR/SSC	Molten Salt Reactor System Steering Committee
EU	Euratom
ARC	Advanced Reactor Concept
RD&D	Research Development and Deployment
NE	Nuclear Energy
DOE	Department of Energy
GIF	Generation IV International Forum
FA	Framework Agreement
Gen IV	Generation IV
MSFR	Molten Salt Fast Neutron Reactor
AHTR	Advanced High-Temperature Reactor
FHR	Fluoride Salt-Cooled High-Temperature Reactor
HTR	High Temperature Reactor
FLiBe	Fluoride salt of Lithium and Beryllium
LFTR	Liquid Fluoride Thorium Reactor
LS-VHTR	Liquid-Salt Very High Temperature Reactor

VHTR	Very High Temperature Reactor
MCNP	Monte Carlo N-Particle Transport Code
SRAC	Standard Thermal Reactor Analysis Code
JAERI	Japan's Atomic Energy Research Institute
MA	Minor Actinide
CR	Conversion Ratio
α_T	Temperature Coefficient of The Reactivity
k_{eff}	Neutron Effective Multiplication Factor
MW_{th}	Megawatt-Thermal
MW_e	Megawatt-Electric
BOL	Beginning of Life
EFPD	Effective Full Power Day
FP	Fission Product
ϕ_v	Maximum Neutron Flux On the Inner Wall of The Vessel
ϕ_G	Maximum Neutron Flux In the Graphite Moderator
Pu	Plutonium
^{233}U	Uranium-233
^{232}Th	Thorium-232

1. INTRODUCTION

A new window on nuclear technology was opened in the 1940s when the basic technologies of molten salt reactor (MSR) were established. MSRs were first studied at Oak Ridge National Laboratory (ORNL). The study started with Aircraft Reactor Experiment (ARE), and followed by five years of successful demonstration of the Molten Salt Reactor Experiment (MSRE), which was criticality achieved for the first time in 1965 [1].

MSRs were designed to bring a better inherent safety and good neutron economy, and their design concepts explored a liquid fuel instead of solid fueled reactors [2]. In 2010, the Molten Salt Reactor System Steering Committee (MSR/SSC) was established to conduct research and studies on MSR technologies that utilize thorium in the composition of a mixed liquid salt fuel. France, EU (Euratom), and Russian joined MSR/SSC in 2013. The United States, the People's Republic of China, Korea, and Japan are welcomed regular observers [3].

1.1. ADVANCED REACTOR CONCEPTS (ARC)

The Advanced Reactor Concepts ARC program was established to facilitate research development and deployment (RD&D) activities to improve nuclear energy technology. ARC program is focused on establishing an international connection of user facilities for nuclear RD&D, improving nuclear economic competitiveness, and reducing the technical and regulatory uncertainties for deploying new nuclear reactor technologies. This will improve safety, economic and technical, sustainability, manageability, security,

proliferation resistance, and environmental friendly of a new and innovative generation of nuclear reactor technologies. The mission of the Office of Nuclear Energy (NE) includes advancements and enhancements of ARC through RD&D activities at the Department of Energy's (DOE) National Laboratories and U.S. universities, in collaboration with the nuclear industry and international partners [4].

1.1.1. Generation IV International Forum (GIF). The Generation IV International Forum GIF is an international collective of 13 countries, which was initiated and chartered in 2000 and 2001, respectively. The charter of the GIF was led by the USA, Russia, Canada, UK, France, China, Japan, Argentina, Brazil, South Korea, Switzerland, South Africa, and Euratom to develop the next generation of nuclear reactor concepts. In the 2005 Framework Agreement (FA), ten members of the GIF were formally committed to join in the development of one or more Generation IV (Gen IV) nuclear concepts. Argentina, Brazil, and the UK did not sign the FA, so they were subsequently appointed as inactive members.

1.1.2. GIF Reactor Concepts. The next generation of nuclear energy technology should be clean, sustainable, safe, and proliferation-resistance. Based on these requirements, six types of reactor concepts were selected from about one hundred concepts by the GIF. Table 1.1 shows the list of the six generation IV reactor designs that are under development by the GIF. Most of these reactor concepts employ a closed fuel cycle in order to minimize the wastes for final disposal. Three of these selected reactors are thermal reactors, and the rest are fast reactors. Three of these reactors operate at low pressure with a significant safety advantage. Most of these reactors' temperatures are

high-range compared with today's light water reactors, so they could be used for thermochemical hydrogen production.

Table 1.1. Generation IV reactor designs under development by the GIF [5].

Reactor type	Coolant	Temperature °C	Fuel	Size (MWe)	Uses
Gas-cooled fast reactors	Helium	850	^{238}U	1200	Electricity & hydrogen
Lead-cooled fast reactors	Lead or Pb-Bi	480-800	^{238}U	20-180, 300-1200, 600-1000	Electricity
Molten salt reactors	Fluoride salts	700-800	UF in salt, or solid fuel with molten salt coolant	1000-1500	Electricity & hydrogen
Sodium-cooled fast reactors	Sodium	550	^{238}U & MOX	30-150, 300-1500, 1000-2000	Electricity
Supercritical water cooled reactors	Water	510-625	UO_2	300-700, 1000-1500	Electricity
Very high temperature gas reactors	Helium	900-1000	UO_2 prism or pebbles	250-300	Electricity & hydrogen

For the MSR, no FA has been signed, but collaborative research and development is conducted by members of the MSR/SSC [6]. The MSR now has two baseline variants:

- The molten salt fast neutron reactor (MSFR) is a fast reactor based on a closed Th/U fuel cycle with no U enrichment and works at 500-800 °C temperature

range. A MSFR will run exclusively on the Th-cycle after breed enough ^{233}U to maintain the chain reaction without need to additional U.

- The advanced high-temperature reactor (AHTR) is the same structure as the VHTR with a coated-solid particle fuel in a graphite core but with molten salt as the coolant instead of helium. The AHTR is also known as the fluoride salt-cooled high-temperature reactor (FHR). The power level is up to 4000 MW_{th} with passive safety systems, and the reactor enables power densities that are 4 to 6 times greater than high temperature reactors (HTRs).

The USA studied and developed the MSR fuel cycle during the 1950s and 1960s. Development started with a successful five years of criticality of a small prototype of MSR with a recent focus on the dissolved thorium and uranium fuel in a Fluoride salt of Lithium and Beryllium (FLiBe) coolant in a fast neutron spectrum.

1.2. MSR HISTORY FROM THE 1940S TO PRESENT

The molten-salt reactor concept was started in the late 1940s by the United States at Oak Ridge as part of a program to develop nuclear powered jet airplane propulsion. The idea started with the use of a liquid fuel consisting of a molten mixture of fluoride salts, including uranium as a fissile material. The fluorides (LiF, BeF_2, UF_4, NaF, ZrF_4, etc…) were nominated to be the most appropriate and the most suitable because of their promising physical and chemical properties. The selected fluorides have high solubility for the fissile material, an extremely low vapor pressure, good thermal conductivity, heat conduction, and no interaction with radiation that would cause damage. The first experiment established at Oak Ridge was the ARE [7,8,9]. The purpose of ARE was to use the molten fluoride as a fuel that could be circulated to remove heat from the core and

to study the nuclear stability. The fuel used was a mixed fluoride salt of Na, Zr with fissile U. It operated successfully for nine days with a working temperature of 1133K and a power level of 2.5 MW_{th} without any chemical or mechanical issues.

After 1956, MacPherson [10] and his group were conducted a series of surveys to determine the best molten salt reactor (in two versions: converters and breeders) for economic power. They studied the nuclear performance and technical characteristics for many of molten salt. They finally concluded that the thermal molten thorium reactor (which is moderated by graphite) was the best candidate of economic power reactor.

By 1960, the efforts united into the development of the MSRE to study the feasibility of MSR [11]. The MSRE core is graphite moderated with molten salt and consists of mixed fluoride salt of uranium, lithium-7, beryllium, and zirconium flowing through channels inside graphite moderator. The MSRE reached criticality for the first time in 1965 with a power level of 8 MW_{th}. The project was ended in 1969 and not much was done with the results of the MSRE project.

Years later, attention was drawn to the thorium MSBR which supposed to use mixed fluoride salt of lithium and beryllium as fuel. Unfortunately, the project was also stopped in 1976 and never allowed to mature [12,13].

In the 1980s, the study of MSR started in Japan with the FUJI project [14]. FUJI is one of the molten salt reactors that uses a molten thorium salt fluid fuel, which is called a liquid fluoride thorium reactor (LFTR). In these reactors, thorium acts the fertile material, uranium-233 as the fissile material, and graphite as the moderator as well as the reflector.

In the 2000s, the very high temperature reactor (VHTR) was selected as a potential design of Gen-IV with liquid-salt-cooled as a fuel version which is commonly called the liquid-salt very high temperature reactor (LS-VHTR) [15]. The LS-VHTR can be operated at a temperature higher than 950 °C with a power level of 2400 MW_{th}.

1.3. ADVANCED FUEL

Waste management, non-proliferation, and optimum fuel utilization are now the main concerns for the nuclear fuel cycle. Production of plutonium (Pu) from the U-fuel cycle in the existing reactors may raise the proliferation of nuclear weapons. This have led scientists to think more about how to develop more advanced and innovative technologies to non-proliferation of nuclear weapons. The thorium fuel cycle, which has been studied for its potential applications in almost all types of reactors (including PWRs, BWRs, FBRs, and MSRs), is a promising choice to start with it. The lower atomic weight of ^{232}Th, compared to ^{238}U, causes it to produce far less alpha-active waste. Also, the highly-penetrating gamma radiation that is emitted as daughter decay of ^{232}U makes ^{233}U hazardous and proliferation resistant [16].

1.3.1. Fuel Type For MSR. There are some requirements for a liquid fuel for MSRs. Some of the chemical and physical properties the proper liquid-fuel should have include:

- A moderate melting temperature at low vapor pressures.
- A high boiling temperature.
- Good thermal properties.
- Stability under irradiation.
- Good solubility of fissile and fertile materials.

- Less waste production of isotopes that are difficult to manage.

The mixed Fluoride Salt of Lithium and Beryllium FLiBe fulfill all these requirements. Therefore, the FLiBe salt is the best candidate fuel [17].

1.3.2. Advantages of Liquid Thorium-Based Fuel. Thorium-based fuel has potential advantages some of which are [18,19]:

- The fuel cannot "meltdown" because it is in molten state.
- The fuel salt can be automatically moved and drained through a freeze plug in the bottom of the reactor core, allowing it to passively cool in specially designed tanks during any accident.
- Most of non-gas fission products stay within the salt during any leak or accident.
- The reactor has no "dead-time" after shutdown because of the continuous removal of the noble gas ^{135}Xe, which has a high neutron absorption cross section.
- The strong negative temperature coefficient increases the safety of MSRs.
- Thorium is three times as abundant as uranium and is found in many countries.
- Using of thorium as fuel enables breeding in the thermal spectrum and produces only tiny quantities of plutonium and other long-lived actinides.

1.4. THORIUM-URANIUM FUEL CYCLE OF MSRS

In the thorium fuel chain of MSRs, the isotope thorium ^{232}Th is not fissionable by thermal neutrons but can be converted into the fissile ^{233}U by neutron absorption (whether by fast or thermal neutron). It becomes ^{233}Th at first (with a short half-life of 22.3 min), and follows with two beta emissions via ^{233}Pa (with a half-life 27 days) (see Figure 1.1).

$$^{232}\mathrm{Th} + {}^{1}_{0}\mathrm{n} \nearrow {}^{233}\mathrm{Th} \xrightarrow[22.3\,\mathrm{min}]{\beta^-} {}^{233}\mathrm{Pa} \xrightarrow[27\,\mathrm{days}]{\beta^-} {}^{233}\mathrm{U} \qquad (1.1)$$

Unlike the uranium ore, the thorium reactor produces less toxic fission product waste that would be used as a low enriched uranium fuel for other reactors like LWRs. In the thorium-based fuel cycle, the actinide waste can be fully recycled.

In the thorium-uranium fuel cycle, when a neutron is absorbed in ^{233}U atom, it either cause fission or transmute the ^{233}U atom to ^{234}U atom which is non-fissile. If the ^{234}U atom captures a neutron, it will be transmuted to ^{235}U, which is a fissile actinide, thereby reducing the probability of further transmutations to higher actinides.

The ^{235}U fissile actinide could be a useful nuclear fuel if it fissions after absorbing a neutron. If it fails to fission, then it will be transmuted to ^{236}U, then ^{237}Np, ^{238}Pu, and, finally ^{239}Pu. The capture-to-fission ratio is about 1:10 for ^{233}U, about 1:6 for ^{235}U, and about 1:2 for ^{239}Pu. The ^{232}Th/^{233}U fuel cycle generates less actinide or transuranic waste than the uranium-plutonium fuel cycle.

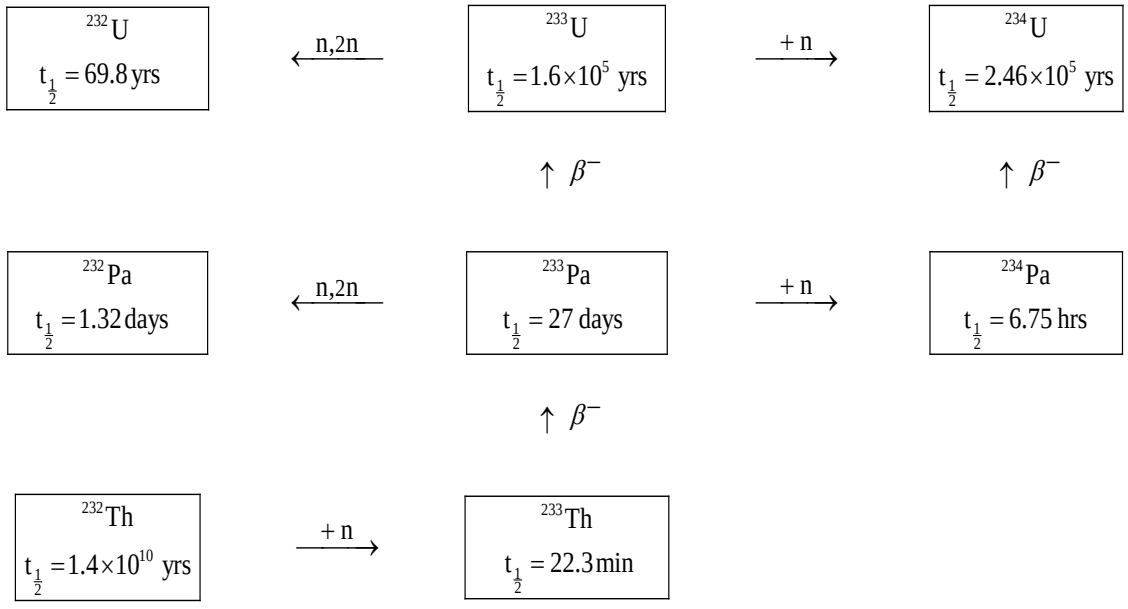

Figure 1.1. Production paths of fissile ^{233}U.

1.5. LATEST ADVANCEMENT AND RESEARCH IN THORIUM-BASED FUEL CYCLES

The following are some of the most recent RD&D efforts in thorium-based fuel applications and molten salt reactor-related research:

- In 2013, an irradiation program test aimed to qualify a fuel of Th/Pu for LWRs. The program was started in the Halden reactor by a Norwegian technology company. The study-tests aimed to determine/focus on some of the key properties of thorium fuels such as thermal conductivity, swelling, and fission gas release with the burn-up process [3].
- In late 2013, Areva and Rhodia signed a memorandum of agreement to develop new applications for the use of thorium-based fuel and the use of thorium/uranium as a potential complementary or alternative fuel to the present uranium/plutonium cycle in the advanced nuclear reactors.
- For decades, Canada showed an interested in thorium (Th) as a fuel alternative to uranium. In 2011, Canada initiated a "Thoria Roadmap Project" in order to identify and address gaps in the understanding of thorium fuel science and technology.
- The IAEA has an existing Coordinated Research Project (CRP), which is an international cooperation on near-term and promising long-term options on the potential of thorium based fuel and for the deployment of thorium energy system [20,21].

1.6. RESEARCH OBJECTIVE AND APPROACH

The objective of this research was to complete feasibility studies of a small commercial thermal liquid fluoride thorium reactor LFTR. The focus was on neutronic calculations in order to prescribe core design parameter such as core size, fuel block pitch (p), fuel channel radius, fuel path, reflector thickness, fuel salt composition, and power.

The expected potential advantage of this small commercial thermal LFTR includes it use in micro-grids where large reactors are not ideal. The advantages also extend to the implementation, factory fabrication, transportation from factory to site, and in situ refueling, etc.

In order to achieve this objective, the following studies were completed:

1. Verified the applicability of Monte Carlo N-Particle Transport Code (MCNP) to MSR modeling. This was done through verification of FUJI-U3-(0) reactor using MCNP code and compared the results with the ones from the original paper, which used the SRAC95 code. These studies are presented in Chapter 3.
2. Prescription for conceptual small thermal LFTR and relevant calculations were performed using MCNP to determine the main neutronic parameters of the core reactor. This includes criticality, neutron energy spectrum, time behavior of k_{eff}, radial and axial fluxes of thermal and fast neutrons inside the core, the burn-up and refueling processes, cycle lengths, and the time behavior of conversion ratio. These studies are presented in Chapter 4.
3. Determined the material balance of actinides, minor actinides (MA), and fission products for five years of operation. These studies are presented in Chapter 4.

2. ANALYSIS TOOL

2.1. CODES HISTORICALLY USED IN ANALYSIS MSR

This chapter shows some codes historically used in the analysis of molten salt reactors MSRs. The descriptions, features, and applications are presented for each code. Any code has limitations, so the reliability and applicability of the MCNP need to be checked to do such an analysis for MSRs.

2.2. SRAC59

2.2.1. History of SRAC. The standard thermal reactor analysis code system (SRAC) was developed in 1978 at Japan's Atomic Energy Research Institute (JAERI). The SRAC was revised in 1986, and SRAC95 was introduced as a potable system on UNIX and OS in 1995. The final version was developed in 2006 and called SRAC2006. The SRAC does a comprehensive neutronics calculation for various types of thermal reactors by producing effective microscopic and macroscopic cross sections. They also perform core calculations including burnup analysis [22].

2.2.2. Features.

1. SRAC can solve for a multi-region cell problem with the PEACO option by doing lethargy mesh in a resonance energy range.
2. Enable many choices of flow calculation by integrating the S_N transport codes ANISN(1D) and TWOTRAN(2D) along with the multi-dimensional diffusion code CITATION into the system.
3. The collision probability calculation (PIJ) is applicable to 16 types of lattice geometries (see Figure 2.1).

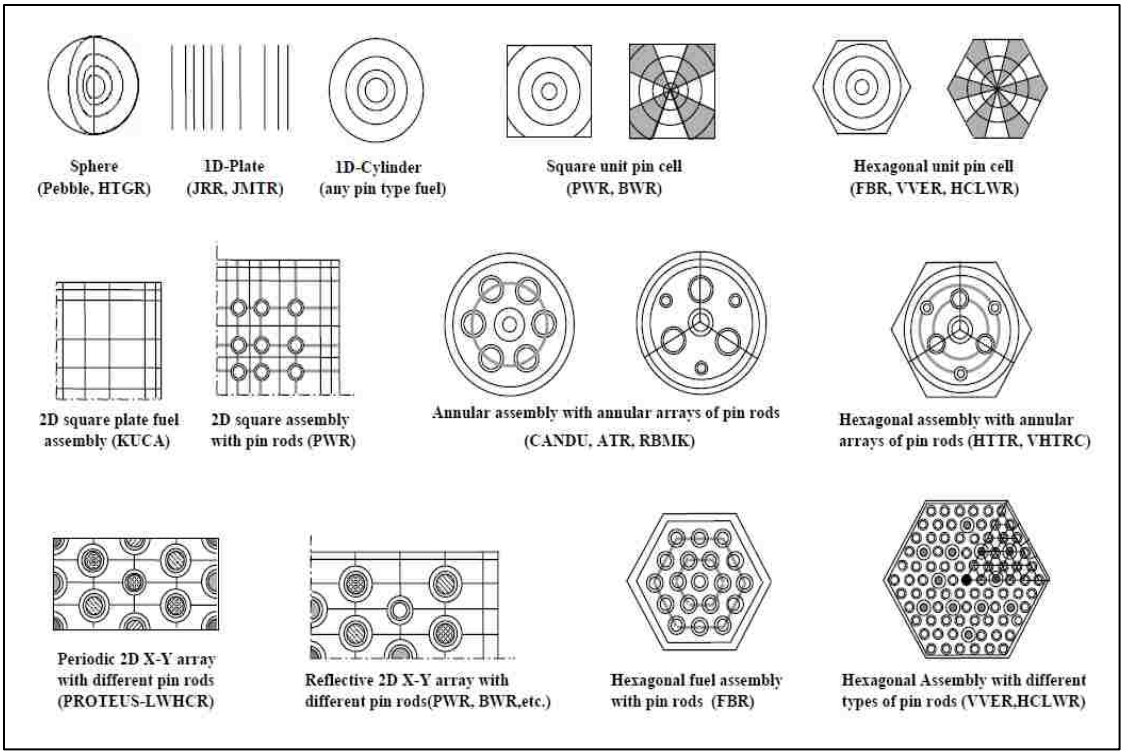

Figure 2.1. Geometrical Models of PIJ [22].

2.2.3. Applications of SRAC in Japan.

1. Testing Reactors and Experimental Analysis of Critical Assemblies (CA):
   - Tank type critical assembly (TCA): pin type fuels with H_2O as a moderator and a low enriched UO_2/MOX fuel.
   - High temperature test reactor (HTTR): coated fuel particles with UO_2 kernel in hexagonal graphite block fuel assemble.
   - Critical assemblies for JAEA material testing reactor (JMTRC): UAI_x-AI plate type fuel with H_2O as a moderator.
   - Kyoto University: high enriched U-AI alloy plate type fuel with polyethylene as a moderator.

2. Core Management and Upgrading of Research Reactor:
    - JRR-2: research reactor with 45% enriched UAI_x-AI cylindrical plate type fuel with D_2O as a moderator.
    - JRR-3M: research reactor with 20% enriched UAI_x-AI cylindrical plate type fuel with H_2O as a moderator.
    - JRR-4: research reactor with 93% enriched U, U-AI alloy fuel with H_2O as a moderator (in 1996).
    - JRR-4: research reactor with 20% enriched U, U_3Si_2-AI dispersed alloy fuel with H_2O as a moderator (in 1998).
    - JMTR: materials testing reactor with 20% enriched U_3Si_2-AI dispersed alloy fuel with H_2O as a moderator.
3. Analysis of Post Irradiation Experiments:
    - PWR by JAEA.
    - BWR by NUPEC.
    - REBUS by JNES.
4. Conceptual Design of Future Reactors [23]:
    - Space power reactors.
    - Design study of reduced-moderation water reactors (RMWRs).
    - Research on plutonium rock-like oxide (ROX) fuels.
    - Conceptual design of molten salt liquid-fuel reactors (MSRs) [24].
5. Integral Testing of JENDL:
    - Benchmark calculation data for more than 1000 experimental data in the ICSBEP benchmark handbook.

2.3. MCNP

2.3.1. Description and Applications. MCNPX (MCNP eXtended) is the latest generation of the series of Monte Carlo N-Particle Transport Codes that started at Los Alamos National Laboratory in the 1940s. It was designed to track photons, electrons, neutrons, protons, and ions over nearly all energies. MCNP is a Fortran90 computer language code that models the interaction of radiation with matter.

MCNPX 2.7.0 is the latest public release of the code, which includes many significant additional features over MCNPX 2.6.0 (released in 2008) like improved physics models, expanded tally options, and improved plotting capability.

MCNP6 is a developed version that combines MCNPX and MCNP5 and has additional modifications beyond MCNPX to track 29 other fundamental particles like protons, muons, pions, sigmas, etc. and four light ions (deuterons, tritons, helions, and alphas) [25,26].

2.3.1.1. Depletion process. MCNP6 is physics rich, which determines the system's eigenvalues, densities, fluxes, reaction rates, and many other physics quantities by running a steady-state calculation. CINDER90 (a FORTRAN code with a data library) then calculates the inventory of nuclides by taking the MCNP6-generated eigenvalues and performing the depletion calculation to generate new number values for the next time step. Another set of fluxes and reaction rates is generated and this process repeats itself until the final time step, which is specified by the user (see Figure 2.2).

The user can determine the list of materials on the MCNP6 material card, and MCNP6 will calculate the parameters from them only. The importance of CINDER90 is that it can track the time reactions of 3400 isotopes in case some information is not

specified from MCNP6, which is only capable of tracking information for isotopes containing transport cross sections.

The nuclide buildup and depletion is calculated by the CINDER90.dat library (which contains the data required for burnup and depletion calculations), which uses the fission yield information for 3400 isotopes, including about 30 fission yield sets and 1325 fission products. The linear depletion equation for a specific isotope is as follows:

$$\frac{dN_i}{dt} = \overline{Y}_i + N_{i-1}(t)\gamma_{i-1} - N_i(t)\beta_i \tag{2.1}$$

where:

$N_i(t)$ = the time-dependent nuclide density of isotope i.

$\overline{Y}_i$ = the production rate.

γ_{i-1} = the total transmutation probability of forming nuclide element N_i.

β_i = the total transmutation probability of isotope i.

Each partial nuclide density N_i is then computed using the following equation:

$$N_n(t) = \prod_{k=1}^{n-1} \gamma_k \left\{ \overline{Y}_m \left[\frac{1}{\prod_{l=1}^{n} \beta_l} - \sum_{j=1}^{n} \frac{e^{-\beta_{jt}}}{\prod_{i=1,\neq j}^{n} \left(\beta_i - \beta_j\right)} \right] + N_1^0 \sum_{j=1}^{n} \frac{e^{-\beta_{jt}}}{\prod_{i=1,\neq j}^{n} \left(\beta_i - \beta_j\right)} \right\} \tag{2.2}$$

The total nuclide density inventory (N_{tot}) for the nuclide is then calculated by the summation of each calculated partial nuclide density N_i from the above equation.

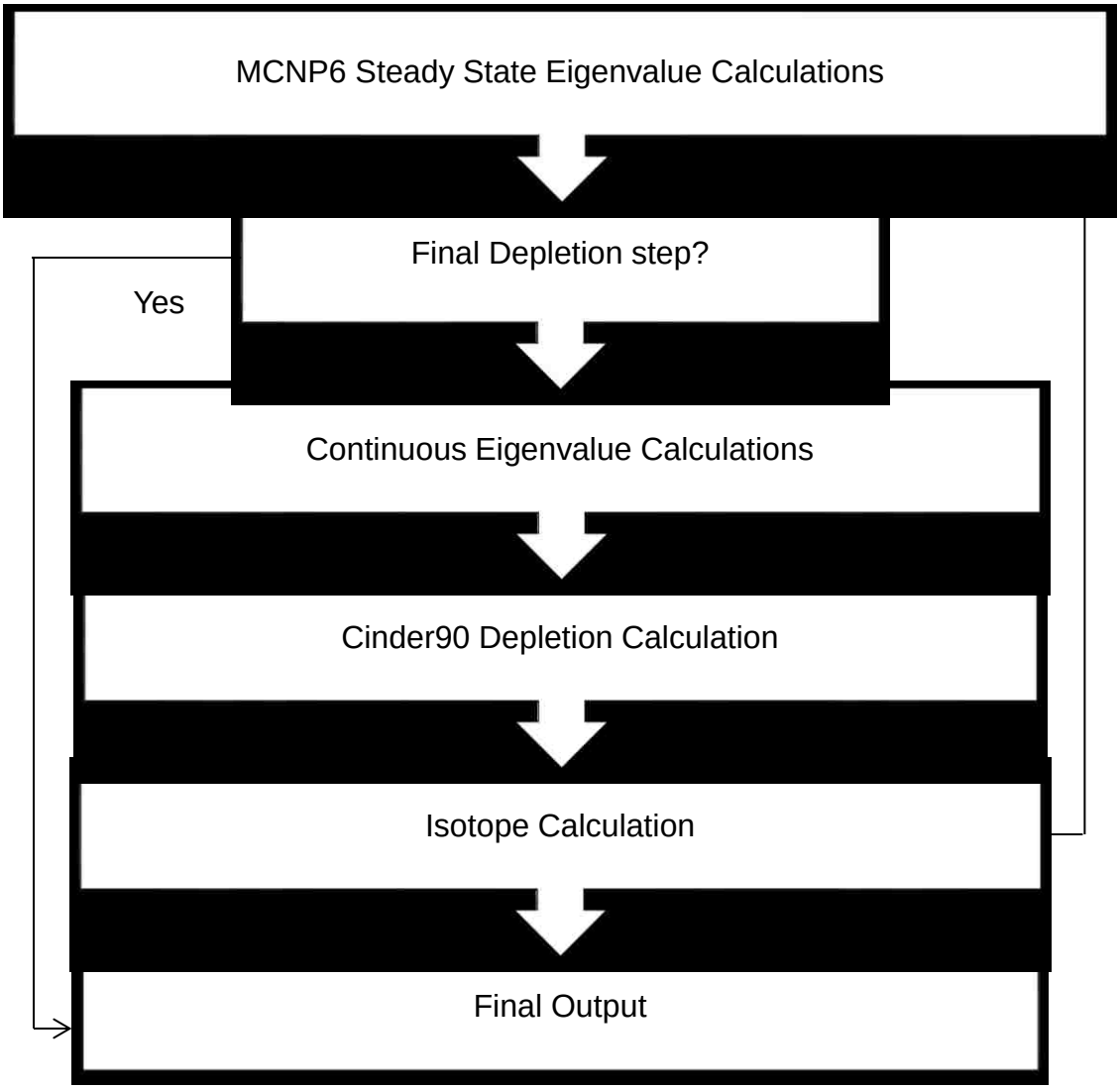

Figure 2.2. MCNP6 linked depletion process.

2.3.1.2. Burn card setup. The setup of a BURN card can be explained as follows:

BURN TIME = t_1, t_2, t_3, ...

PFRAC = f_1, f_2, f_3, ...

POWER = p

$$MAT = \pm m_1, \pm m_2, \pm m_3, ...$$

$$OMIT = m_1\ n_1\ j_{11}\ j_{12} ... j_{1n_1},\ m_2\ n_2\ j_{21}\ j_{22} ... j_{2n_2}, ...$$

$$MATVOL = v_1\ v_2 ... v_n$$

$$MATMOD = ...$$

$$BOPT = b_1\ b_2$$

where,

t_i = duration of burn step *i* in days,

f_i = power fraction for each time step,

p = power level (in MW_{th}),

m_i = material number to be burned,

n_i = number of omitted nuclides listed for the m_i material,

j_{i,n_k} = omitted nuclides for the m_i material. Each j must be provided in the form ZZZAAA, where ZZZ is the isotope's atomic number and AAA is its atomic mass number,

v_i = total volume of all cells (cm^3) containing burn material m_i,

b_1 = Q value multiplier, (Default is 1.0), and

b_2 = control of the ordering and content of the output files. It takes the value of the additive result of two integer values $b_2 = I_1 + I_2$.

$$\text{If } I_1 = \begin{cases} 0\ ; & \text{include only Tier 1 fission products.} \\ 10\ ; & \text{include Tier 2 fission products.} \\ 20\ ; & \text{include Tier 3 fission products.} \end{cases}$$

$$\text{If } I_2 = \begin{cases} 1\ ; & \text{order output inventory high to low, based on mass.} \\ 2\ ; & \text{order output inventory high to low, based on total activity.} \\ 3\ ; & \text{order output inventory high to low, based on specific activity.} \\ 4\ ; & \text{order output inventory based on increasing ZZZAAA.} \end{cases}$$

If $b_2 > 0$, output will be printed at end of job only.

If $b_2 < 0$, output will be printed at end of each burn step.

2.3.1.3. MATMOD (material modification)

$$\begin{array}{lllllllllll}
\text{MATMOD} = \text{nt} & ts_1 & nm_1 & mn_{1,1} & k_{1,1} & z^1_{1,1} & c^1_{1,1} & z^2_{1,1} & c^2_{1,1} & \ldots & z^{k_{1,1}}_{1,1} \quad c^{k_{1,1}}_{1,1} \\
 & . & . & . & . & . & . & . & . & \ldots & . \quad . \\
 & . & . & . & . & . & . & . & . & \ldots & . \quad . \\
 & . & . & . & . & . & . & . & . & \ldots & . \quad . \\
 & . & . & mn_{1,nm_1} & k_{1,nm_1} & z^1_{1,nm_1} & c^1_{1,nm_1} & z^2_{1,nm_1} & c^2_{1,nm_1} & \ldots & z^{k_{1,nm_1}}_{1,nm_1} \quad c^{k_{1,nm_1}}_{1,nm_1} \\
 & . & . & & & & & & & & \\
 & ts_{nt} & nm_{nt} & mn_{nt,1} & k_{nt,1} & z^1_{nt,1} & c^1_{nt,1} & z^2_{nt,1} & c^2_{nt,1} & \ldots & z^{k_{nt,1}}_{nt,1} \quad c^{k_{nt,1}}_{nt,1} \\
 & & & . & . & . & . & . & . & \ldots & . \quad . \\
 & & & . & . & . & . & . & . & \ldots & . \quad . \\
 & & & . & . & . & . & . & . & \ldots & . \quad . \\
 & & & mn_{nt,nm_{nt}} & k_{nt,nm_{nt}} & z^1_{nt,nm_{nt},1} & c^1_{nt,nm_{nt},1} & z^2_{nt,nm_{nt},1} & c^2_{nt,nm_{nt},1} & \ldots & z^{k_{nt,nm_{nt}}}_{nt,nm_{nt}} \quad c^{k_{nt,nm_{nt}}}_{nt,nm_{nt}}
\end{array}$$

where,

nt = number of the time step,

ts_i = the ordinal position of the time step (integer number) for which to manually change the nuclide concentration of the material,

nm_i = total number of materials at time step ts_i that incur nuclide concentration changes, and

mn_{i,j_i} = j^{th} material number for which to manually change nuclides at time step ts_i. A positive value indicates atom/wt. concentration fraction. A negative value indicates atom/gram density.

k_{i,j_i} = number of nuclides to manually change for the j^{th} material,

$z_{i,ji}^{k_{i,ji}}$ = k^{th} nuclide (in ZZZAAA format) of material mn_{i,j_i} for which a new concentration will be specified,

$c_{i,ji}^{k_{i,ji}}$ = concentration value for the nuclide $z_{i,ji}^{k_{i,ji}}$ of material mn_{i,j_i}. Positive values are given for atom fractions or atom densities. Negative values are given for weight fractions or gram densities.

2.3.2. Applicability of MCNP to MSR Analysis. A verification for the FUJI-U3-(0) model was performed and the results were compared with the results obtained from the FUJI-U3-(0) using the SRAC95 to check the applicability of MCNP to a molten salt reactor analysis. The applicability of MCNP is discussed in Chapter 3.

2.3.3. Advantages and Limitations of MCNP. The MCNP is a physics rich program that uses the best data, models, and theories. With more than 10,000 users around the world, MCNP is the way to study/focus on many hot and interesting areas such as: fission and fusion reactor design, nuclear criticality safety, radiation shielding,

waste storage/disposal, detector design and analysis, health physics and dosimetry, medical physics and radiotherapy, transmutation, activation, burnup, aerospace applications, and nuclear safeguards [26].

MCNP is capable of calculating nearly any physical quantity and using unique features for nuclear physics calculations such as:

- Flux and current,
- Energy and charge deposition,
- Heating and reaction rates,
- Response functions,
- Detector response (pulse-height tallies),
- Mesh tallies and radiography images,
- K-effective, beta-eff, and lambda-eff,
- Fission distributions,
- Shannon entropy of the fission source for assessing convergence,
- Stochastic geometry,
- Isotopic changes with burnup,

Some of limitations that apply to the energies and particles beyond MCNP include[27,28]:

1. MCNP gives a fatal error if it is run for problems above the MCNP energy range or beyond the MCNP particle set.
2. KCODE criticality calculations work only with the available actinide nuclear data libraries and have not been extended to include high-energy neutrons.

3. Charged-particle reaction products are not generated for some neutron reactions below 20 MeV in the LA150N library.
4. The results of an F6:P tally must be checked for small cells when running a photon or photon/electron problem.
5. Users should avoid densities lower than about 1e-9 g/cm^3 for heavier charged particles and densities lower than about 1e-15 g/cm^{3}for electrons because numerical problems may occur in the straggling routines.
6. The upper energy limit is 100 GeV for photon transport and 1 GeV for electron transport.
7. Continued runs that include mesh tallies must use the last available complete restart dump.
8. Specifying different densities for the same material is a fatal error.
9. Positrons may not be used as source particles.
10. Storage limitations have to be considered when setting up a problem.

3. MSR CORE VERIFICATION WITH MCNP

This section includes a modeling of FUJI type reactor. In order to develop a small fuel thorium reactor (LFTR); a verification for FUJI-U3-(0) (a molten salt reactor) was performed. The reactor used LiF-BeF_2-ThF_4-UF_4 as the mixed liquid fuel salt, and the core was graphite moderated. The MCNP6 code was used to study the reactor physics characteristics for the FUJI-U3-(0) reactor. Results for reactor physics characteristics of the FUJI-U3-(0) exist in literature, which were used as reference. The reference results were obtained using SRAC95 (a reactor analysis code) coupled with ORIGEN2 (a depletion code). Some modifications were made in the reconstruction of the FUJI-U3-(0) reactor in MCNP due to unavailability of more detailed description of the reactor core. The assumptions resulted in two representative models of the reactor. The results from the MCNP6 models were compared with the reference results obtained from literature. The results were comparable with each other, but with some notable differences. The differences are because of the approximations that were done on the SRAC95 model of the FUJI-U3-(0) to simplify the simulation. Based on the results, it is concluded that MCNP6 can be reliably employed in the analysis of molten salt reactors.

3.1. FUJI-U3-(0)

The original FUJI-U3-(0) reactor (also referred to as FUJI-U3) used a mixed liquid fuel salt comprised of LiF, BeF_2, $^{232}ThF_4$, and $^{233}UF_4$ initially composed at 71.76 mol. %, 16 mol. %, 12 mol. %, and 0.24 mol. %, respectively. The core was graphite moderated and consisted of a hexagonal prism (p=19 cm) as its unit fuel cell, which was modeled as a cylindrical element (D=20 cm). The fuel channel was a cylindrical bore

(d=variable) through the hexagonal graphite prism [24]. The neutron flux inside the reactor vessel of the FUJI-U3 was not to exceed the neutron irradiation limits (based on MSBR design [29]) in order to avoid replacing the graphite before 30 years of the reactor operational lifetime. These limits were tabulated based on the fast neutron irradiation limits and thermal neutron irradiation limits, as shown in Table 3.1.

For these irradiation limit conditions, three regions were created inside the core (Core 1, Core 2, and Core 3), as shown in Figure 3.1, to reduce the neutron flux at the center of the core. The radius, height, and fuel volume fraction are tabulated for each core in Table 3.2. Based on the FUJI-U3, the entire core was covered with a vessel made basically of Hastelloy-N, and there was a narrow fuel path between the graphite-reflector and core-3. There were fuel ducts at the top and bottom of the core.

FUJI-U3 used the nuclear analysis code SRAC95 [30] for the criticality calculation and used JENDL3.2 [31] as a nuclear library. Based on FUJI-U3, the assumption of a constant temperature in the fuel cell calculation had little influence on the neutron flux difference between the upper lower parts of the core, which was approximately 2%. Therefore a constant temperature (900 K) was assumed for the entire core.

Table 3.1. The irradiation limit of fast/thermal neutron flux based on MSBR design.

Irradiation limit (1/ cm^2.s)	Fast neutron flux		Thermal neutron flux < 1 eV
	> 52 keV	> 0.8 MeV	
Graphite moderator	4.2×10^{13}	-	-
Vessel	-	1.4×10^{11}	7.1×10^{12}

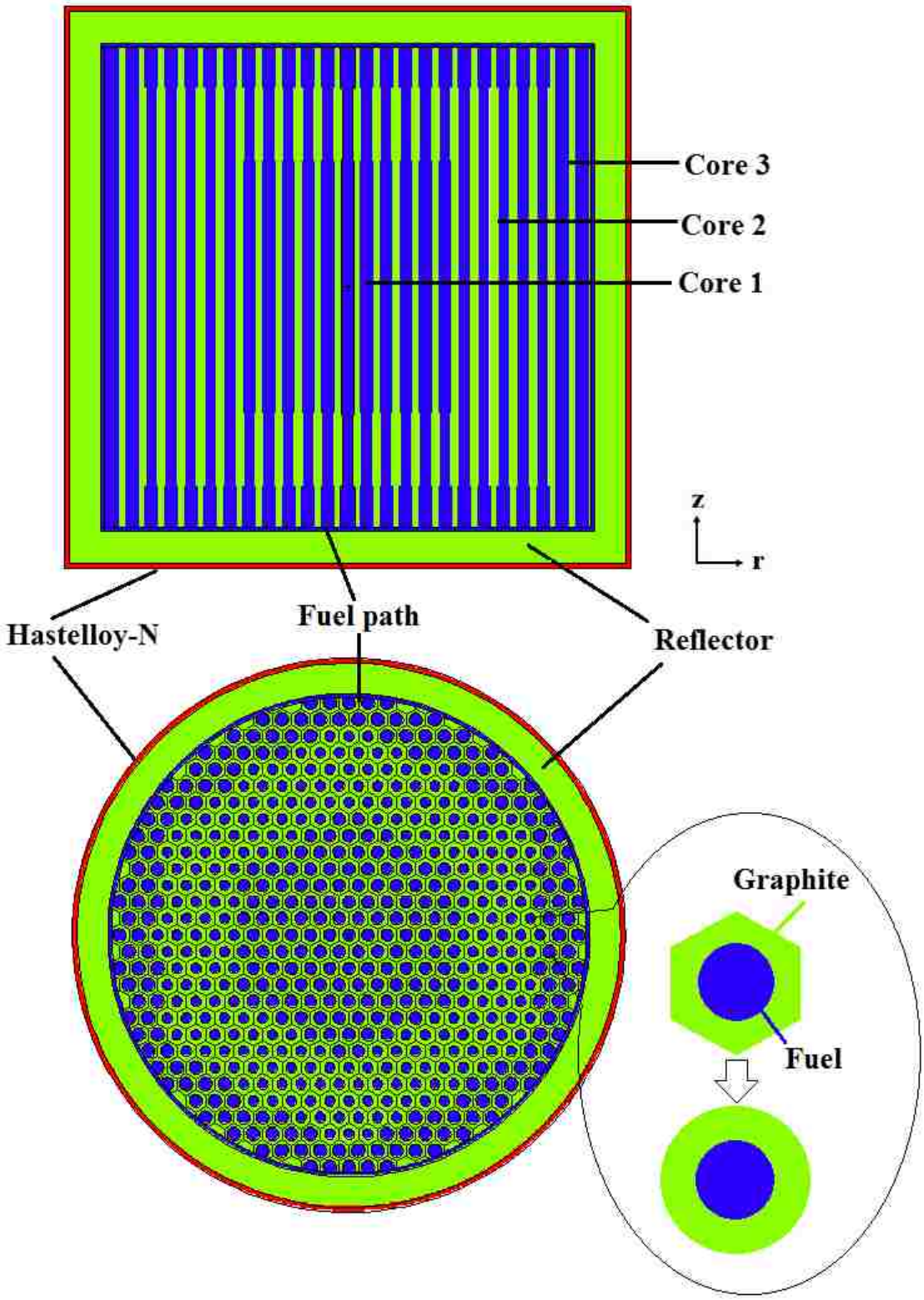

Figure 3.1. Original FUJI-U3-(0) core configuration.

Table 3.2. Parameters for the three region cores.

	Core 1	Core 2	Core 3
Δr (m)	1.16	0.8	0.4
Δh (m)	1.23	0.7	0.4
Fuel vol. %	0.39	0.27	0.45

3.2. PARAMETERS AND CHARACTERISTICS TO BE VERIFIED

The main parameters of the FUJI-U3 that were followed in the verification are listed in Table 3.3. The MCNP6 code was used to perform the calculations but some modifications were made on the FUJI-U3 design to attain a realistic configuration for the verification process. The following reactor physics characteristics were determined with MCNP6: the effective multiplication factor (k_{eff}) for the first 40 days of operation, the temperature coefficient of the reactivity (α_T), the radial and axial distribution for both fast and thermal neutron flux at the center of the core at the beginning of life (t=0), the fuel conversion ratio (CR), the maximum neutron flux (ϕ_v) on the inner wall of the vessel for fast and thermal neutron flux, and the maximum neutron flux (ϕ_G) in the graphite moderator. The results from the MCNP code were compared with the results from the literature on FUJI-U3 that used the SRAC95 analysis code.

Table 3.3. The main parameters of FUJI-U3-(0).

Thermal output/efficiency Electrical output	450 MW_{th}/ 44.4% 200 MW_e
Reactor :- Diameter/height (inner) Thickness	 5.40 m/ 5.34 m 0.05 m

Table 3.3. The main parameters of FUJI-U3-(0) (cont.).

Core :- Diameter/height Fuel vol. %	 4.72 m/ 4.66 m 36 vol. %
Fuel path/ducts :- Width Fuel vol. %	 0.04 m 90 vol. %
Reflector :- Thickness Fuel vol. %	 0.30 m 0.5 vol. %
Volume of primary loop	38.8 m^3
Inventory of primary loop :- 1- ^{233}U 2- ^{232}Th 3- Graphite	 1.133 ton (Initial condition) 56.4 ton (Initial condition) 163.1 ton

3.3. MCNP MODEL OF FUJI-U3-(0)

Calculations were performed to determine the radii of the fuel channel (d=variable) in the three core regions (Core 1, Core 2, and Core 3) used in the original model based on the design parameters of the FUJI-U3 listed in Tables 3.2 and 3.3. The results for Core 1, Core 2, and Core 3 were 6.28 cm, 5.18 cm, and 6.7 cm, respectively. The density of the fuel salt was also determined to be 3.33 g/cc at 900 K. The density of the graphite was 1.84 g/cc.

Two modeling approaches were taken, and some modifications were made to the FUJI-U3 model to simplify the simulation. In the first model (Model 1), the graphite moderator was kept as a hexagonal prism (p=19cm). The fuel volume fraction in the

reflector (0.5 vol. %) was added to the fuel volume fraction in the fuel path (90 vol. %) in order to have 100 vol. % of the fuel salt in the fuel path/ducts. Thus, the width was reduced to (3.776 cm). The reflector thickness was changed to 30.224 cm with 100 vol. % of graphite. The vessel was made of Hastelloy-N (Ni/Mo/Fe/Cr/Nb/Si in amounts of 73.9 wt. %, 12.0 wt. %, 5.0 wt. %, 7.0 wt. %, 2.0 wt. %, and 0.1 wt. %, respectively).

Because a hexagonal graphite moderator prism was used, some of the fuel rods were cut at the edge of the core (see Figure 3.2). Therefore, another approach was modeled (Model 2) with the same specifications used in Model 1 but with a modification to fit all of the fuel rods inside the core by increasing the radius of the core by 5 cm. This modification allowed the same volume/mass of the fuel salt to be kept inside the core. The final main characteristics of the modified FUJI-U3 core are listed in Table 3.4. It should be noted that the hexagonal graphite moderators were approximated as cylinders with equivalent diameter of 20 cm in SRAC95 analysis of the FUJI-U3 reactor.

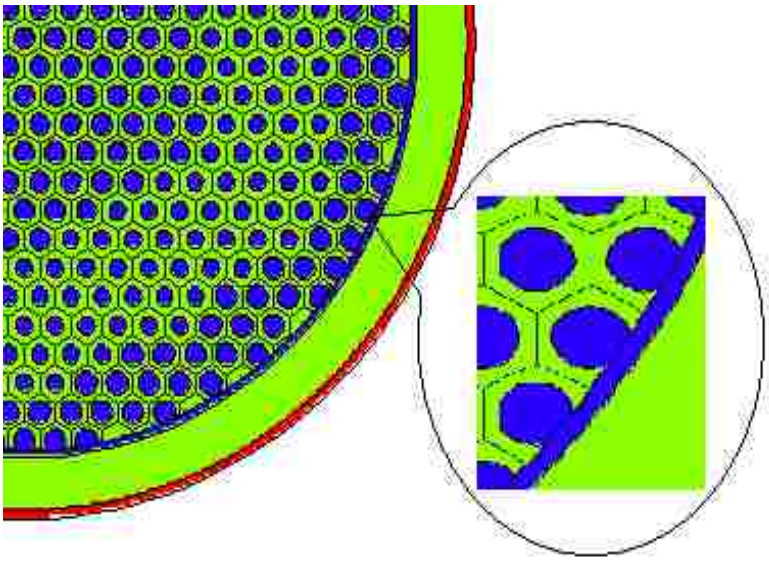

Figure 3.2. The cut of the fuel rods at the edge of the core.

Table 3.4. Modified FUJI-U3 design parameters.

	Model 1	Model 2
Thermal output	450 MW_{th}	450 MW_{th}
Reactor vessel :- Diameter/height Thickness	 5.40 m/5.34 m 0.05 m	 5.48 m/5.32 m 0.05 m
Core :- Diameter/height Fuel vol. %	 4.72 m/4.66 m 36%	 4.82m/ 4.66 m 34.5%
Fuel path :- Width Fuel vol. %	 0.03776 m 100 %	 0.03674 m 100 %
Reflector :- Thickness Graphite vol. %	 0.302 m 100%	 0.296 m 100%

3.4. COMPARISON OF MCNP RESULTS WITH LITERATURE

The k_{inf} vs. graphite/^{233}U atom density ratio was plotted using MCNP5, as shown in Figure 3.3, in order to compare the range of moderator-to-fuel ratio in which the FUJI-U3 core was designed to remain under-moderated. The results obtained using MCNP6 were comparable to those of the reference FUJI-U3.

The beginning-of-life radial thermal neutron flux was calculated at the center of the FUJI-U3 core. Thermal neutron energy cut-off was set at 1.0 eV as in agreement with the energy cut-off used in the reference FUJI-U3 literature.

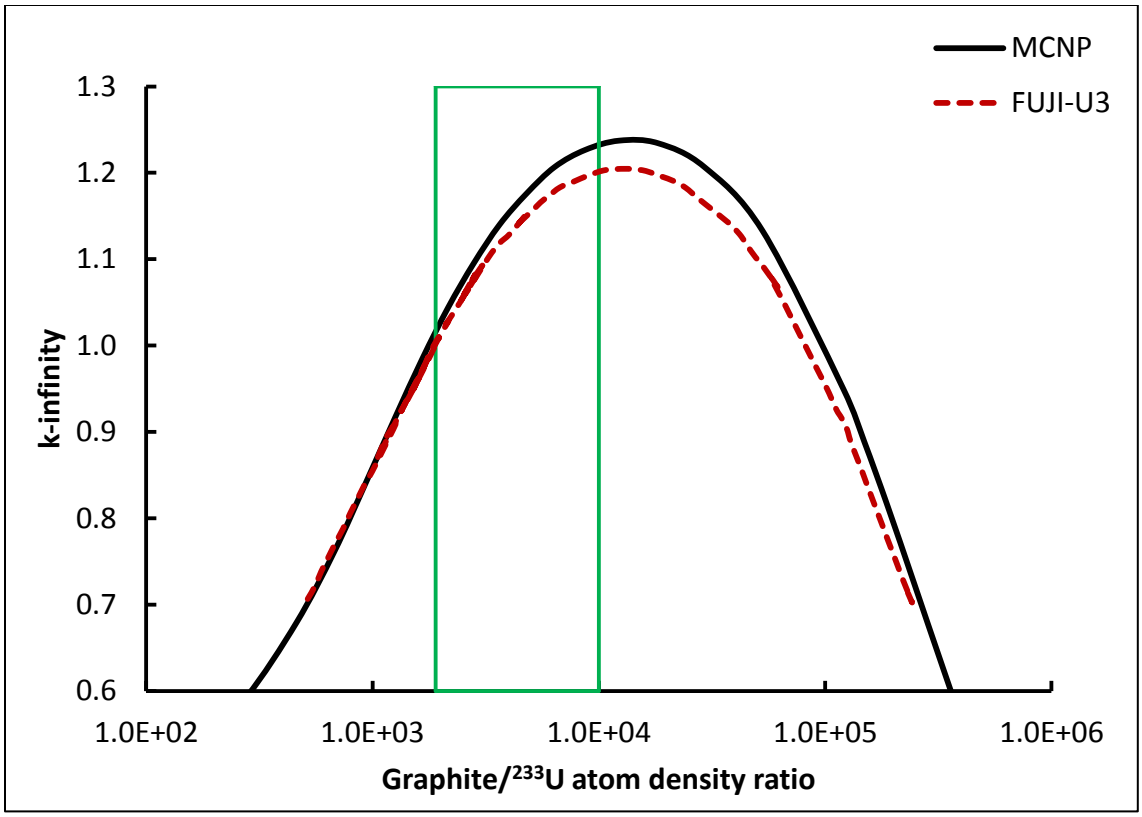

Figure 3.3. The k-infinity vs. graphite/^{233}U atom density ratio using MCNP5.

The results are provided in Figure 3.4 with the reactor radius normalized to unity with respect to outer vessel radius (R_v) for the reactor models and reference flux data. Radially, Core 1 extends to normalized radius of 0.43, Core 2 is from 0.43 to 0.73, and Core 3 extends from 0.73 to 0.87. The results of the radial thermal flux for both MCNP models were comparable with each other. The MCNP results showed deviation from the reference flux data (see Figure 3.4). In Core 1 region, the MCNP6 and reference flux values are about 2.1E+13 n/cm^{2}s and 3.2E+13 n/cm^{2}s respectively. The peak flux values are in Core 2 with values of 4.1E+13 n/cm^{2}s and 5.5E+13 n/cm^{2}s for MCNP6 and reference FUJI-U3 models respectively. The "hump" between normalized radius 0.87 and

1.0 is due to thermalization in the radial reflector of the reactor. Aside from the difference in magnitude, the flux profiles are generally similar for all data sets.

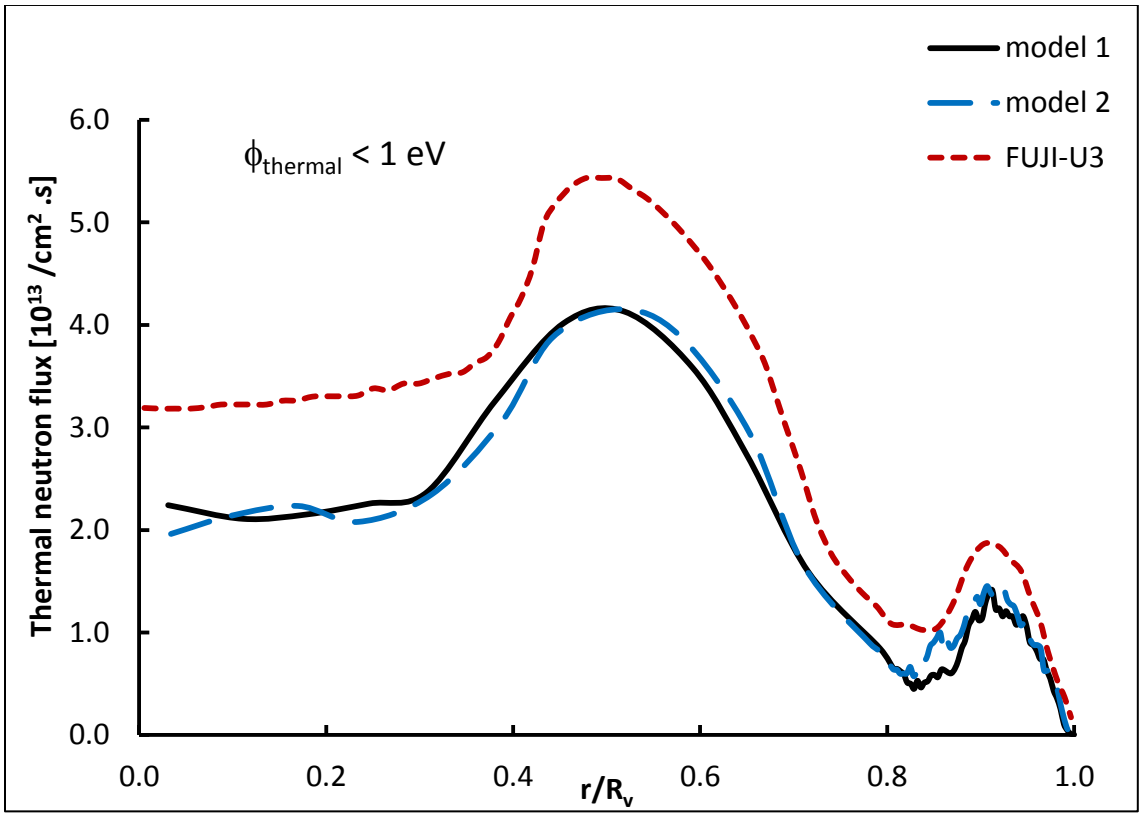

Figure 3.4. Radial distribution of thermal neutron flux of Model 1 vs. Model 2.

Figure 3.5 shows the radial distribution of beginning-of-life fast neutron flux at the center of the FUJI-U3 core for each model. The low end of the fast energy range is set at 52 keV. The radii are normalized to unity as described earlier. The reference FUJI-U3 distribution for fast neutrons was less than the irradiation limit. Similarly, the MCNP6 results provided flux profiles less than the irradiation limit. The results from the two MCNP6 models were comparable to each other. The magnitude of the fluxes obtained through MCNP6 are however lower than the results obtained for the reference reactor.

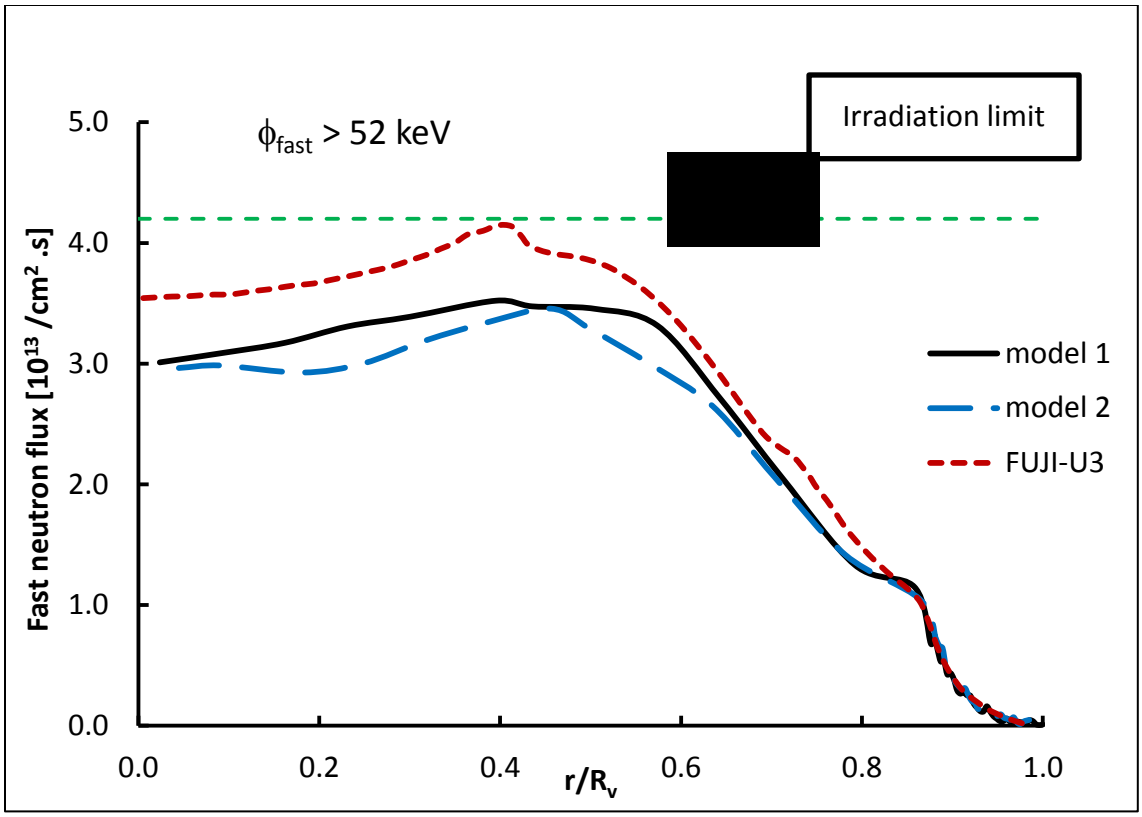

Figure 3.5. Radial distribution of fast neutron flux of Model 1 vs. Model 2.

Figures 3.6 and 3.7 show the beginning-of-life axial distributions of the thermal neutron flux and fast neutron flux at the center of the FUJI-U3 core respectively. The radial normalization scheme was adapted for the axial dimension. All axial dimensions were normalized to unity with respect to the outer vessel half-height (H_v). The axial center of the core is at normalized half-height zero. Axially, Core 1 extends to normalized half-height of 0.46, Core 2 is from 0.46 to 0.72, and Core 3 extends from 0.72 to 0.87. The results of the axial distributions of thermal and fast neutron fluxes from MCNP6 models were comparable with each other, but different in magnitude from the reference flux data calculated with SRAC95 (see Figures 3.6 and 3.7). Observations made in axial flux profiles are similar to those observations discussed in the radial flux profiles.

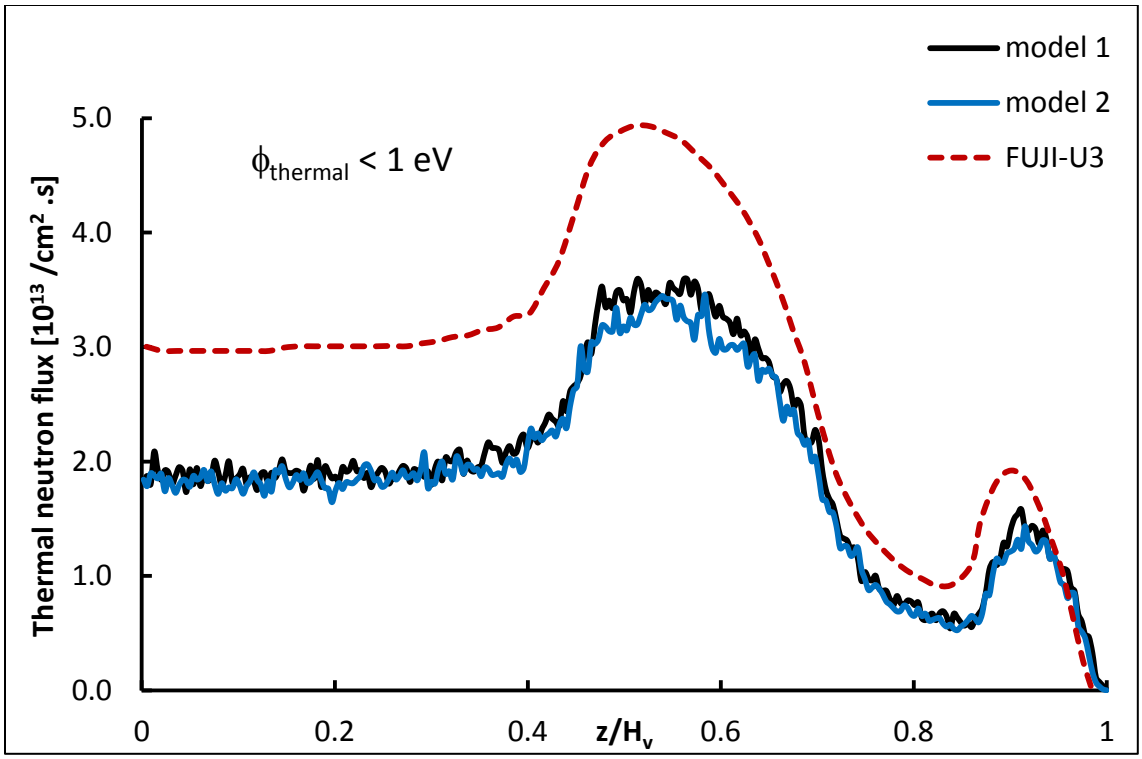

Figure 3.6. Axial distribution of thermal neutron flux of Model 1 vs. Model 2.

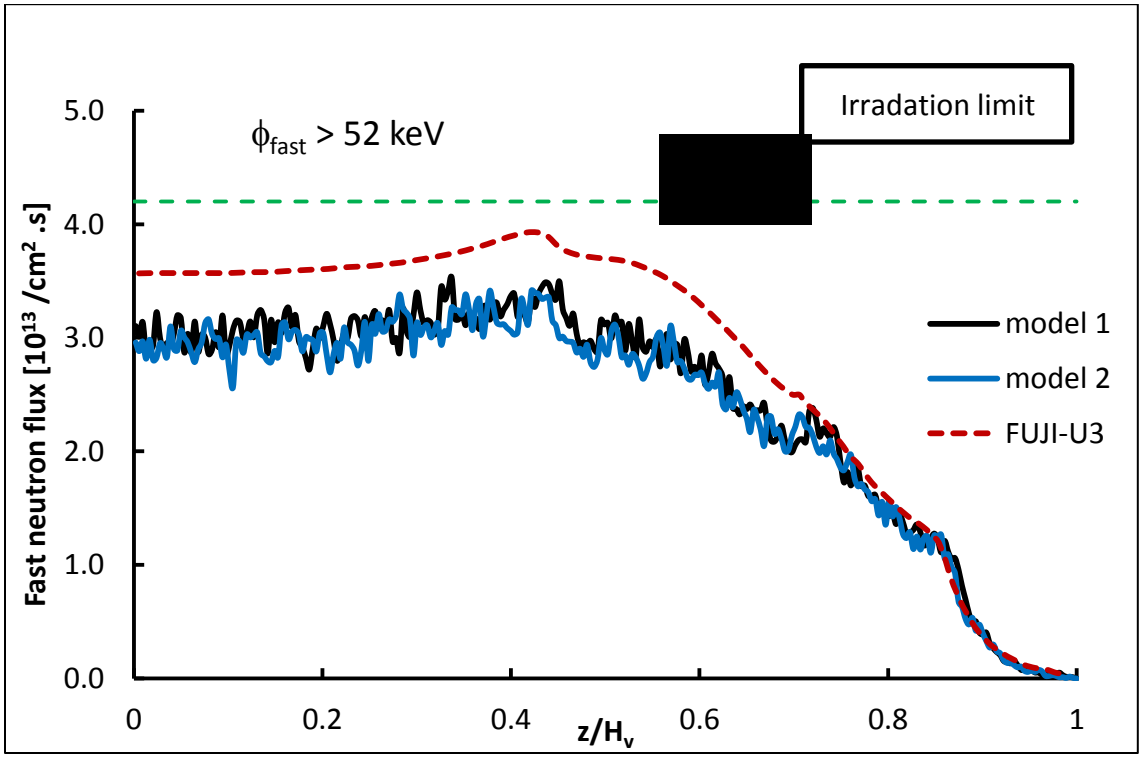

Figure 3.7. Axial distribution of fast neutron flux of Model 1 vs. Model 2.

Burnup calculations with a 75% load factor were done for 100 days for the two models. Figure 3.8 shows the time behavior of k_{eff} for Model 1 and Model 2. In the original FUJI-U3, the time needed for the k_{eff} to drop to the value 1.01 was about 40 days. This implies that (based on the FUJI-U3 design) the reactor should be fed with a new fuel salt every 40 days to maintain the core's criticality. The results obtained using MCNP for the modified FUJI-U3 core in Model 1 and Model 2 showed that the time needed for the k_{eff} to drop to the point 1.01 was also 40 and 41 days, respectively. This was the same as the reference FUJI-U3.

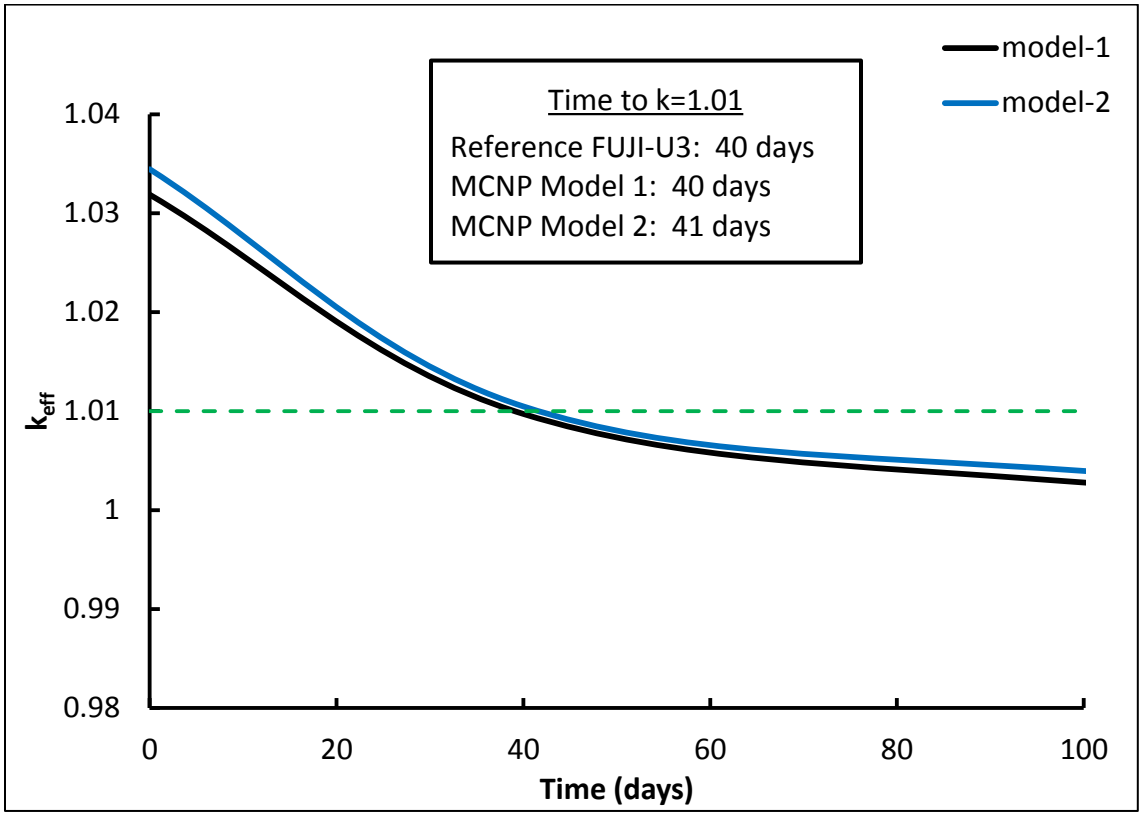

Figure 3.8. Time behavior of k_{eff} for Model 1 vs. Model 2.

Table 3.5 shows the main characteristics of the modified FUJI-U3 at the beginning-of-life (t=0). The effective neutron multiplication factor k_{eff} started with the

value 1.027 (super-critical) for the reference FUJI-U3 at the beginning-of-life. For Model 1 and Model 2, MCNP6 calculated 1.032 and 1.034, respectively. These values are within 0.5% and 0.7% of the reference k_{eff} for Model 1 and Model 2 respectively.

Table 3.5. The main characteristics of the modified FUJI-U3 at t=0.

Model	k_{eff}	CR	α_T [1/K] ($\times 10^{-5}$)	ϕ_G [1/cm^2.s] > 52 KeV ($\times 10^{13}$)	ϕ_v [1/cm^2.s]	
					>0.8 MeV ($\times 10^{11}$)	<1.0 eV ($\times 10^{12}$)
FUJI-U3	1.027	1.034	-3.10	4.10	1.34	2.46
Model 1	1.032	1.04	-5.01	3.53	0.80	3.13
Model 2	1.034	1.04	-5.06	3.46	0.88	3.37

The conversion ratio (CR) for the reference FUJI-U3 model was 1.034. For the two MCNP6 models, this value was 1.04, which is within 0.6% of the reference CR. The temperature coefficient of reactivity, α_T (a measure of the change in reactivity caused by a change in one degree temperature (K) of the core components and defined as $\alpha_T = \frac{\Delta\rho}{\Delta T}$) was -3.1×10^{-5} 1/K from the reference data of the FUJI-U3. The temperature coefficient of reactivity was determined in MCNP6 by performing simulations at 900K and 1200K, and using the criticality result to calculate the reactivity effect. The results for Model 1 and Model 2 were -5.01×10^{-5} 1/K and -5.06×10^{-5} 1/K, respectively. The results are more

negative temperature reactivity coefficient, which is desirable. The MCNP6 results of maximum fast flux in the graphite moderator (ϕ_G) are lower than the reference data, which is 4.1E+13 n/cm^{2}s. The ϕ_G values from MCNP6 are 3.53E+13 n/cm^{2}s and 3.46E+13 n/cm^{2}s for Model 1 and Model 2 respectively. At the inner surface of the reactor vessel, maximum thermal and fast fluxes (ϕ_V) were calculated. The fast neutron cut-off was redefined as 0.8 MeV for this calculation, while the thermal cut-off remained at 0.1 eV. The maximum fast flux at the inner surface of the vessel were 8.0E+10 n/cm^{2}s and 8.8E+10 n/cm^{2}s for Model 1 and Model 2 respectively, which are lower than 1.34E+11 n/cm^{2}s from the reference data. However, the maximum thermal fluxes at the vessel, calculated by MCNP6 are higher than the reference data.

3.5. CONCLUSION

The results from both MCNP models are comparable to each other, indicating that the approximations made in arriving at detail FUJI-U3 reactor model had insignificant impact on the neutronics. In all cases of flux profile, MCNP6 provided flux magnitudes lower than the reference results from SRAC95. However, the flux profiles are apparently similar between the MCNP6 results and the reference data. The difference in flux magnitude between the MCNP models and reference data may be attributed to the approximation of the graphite blocks as cylinders in the SRAC95 model used to analyze the reference FUJI-U3 core. The MCNP6 results are deemed more accurate since the geometries of the reactor core component were explicitly modeled in MCNP, while the SRAC95 model employed approximations. It also makes sense that the higher flux values from SRAC95 are conservative since irradiation limits were principal constraints in the design of the FUJI-U3 reactor. The temperature coefficients of reactivity were negative in

all cases, although the MCNP6 calculations resulted in more negative reactivity coefficient than the reference data. Other neutronic characteristics calculated were comparable to the reference data within less than one percent error. From all results, the conclusion drawn is that MCNP6 provides results which are as good as the reference results available in literature. MCNP6 is thus a viable and reliable tool in the analysis of molten salt fueled reactors.

4. CONCEPTUAL DESIGN OF THERMAL LFTR

This section presents a prefatory design study for a small thermal liquid fluoride thorium reactor (LFTR). A series of survey calculations were conducted using MCNP6 to obtain the prospective core. The calculations started by determining the candidate fuel composition system with a ($^{233}U/^{232}Th$) % atom ratio that would achieve the minimal change of reactivity. The calculations ended with a full-scale reactor core with a power level of 125–175 MW_{th}. A description of the LFTR model, its design parameters, and the reactor physics calculations are presented below.

4.1. LFTR CONCEPT

Molten salt reactor (MSR) is one of six reactors selected by the Generation IV International Forum (GIF). The liquid fluoride thorium reactor LFTR is a MSR concept based on thorium fuel cycle. LFTR uses liquid fluoride salts as a nuclear fuel. It uses ^{232}Th and ^{233}U as the fertile and fissile materials, respectively. Fluoride salt of these nuclides is dissolved in a mixed carrier salt of lithium and beryllium (FLiBe). An attractive point: these kinds of reactors don't have to operate at a high pressure. They don't have to use water for cooling, and there is nothing in the reactor that would cause a big change in density. In normal operation, there is a little piece of freeze plug. If there is an emergency and all the power of nuclear power plant is lost, the freeze plug of salt melts, and the liquid fluoride fuel inside the reactor drains out of the vessel to another tank, called the drain tank.

4.1.1. Description and Specification. The goal was to outline a preliminary feasible design of a small thermal commercial LFTR by conducting a series of survey

calculations to obtain the optimum prospective of an initial core. This was done by changing the parameters, including core size, hexagonal graphite pitch, fuel channel radius, fuel path, reflector graphite thickness, fuel composition system, and thermal power level.

4.1.2. K-Infinity, Geometry and Calculations. This part presents some of the different fuel compositions of different ($^{233}U/^{232}Th$) % enrichments that were examined in order to find the proper enrichment ratio that would achieve the minimum change of reactivity. A single fuel rod was modeled with specular reflectors to eliminate the leakage of neutrons and aid in finding the proper ratio. The fuel channel was a cylindrical bore through a hexagonal graphite moderator prism, as illustrated in Figure 4.1. The selected fuel was a mixture of fluoride salt of lithium, beryllium, Thorium-232, and Uranium-233 with different compositions and different ($^{233}U/^{232}Th$) % enrichments, where ^{233}U was the fissile material, ^{232}Th was the fertile material, and Li was (99.995 mol %) ^{7}Li. It is desirable for these kinds of reactors to have relatively small mole fractions of ^{233}U to keep the physical properties (like the melting point) for the corresponding binary, ternary, or quaternary systems of the diluents under control [32].

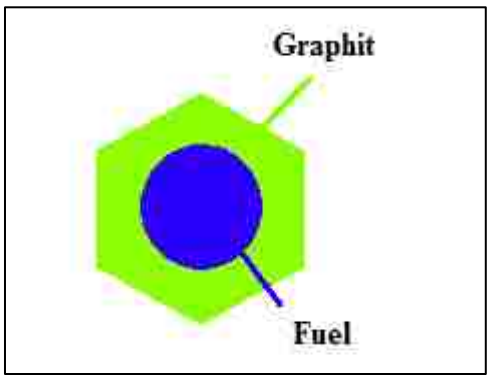

Figure 4.1. Single fuel rod model.

Table 4.1 shows fuel systems of different compositions for example. This is not an exhaustive enumeration of all systems because of the difficulty in conducting experiments for every fuel composition to get the physical and chemical information.

Table 4.1. Different fuel salt composition systems.

Fuel Salt Composition (mol. %) $^{7}LiF - BeF_2 - ThF_4 - UF_4$	Melting Temperature (°C)	Density (g/cc) at T=900K	Enrichment - Atom Ratio ($^{233}U/^{232}Th$) × 100%
60.00 – 38.00 – 1.00 – 1.00 [33]	442	2.197	100.43
63.00 – 35.50 – 1.00 – 0.50 [33]	456	2.140	50.22
65.00 – 30.00 – 4.00 – 1.00 [33]	448	2.548	25.11
65.00 – 30.50 – 4.00 – 0.50 [33]	453	2.492	12.55
71.76 – 16.00 – 12.0 – 0.24 [24]	457	3.330	2.01

The densities of the different compositions were calculated using the rule of additivity of molar volumes [34,35]. A FORTRAN program was written for this purpose and used to carefully transform the molar ratios of the salt compositions into weight fractions to be used in the MCNP6 material card.

For the initial calculation, MCNP5 was used to calculate the k_{inf} vs. graphite/^{233}U atom density ratio to determine a mutual range at which all of these different fuel composition systems were under-moderated and supercritical at the same time. The fuel channel had a radius (r = variable) with a height of 300 cm. In this test, the hexagonal graphite pitch was chosen to be p=28 cm. All of these values were just initial values for the test and could be changed later for calculations for a full-size reactor. Figure 4.2 shows the k_{inf} vs. graphite/^{233}U atom density ratio for all of the different fuel composition

systems. The curved regions enclosed inside the rectangle are satisfy the two conditions mentioned above.

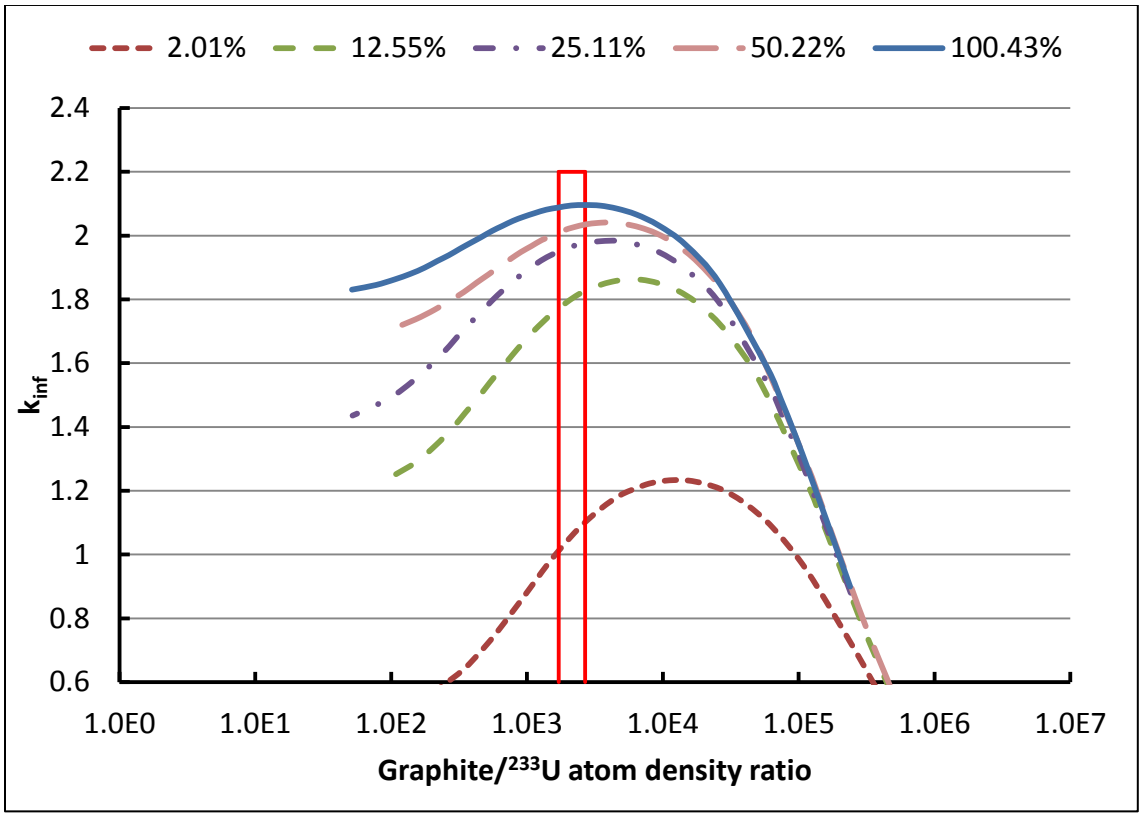

Figure 4.2. The k_{inf} vs. graphite/^{233}U for different fuel composition systems.

The burnup calculations were conducted within the range illustrated in Figure 4.2 for all systems. MCNP6 was used to calculate the k_{inf} vs. time (days) to determine the proper enrichment for a full-scale LFTR. The k_{inf} values for all fuel composition systems were run using the same single fuel rod geometry illustrated in Figure 4.1. They were burned up to 1200 days at a power level of 1 MW_{th}, as an arbitrary initial value test, with a working temperature of 900K.

Figure 4.3 shows the results of the k_{inf} calculations for all composition systems. The purpose of this study was to determine the best fuel composition that would bring the

smallest change in reactivity. In other words, a balance of consumption and production of fissionable material that brings a minimal change in reactivity was sought.

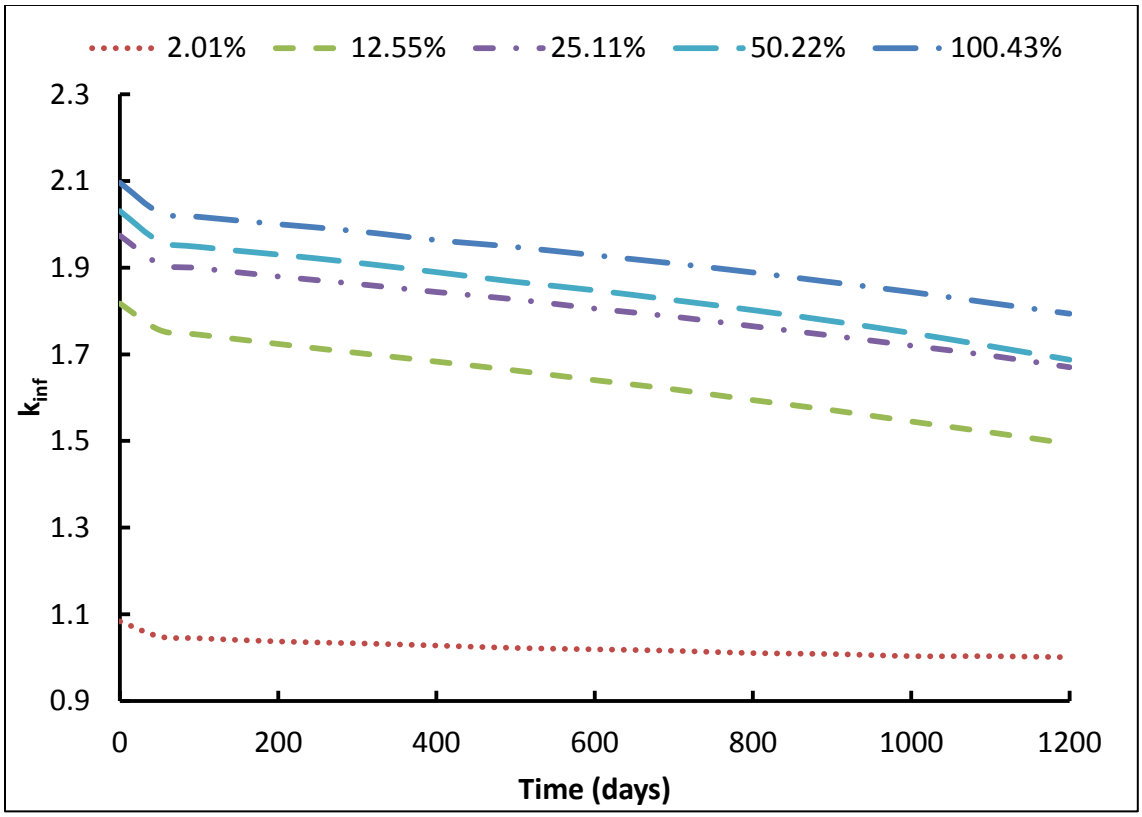

Figure 4.3. The k_{inf} vs. time for different fuel salt composition systems.

Figure 4.3 shows the decrease in k_{inf} values for all systems with the increase of burnup time. There was at first a decrease in the k_{inf} values for nearly 50 days for the system with the ($^{233}U/^{232}Th$ = 2.01%) atom ratio. Then, it almost flattened. The initial decrease in k_{inf} was due to the production of Protactinium-233 (^{233}Pa), as shown in the following the reaction:

$$^{232}_{90}\mathrm{Th} + {}^{1}_{0}\mathrm{n} \rightarrow {}^{233}_{90}\mathrm{Th} \xrightarrow[22.3\ \mathrm{min}]{\beta^-} {}^{233}_{91}\mathrm{Pa} \xrightarrow[27\ \mathrm{d}]{\beta^-} {}^{233}_{92}\mathrm{U} \qquad (4.1)$$

^{233}Pa has a 27 day half-life, so there was a delay between the production of neutrons (k_{inf}) from the fission reaction of ^{233}U to the production of new fissile material ^{233}U. The results showed that the fuel composition with the enrichment (^{233}U/^{232}Th) = 2.01 % had the least reactivity swing during the burnup time. The k_{inf} value at the beginning of life (BOL) (t=0) was close to unity, which allowed for the design of a thermal reactor. The rest of the fuel types showed a decrease in the k_{inf} profile's burnup time. Moreover, these fuels started with very high k_{inf} values at the BOL. A reduction in fuel channel size will be necessary to reduce the k_{inf} if these fuels are to be used in thermal reactor configuration.

At this point, based on the results shown in Figure 4.3, the fuel composition of (71.76% – 16.0% – 12.0% – 0.24%) with the enrichment (^{233}U/^{232}Th) = 2.01% was chosen as the optimal fuel composition to start the next calculations toward designing a full-scale conceptual-commercial thermal liquid fluoride thorium reactor LFTR.

4.2. LFTR MODEL

The LFTR core model was graphite moderated (with a density of 1.84 g/cc) with a radius of 140 cm and a height of 260 cm. It consisted of 91 fuel channels that passed through hexagonal prisms with a pitch (p=26cm), as shown in Figure 4.4. Each fuel channel was a cylindrical hole with a radius of (d=variable). The variation corresponded to the range of the under-moderated region until criticality was achieved. The fuel had a density of 3.33 g/cc and was composed of LiF, BeF_2, $^{232}ThF_4$, and $^{233}UF_4$, with mole fractions of 71.76%, 16.0%, 12.0%, and 0.24%, respectively. The entire core was covered by a vessel made of Hastelloy-N (Ni-based) with a thickness of 5 cm. There was a fuel

path between the reflector (graphite) and the core with a thickness of 7 cm. MCNP6 was used in the calculations of the criticality of the core with a working temperature of 900K.

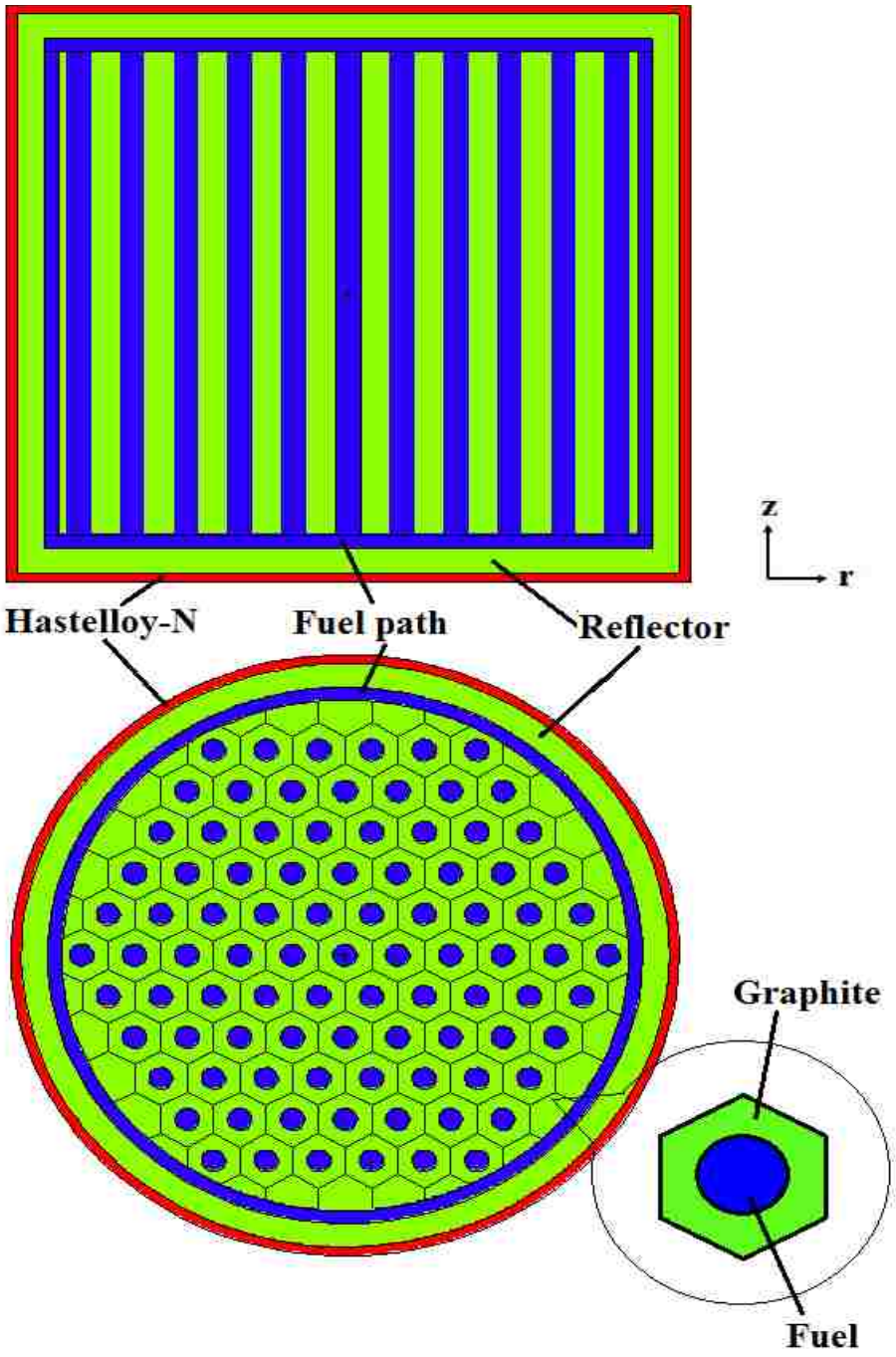

Figure 4.4. Small LFTR core model configuration.

4.3. DESIGN PARAMETERS

The core operated with a thermal power equal to 150 MW_{th} at a temperature of 900 K. Table 4.2 shows the main characteristics of the LFTR core reactor.

Table 4.2. The main parameters of the small LFTR design.

Thermal output Thermal efficiency Electric output	150 MW_{th} 33.0 % - 44.0 % (50 - 66) MW_e
Reactor vessel; Diameter/Height (inner) Thickness	 340 cm / 320 cm 5 cm
Core; Diameter/Height Fuel volume fraction	 280 cm / 260 cm 16.71 vol. %
Fuel path; Width	 7 cm
Reflector (graphite); Density Thickness	 1.84 g/cc 23 cm
Power density within core	9.37 MW_{th}/liter
Fuel salt; Composition Mol% Volume in reactor Temperature	 ^{7}LiF-BeF_2-ThF_4-UF_4 71.76 - 16.0 - 12.0 - 0.24 5.27 m^3 900 K
Hastelloy–N [29]; Compositions Wt. %	 (Ni/Mo/Fe/Cr/Nb/Si) 73.9 - 12.0 - 5.0 - 7.0 - 2.0 - 0.1

4.3.1. Things to Analyze: k_{inf} Vs. Graphite/^{233}U Density Ratio. The k_{inf} vs. graphite/^{233}U atom density ratio calculations were made using MCNP5 for a 2-D infinity array of the unit fuel cell. The calculations were then plotted, as shown in Figure 4.5, to determine the range at which the LFTR core should be designed. The curve enclosed inside the rectangle is the range that was sought to satisfy the condition for under-moderation. The height and radius of the reactor core were fixed. The k_{eff} above 1 (super-critical) was achieved by varying the lattice side hexagonal graphite moderator and the flow-hole diameter of the fuel inside the graphite moderator (corresponding to the range within the under-moderated region) in order to calculate criticality.

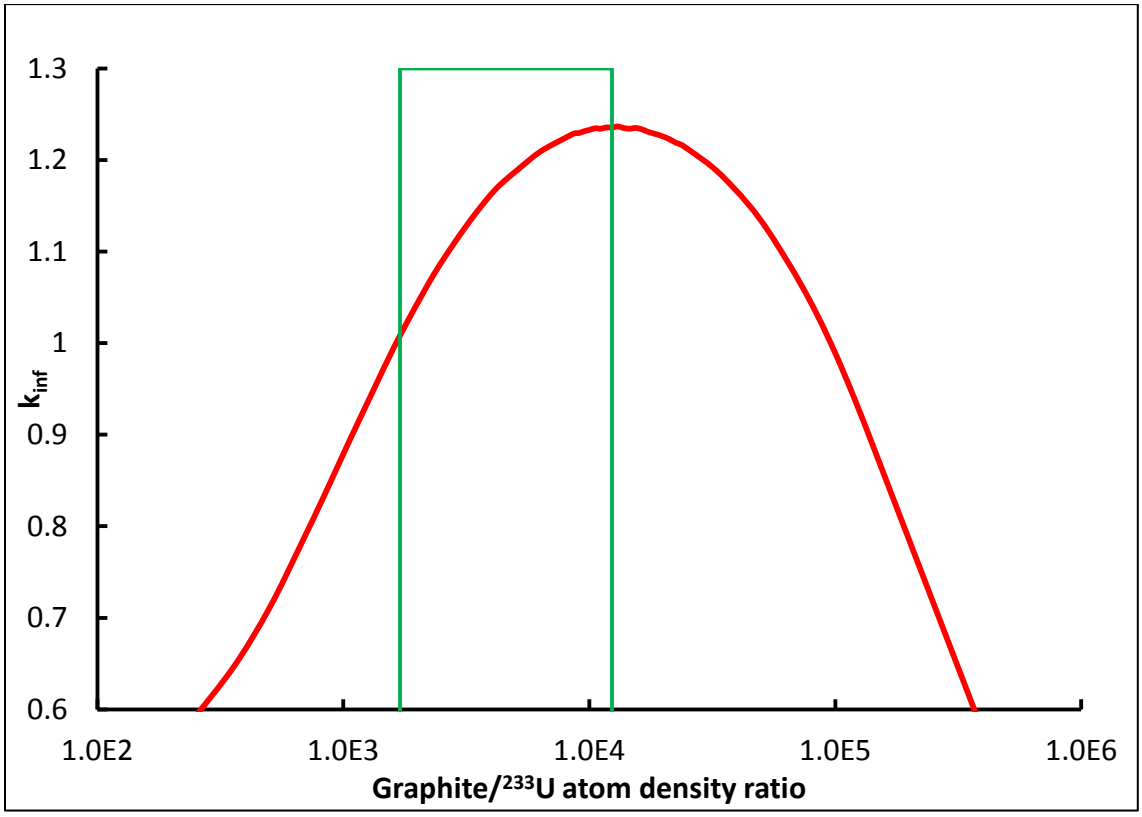

Figure 4.5. Moderator-to-fuel atom density ratio vs. k_{inf} for LFTR composition.

The maximum graphite to ^{233}U atom density ratio was about 13000 in order to achieve under-moderation. The region-curve inside the rectangle is the range at which the core is designed for safety. In this region, if the temperature increases due to fission, the number density of the graphite moderator will decrease. This leads to a decrease in the G/U ratio, which means fewer thermalized neutrons. This leads to a decrease in the fission rate, the temperature, and k-infinity, leading to the core being in a place of safety.

4.3.2. Energy Spectrum. The evaluation of the energy spectrum in the fuel cell was determined for this moderate-to-fuel atom density ratio, which is essential for the analysis of the core irradiation characteristics (see Figure 4.6). Two clear peaks were identified in the fuel channel: one in the thermal energy region and another in the fast energy region. The LFTR is a thermal reactor because of the existence of the thermal peak. The fuel cell showed a thermal spectrum with a notable epithermal neutron contribution. The thermal cross fission section for ^{233}U is about 150 times the absorption cross section in the natural thorium ^{232}Th (see Figure 4.22). Hence, more neutron absorption in the fissile content is expected at thermal energies. However, thorium resonances compete with those of ^{233}U. In particular, the dip in the spectrum (noted by 'A' in Figure 4.6 at about 22 eV) is a result of the first huge resonance of ^{232}Th at the same energy. The dip (noted by 'B' in the spectrum at about 1.26 eV) is due to the early fission cross section resonance of ^{233}U. As fuel burnup progresses, the production of ^{233}Pa, which has a relatively long half-life of 27 days, may result in an increase in the parasitic loss of neutrons in the core. The early radiative capture resonance in ^{233}Pa competes with that of ^{233}U and is up to 1000 times larger than the absorption cross section in thorium at these energies. Under ideal conditions, most of the ^{233}Pa produced

would decay to ^{233}U, thereby breeding new fuel. The likelihood of radiative capture in early resonance of ^{233}Pa is counterproductive to the creation of new fissile fuel.

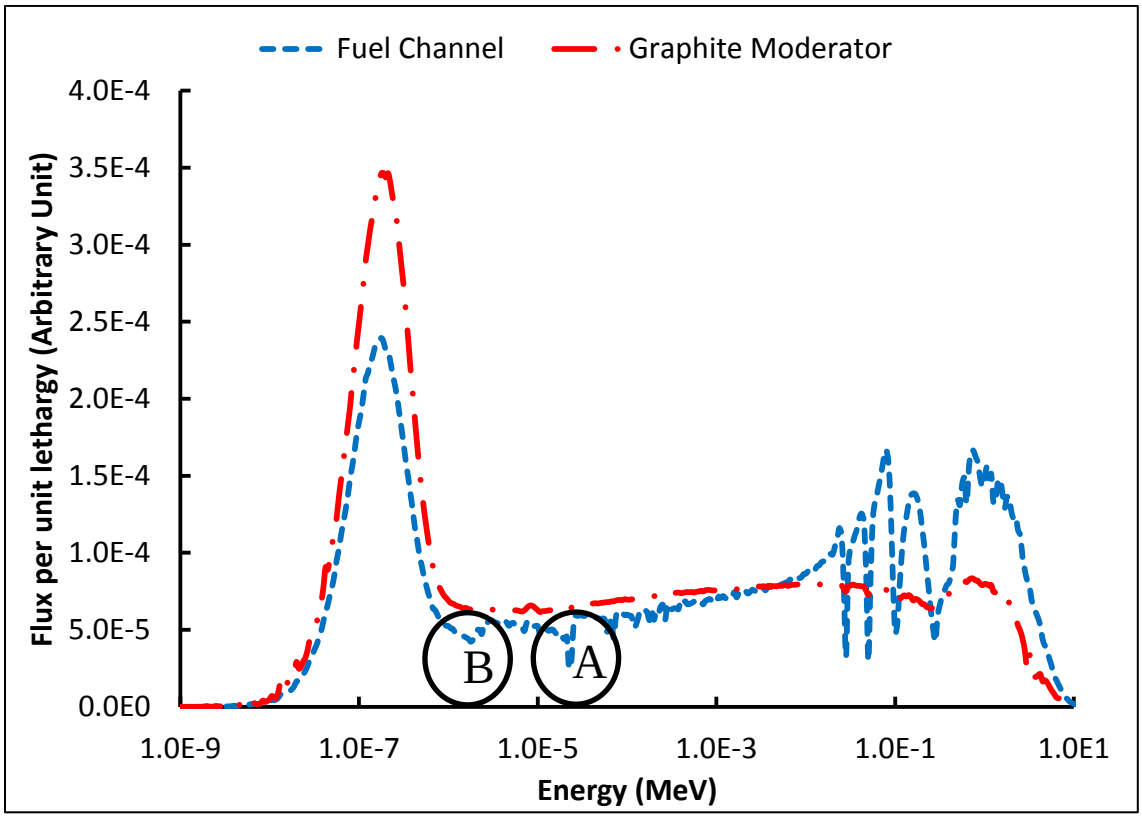

Figure 4.6. Neutron energy spectrum in a unit cell of the LFTR.

4.3.3. Time Behavior of k_{eff}. In the burnup/depletion calculations, the number of fission products to include in the MCNP input code must be determined for accurate results and efficiency in calculations. This is done by testing the built-in "Tiers" of fission products in the MCNP input file.

There are three built-in "Tiers" of fission products available to the user in the "Burn" card. Tier-1 is the default with the main 12 fission products: ^{93}Zr, ^{95}Mo, ^{99}Tc, ^{101}Ru, ^{131}Xe, ^{134}Xe, ^{133}Cs, ^{137}Cs, ^{138}Ba, ^{141}Pr, ^{143}Nd, and ^{145}Nd. Tier-2 has 87 fission products. In Tier-3, all isotopes are contained in the fission product [27].

In the burnup calculations, undue use of Tier-2 or Tier-3 will waste the running time by including hundreds of fission products. A test was done on the fuel composition system listed in Table 4.1 to compare the change in criticality between the three tiers and distinguish which tier is required. Figure 4.7 shows the results of the evaluation of the three tiers after depletion at a power level of 1 MW_{th} for 800 days. The same single fuel rod geometry was used for all three tiers. This is illustrated in Figure 4.1, in which the fuel channel had a radius of 6 cm, a height of 260 cm, and a hexagonal graphite pitch p=26 cm.

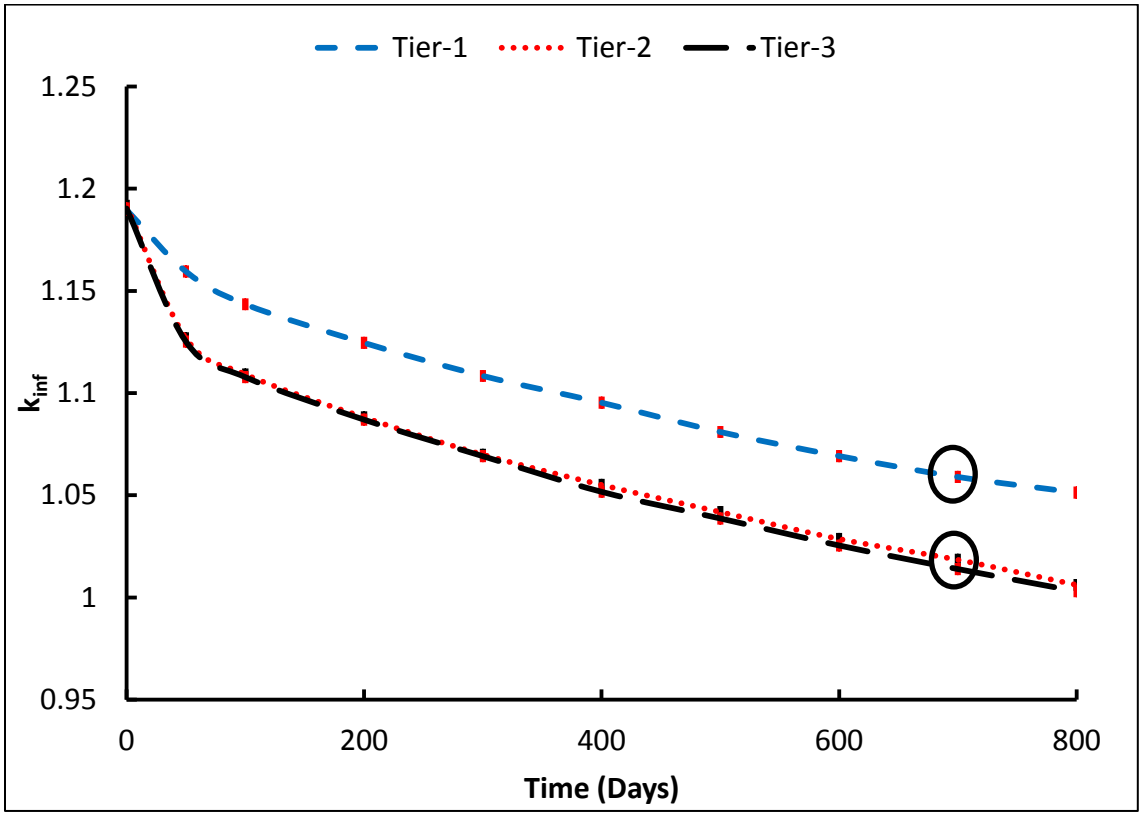

Figure 4.7. The k_{inf} as a function of time for the three tiers.

Figure 4.7 shows the visible difference in the k_{inf} values between Tier-1 and Tier-2, and a negligible difference in the k_{inf} between Tier-2 and Tier-3, where the dots inside

the circles represent the standard deviation. This indicated that Tier-3 did not need to be included for the next calculations, which saved computational time. Tier-2 fission products needed to be included for accuracy in all future calculations.

Figure 4.8 shows the time behavior of k_{eff} for 200 days of burnup calculations (with a 100% load factor) with a fuel channel radius of 6 cm and with no control rods incorporated within this analysis. It took 140 days for the k_{eff} to drop to the value of 1.0. Work will be done to increase this cycle length for the next calculation. The core will be fed with more fissile material ^{233}U to keep it just critical enough to operate for five years.

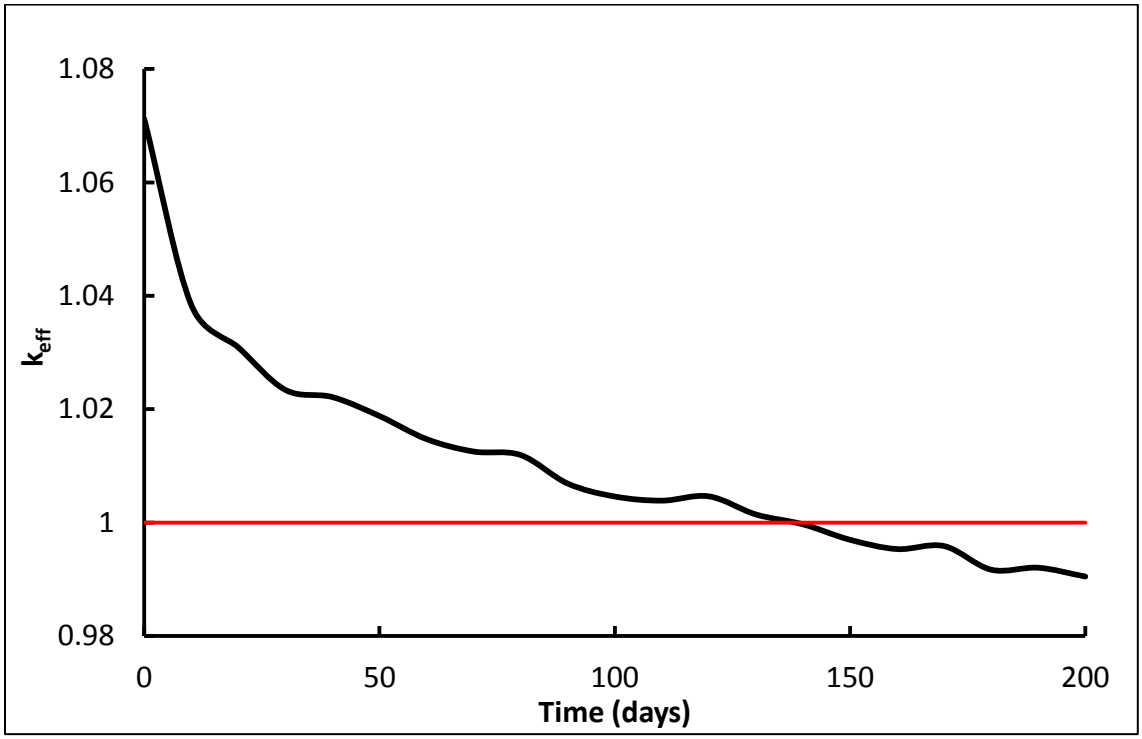

Figure 4.8. Time behavior of k_{eff} for 200 days of burnup.

4.3.4. Flux Profile. The radial distribution of the thermal neutron flux was calculated at the center of the core (z=0, θ=0) with energy lower than 1.0 eV at the beginning of the life (t=0), where the cadmium cutoff was used as a thermal energy

boundary, as shown in Figure 4.9. The x-axis was normalized to 1.0 for the outer radius vessel (R_v). The tops represent the flux at the graphite boundaries (zones) with a maximum value of thermal neutron flux at about (2.0×10^{14} n/cm^2.s). The bottoms represent the flux at the mixed fuel zones with a maximum value of thermal neutron flux at about (1.5×10^{14} n/cm^2.s).

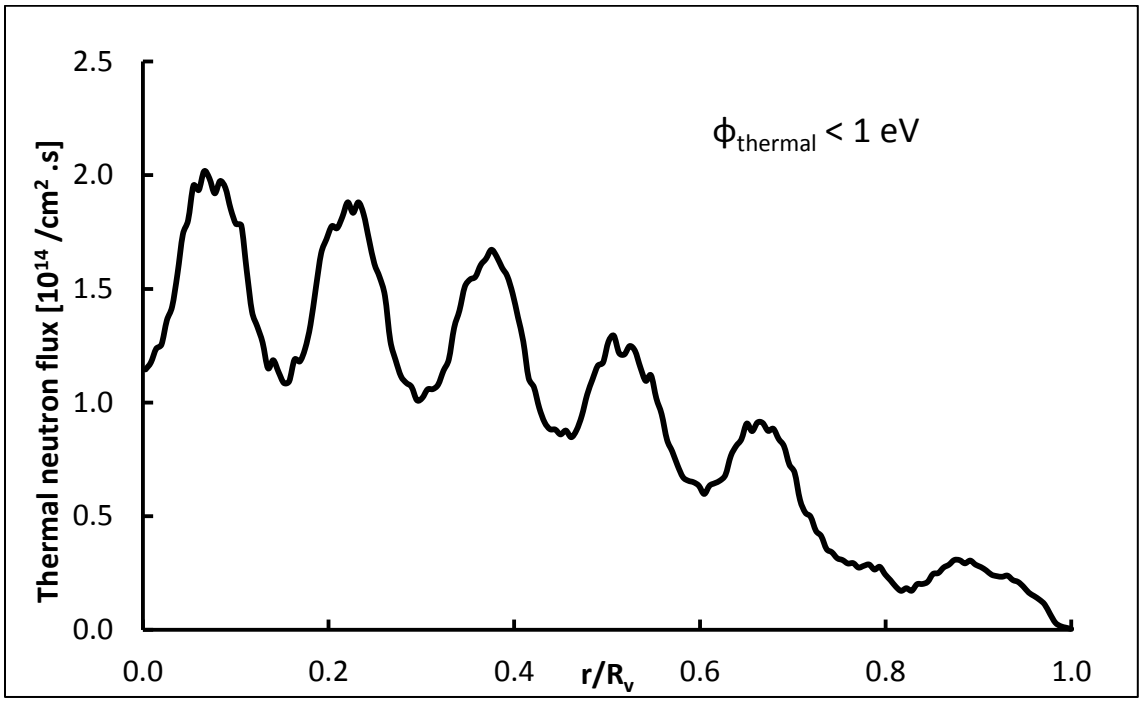

Figure 4.9. Radial flux distribution of thermal neutrons at the center of the core.

Figure 4.10 shows the radial distribution of the fast neutron flux at the center of the core (z=0, θ=0) with energy higher than 52 keV at the beginning of life (t=0). The x-axis was normalized to 1.0 for the outer radius vessel (R_v). The tops represent the flux at the mixed fuel zones with a fast neutron flux maximum value of about (1.55×10^{14} n/cm^2.s). The bottoms represent the flux at the graphite zones with a fast neutron flux maximum value of about (7.5×10^{13} n/cm^2.s).

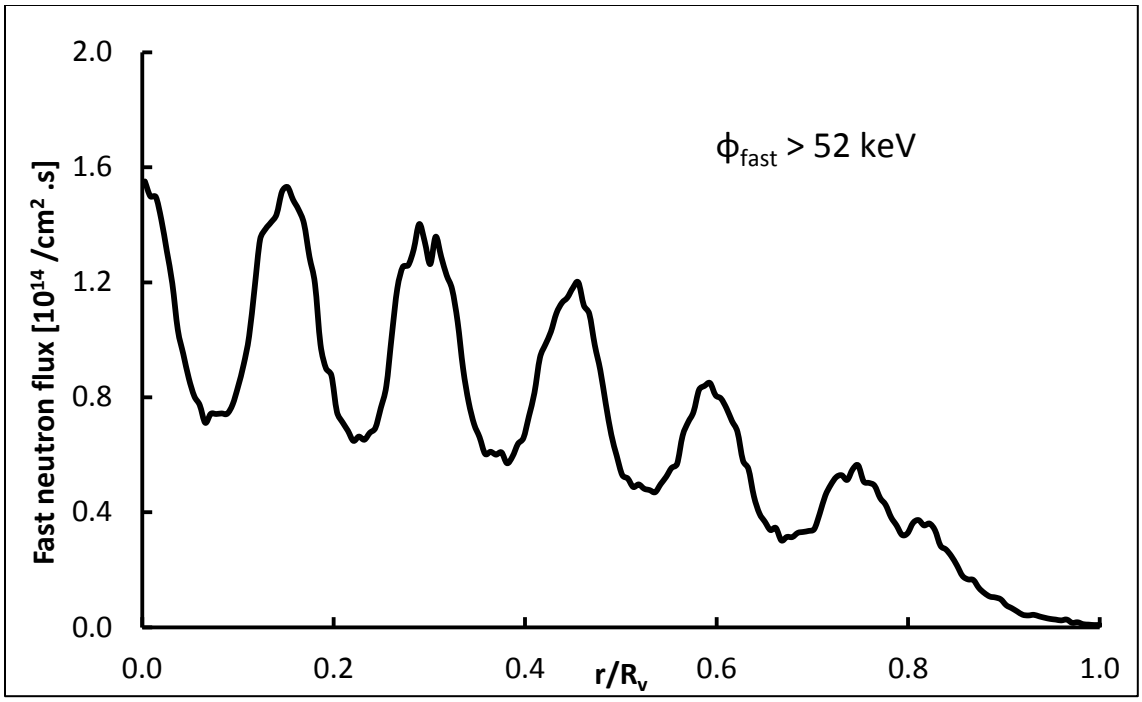

Figure 4.10. Radial flux distribution of fast neutrons at the center of the core.

Figure 4.11 shows the axial flux of thermal neutrons for five different points along the radius of the reactor, where the y-axis represents the height and the x-axis represents the normalized flux. Two of these points are in the fuel zone at (x_1=0.5 cm, x_3=104.1 cm), two points are in the graphite-moderator zone at (x_2=13.6 cm, x_4=116.2 cm), and the last point, at x_5=174.5 cm, is in the Hastelloy-N zone. The thermal flux in the graphite zone close to the center of the core (the location of the initial fission source) is higher than the thermal flux in the fuel zone close to the center, as shown from the two points at x_1=0.5 cm and x_2=13.6 cm. That is because the thermal neutrons were absorbed in the fuel to get fission while the graphite worked as a moderator, and more thermal neutrons were born inside it by slowing more fast neutrons. Moving far away from the center of the core along the core's radius, the thermal neutron flux decreases in both the radial and axial directions as compared to the flux at the point of x_1=0.5 cm and the point

of x_3=104.1 cm, which are both in the fuel or between the two points at x_2=13.6 cm and x_4=116.2 cm (both in the graphite). The thermal flux at the outer reactor vessel (x_5=174.5 cm) is almost zero (negligible). At any point on the radial radius, the thermal neutron flux decreases with the height. At a height of about z = ±137 cm (start region of reflector graphite), the thermal neutron flux began to increase symmetrically for all points but with different values. It then decreased until it vanished in the Hastelloy-N zone.

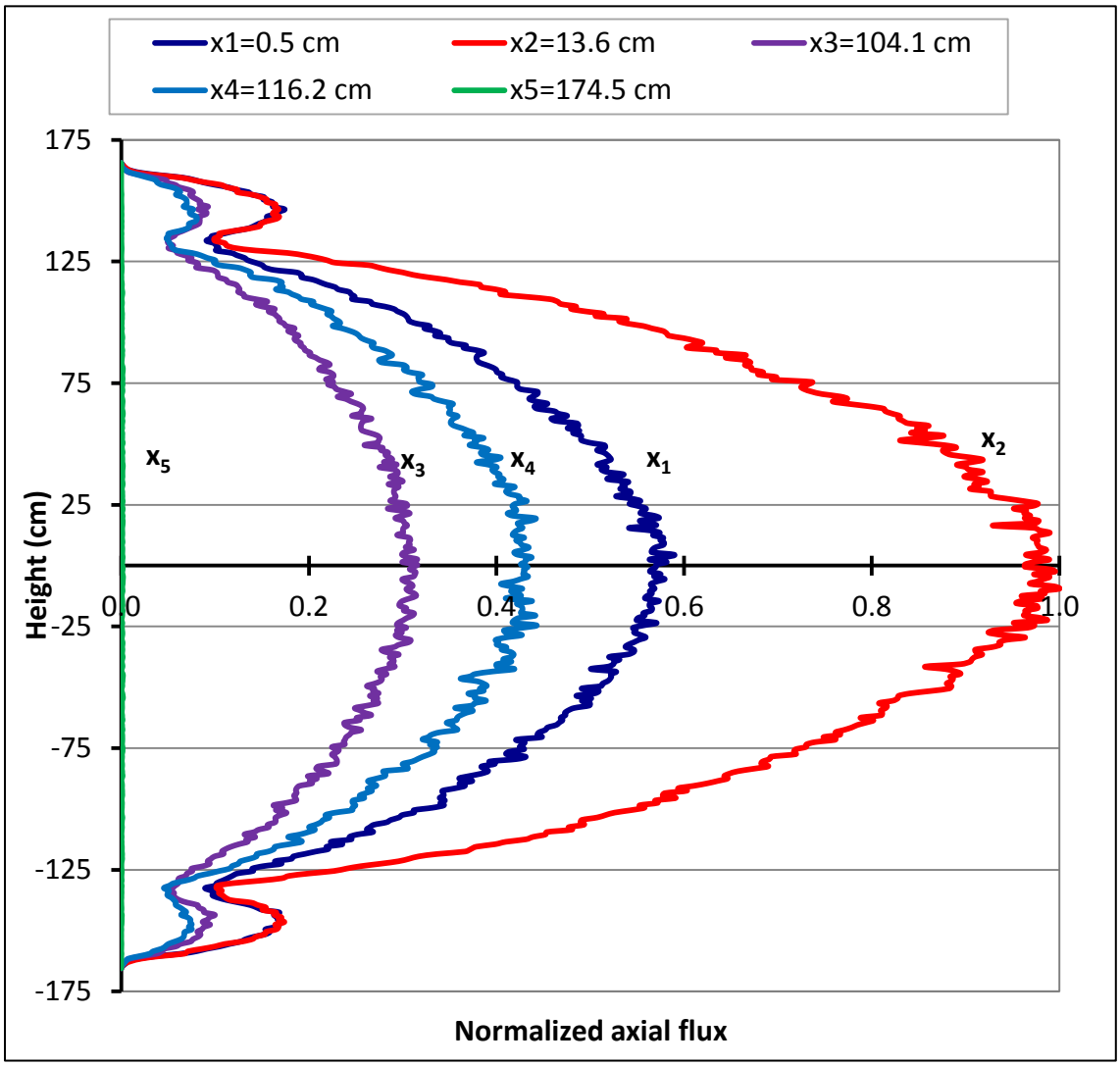

Figure 4.11. Axial flux distribution of thermal neutrons at five different radial points.

Figure 4.12 shows the axial flux of fast neutrons for the same five points explained in the previous section. The fast flux in the fuel zone located near the center of the core is higher than the fast flux in the graphite zone located near the center, as shown from the two points at x_1=0.5 cm and x_2=13.6 cm. That is because the fast neutrons were born in the fuel and then moderated in the graphite. Moving far away from the center of the core along the radius of the core, the fast neutron flux decreased in both the radial and axial directions as compared to the flux at the point x_1=0.5 cm and the point at x_3=104.1 cm, which are both in the fuel or between the two points at x_2=13.6 cm and x_4=116.2 cm, which are both in the graphite. The fast flux at the outer reactor vessel (x_5=174.5 cm) is almost zero (negligible).

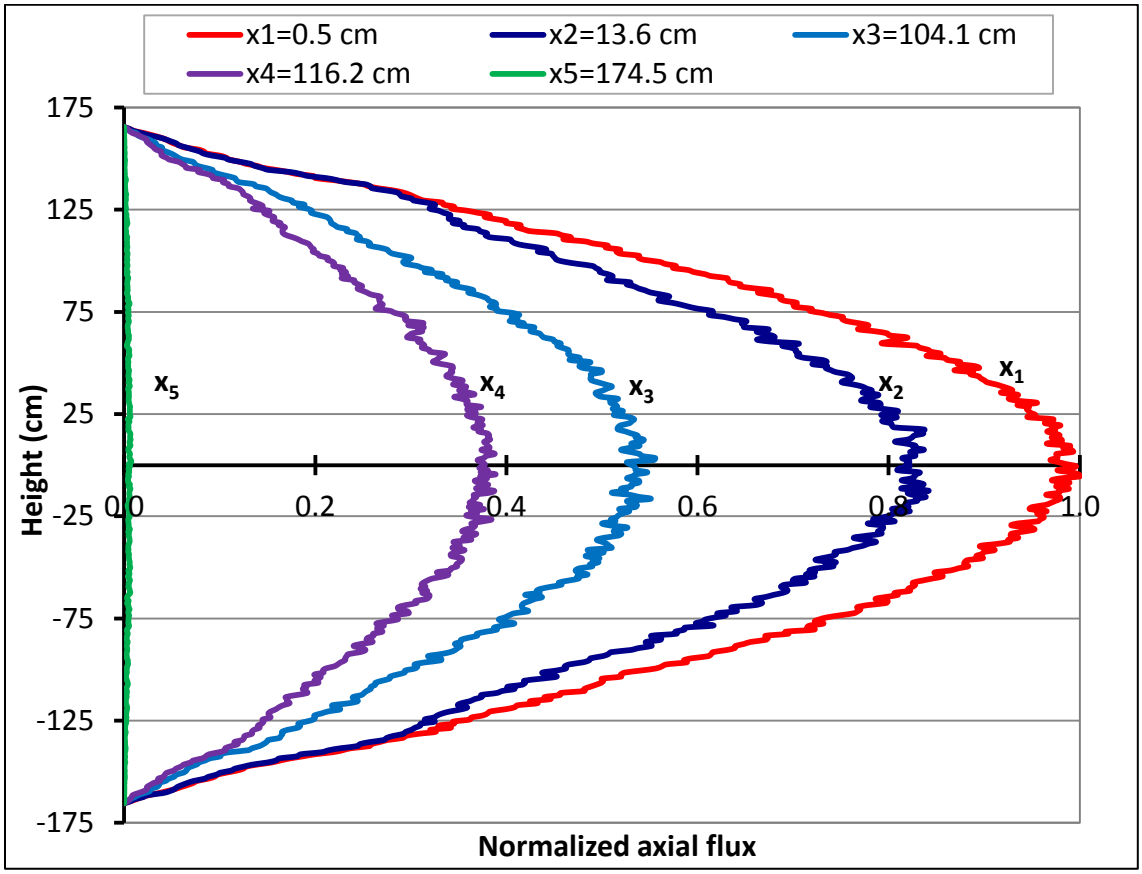

Figure 4.12. Axial flux distribution of fast neutrons at five different radial points.

Figures 4.13 and 4.14 show the thermal neutron flux distribution at the beginning of life (t=0) for the entire reactor vessel at (z=0) in 2-D and 3-D vision, respectively, with energy lower than 1 eV. The maximum thermal neutron flux was in the graphite regions around the center of the core with maximum-to-average of 1.87. The value of the thermal neutron flux decreased while moving far from the center of the core toward its edge.

Figures 4.15 and 4.16 show the fast neutron flux distribution at the beginning of life (t=0) for the entire reactor vessel at (z=0) in 2-D and 3-D vision, respectively, with energy higher than 52 keV. The maximum fast neutron flux was at the center of the core with maximum-to-average of 2.78. The value of the fast neutron flux decreased while moving far from the center of the core toward the edge of the vessel.

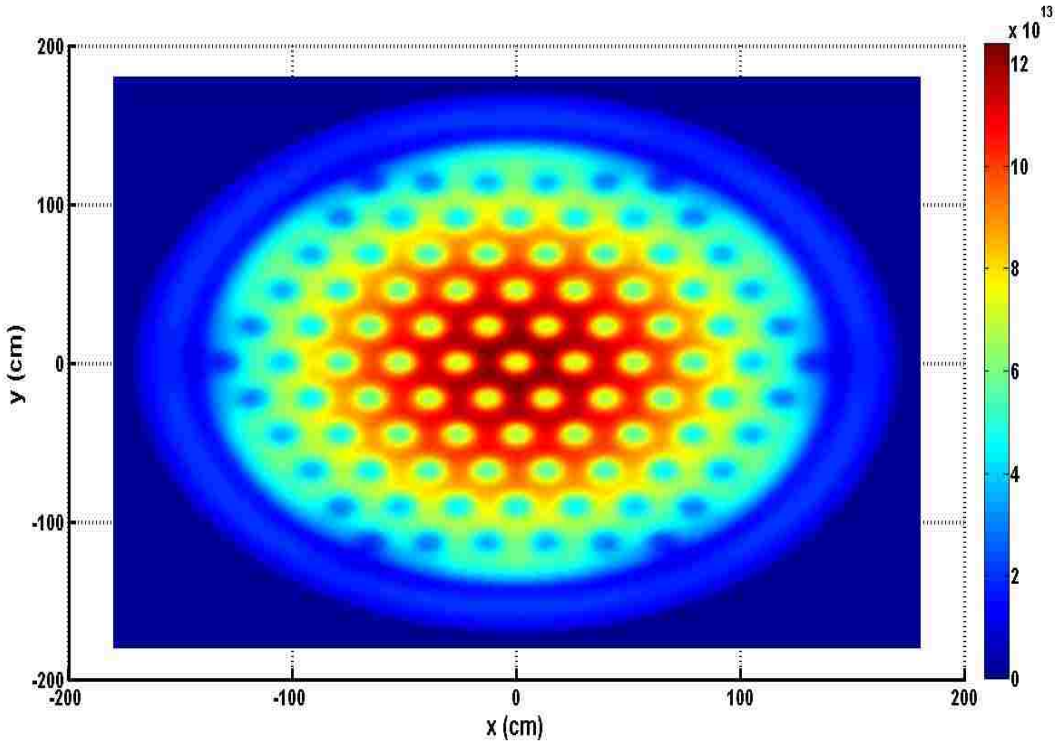

Figure 4.13. 2-D thermal flux distribution ϕ_{th} < 1 eV.

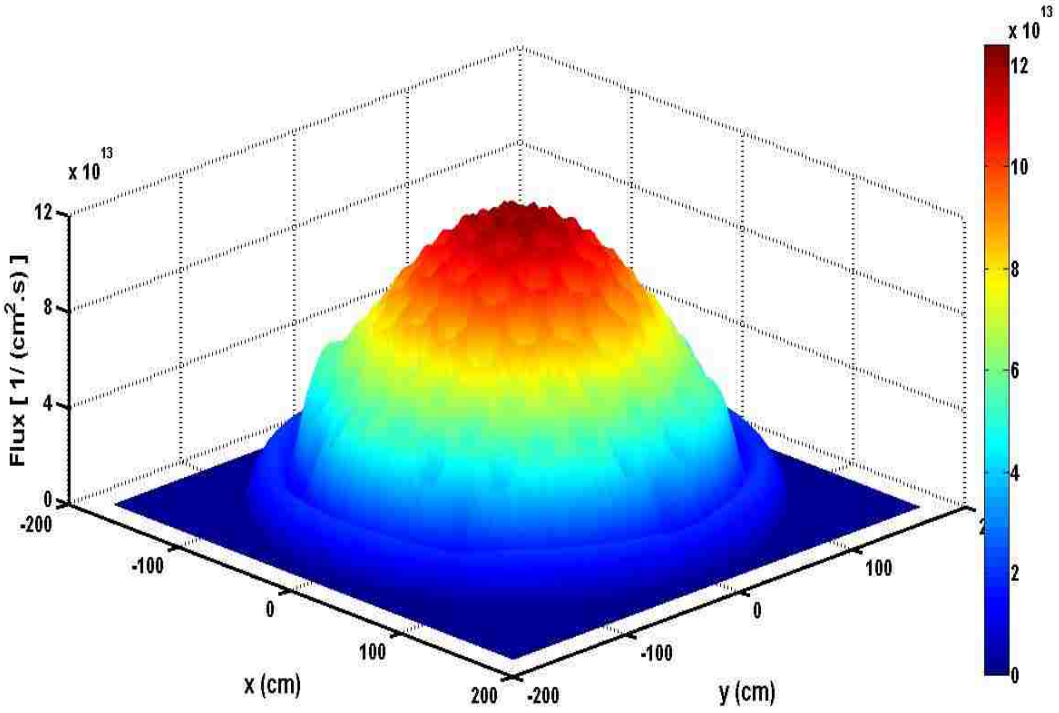

Figure 4.14. 3-D thermal flux distribution ϕ_{th} < 1 eV.

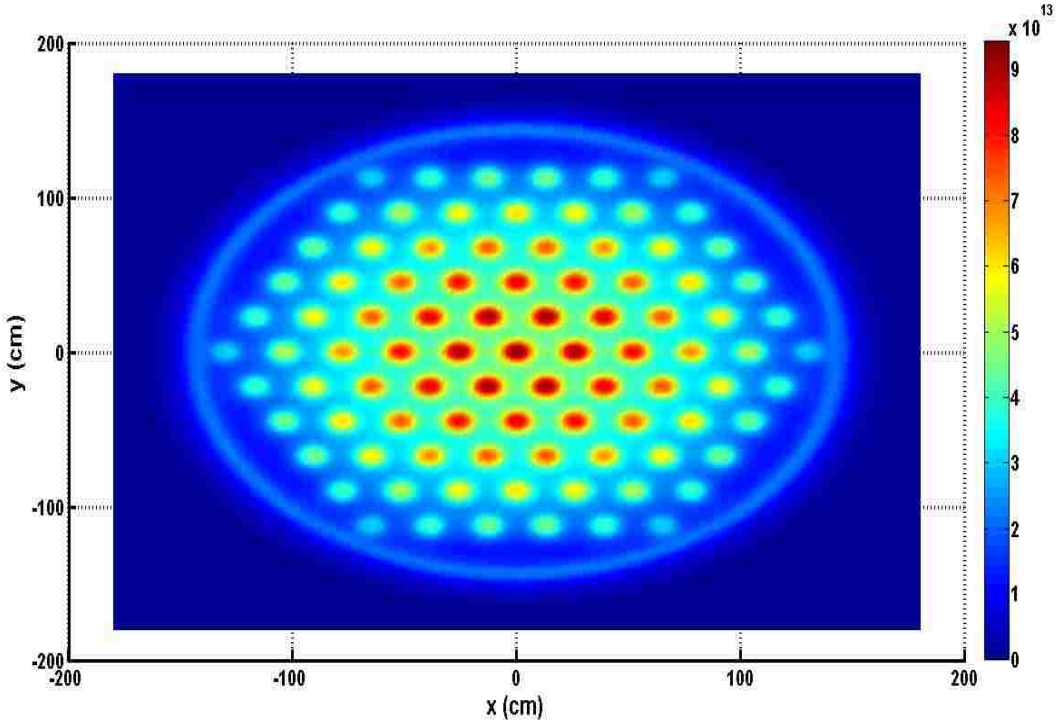

Figure 4.15. 2-D fast flux distribution ϕ_f > 52 keV.

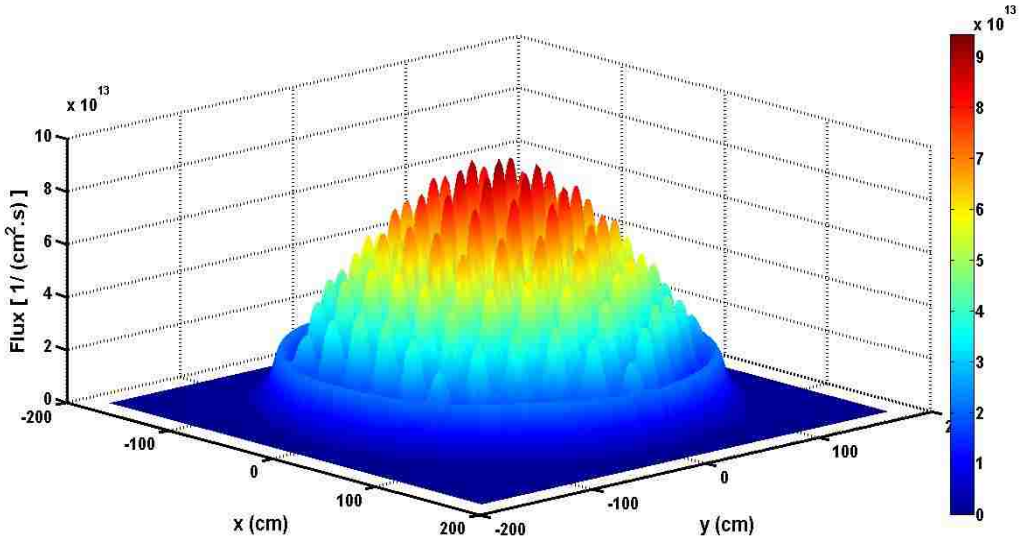

Figure 4.16. 3-D fast flux distribution ϕ_f > 52 keV.

Figures 4.17 and 4.18 show the total neutron flux distribution at the beginning of life (t=0) for the entire reactor vessel at (z=0) in 2-D and 3-D vision, respectively. The maximum-to-average of total flux was 1.68. The value of the total neutron flux decreased while moving far from the center of the core toward the edge of the vessel.

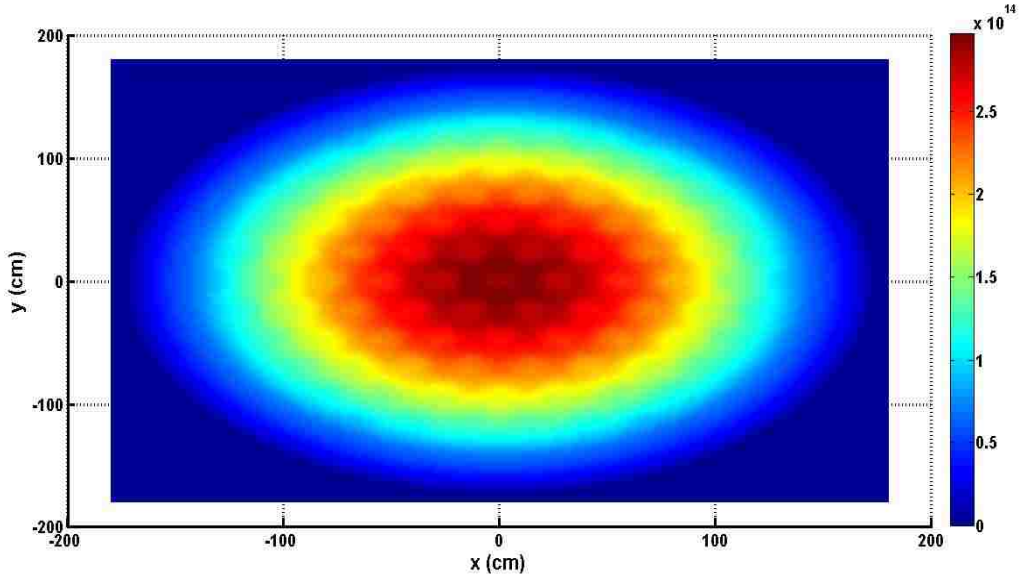

Figure 4.17. 2-D total flux distribution ϕ_{total}.

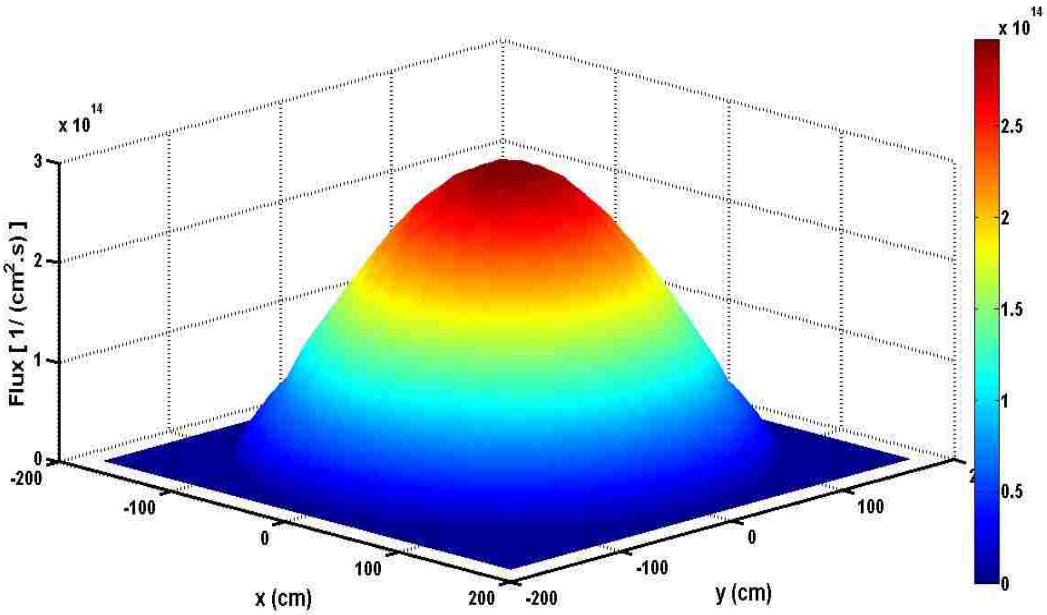

Figure 4.18. 3-D total flux distribution ϕ_{total}.

4.3.5. Burnup Calculations. The burnup characteristics were calculated using the Monte Carlo N–Particle (MCNP) Transport Code. Tier-2 (with 87 fission products) was used to perform this calculation. In the burnup calculation, the continuous removal of fission product FP gases (such as H, He, Ne, Kr, and Xe) from the fuel salt was done for every 10 days by the material modification (MATMOD) feature from the input BURN card. It was assumed that 100 % of gaseous FP was removed with no residual remains for every 10 day interval.

Figure 4.19 shows the time behavior of k_{eff} where the x-axis shows the effective full power day EFPD of burnup of 1880 days with a load factor of 100 %, corresponding to almost 5 years of operation. At the beginning of life (t=0), the k_{eff} started with the value of about 1.07. Then, k_{eff} was calculated every 10 days with FP gases being removed at every 10 day interval. The k_{eff} took about 300 days to drop to the value of almost 1.002.

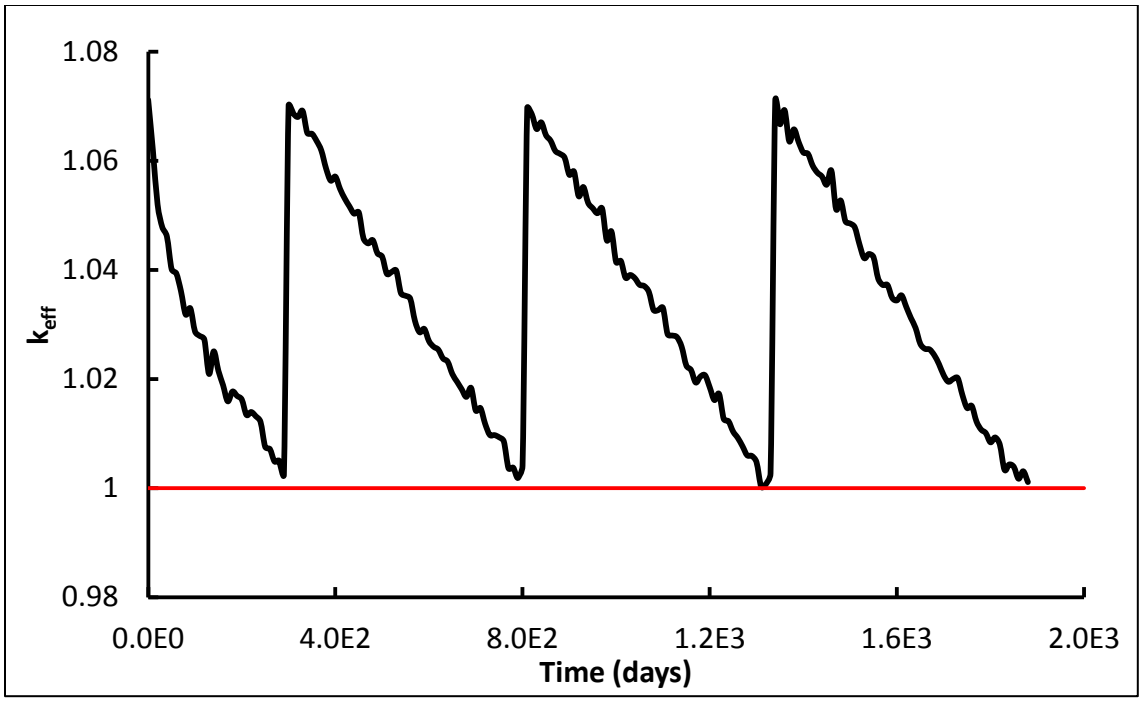

Figure 4.19. Time behavior of k_{eff} for up to five years of operation.

The k_{eff} was maintained at a critical status by feeding the reactor with a new fuel salt on the 300th day. This fed fuel was in the form of frozen eutectic salt for replenishment, which composed of a mixture of LiF (73 mol. %) and UF_4 (27 mol. %). The same scenario was repeated for the next time of burnup with the removal of FP gases every 10 days and calculations of the k_{eff}. To operate the reactor to almost five years, it was fed 3 times during the burnup process. The total net feed for the first time was 25 kg of ^{233}U on the 300th day. This was enough to increase the k_{eff} to almost the same point as the beginning of life (1.07). The reactor was fed with 27 kg of ^{233}U for the second feeding, which was on the 810th day; the k_{eff} increased to 1.07. For the last time of feeding, 29 kg of ^{233}U was fed to the reactor on the 1340th day, which brought the k_{eff} back to 1.07. The first cycle length was 300 days, the second cycle length was 510 days, the third cycle length was 530 days, and the last cycle length was 540 days. There was an

increase in the fuel cycle length because of the increase in the (fission/fertile) % after each feeding (see Table 4.3).

Figure 4.20 shows the phase diagram equilibria for the binary system LiF - UF_4. The phase diagram plots relative concentrations of LiF and UF_4 along the x-axis and temperature along the y-axis. The temperature has a eutectic point at the concentration of 73 mol. % - 27 mol. %. The term “eutectic point” comes from the Greek 'eutektos', meaning easily-melted. This is the point where the liquid phase borders directly on the solid phase; it represents the minimum melting temperature of the binary system LiF – UF_4 at 480 °C.

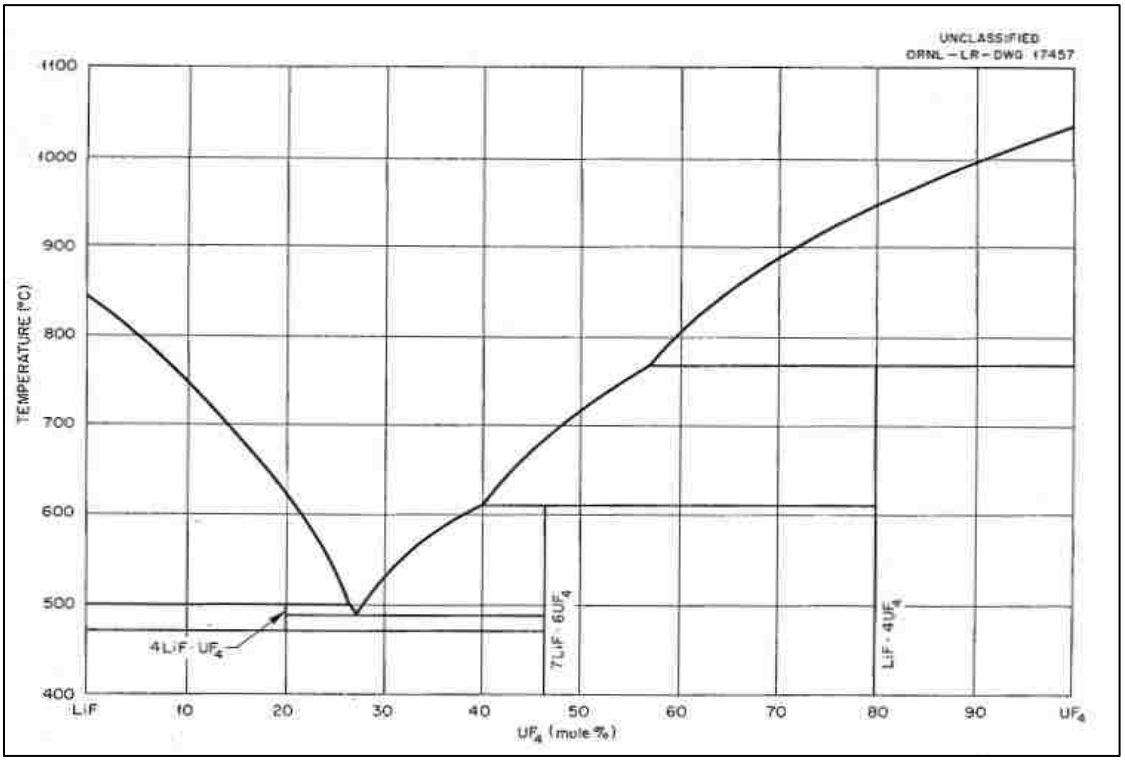

Figure 4.20. Phase equilibria for the binary system LiF – UF_4 [33].

Table 4.3 shows the change of LFTR characteristics for almost of 5 years of operation. The k_{eff} and the conversion ratio CR values were calculated at the beginning of

life (t=0), at the beginning of each cycle length, and prior to feeding. The fissile-to-fertile ratios and the temperature coefficient of reactivity α_T values were calculated at the beginning of life (t=0) and at the beginning of each cycle length.

Table 4.3. Time behavior of LFTR characteristics during 1880 days of operation.

Operation Period (EFPD)	k_{eff}	CR	Fission/Fertile %	α_T [1/K] ($\times 10^{-5}$)
0 290	1.071 1.002	0.0 0.77	0.0201	-2.83
300 800	1.070 1.004	1.24 0.84	0.0227	-2.39
810 1330	1.070 1.003	1.14 0.81	0.0244	-1.58
1340 1880	1.071 1.001	1.13 0.78	0.0260	-2.79

4.3.6. Conversion Ratio. By following the production paths of ^{233}U (which was explained in Figure 1.1), one can easily estimate the value of the conversion ratio (CR), which is defined as the ratio of the production of fissile material to the consumption. When a ^{232}Th atom absorbs a neutron, it is converted to a ^{233}Th atom with a half-life of 22.3 minutes. After that, ^{233}Th decays by beta emission to ^{233}Pa, with a half-life of about 27 days. Finally, the ^{233}Pa converts to ^{233}U by beta decay emission.

Figure 4.21 shows the time behavior of the fuel conversion ratio (CR), as well as the build-up mass of ^{233}Pa. The x-axis represents the burnup time, the major y-axis represents the CR values, and the minor y-axis represents the build-up mass of ^{233}Pa. At the beginning of life, the CR had a very low value. There was a dip after about 10 days

due to the accumulation of ^{233}Pa (with a half-life of 27 days), which has a high absorption cross section of slow neutrons. After almost 20 days, the CR values increased rapidly. When the core was fed with a new fuel, the CR peaked due to the sudden increase in the fissile material ^{233}U. Figure 4.21, shows the peaks at the three points of feeding: 300, 810, and 1340 days.

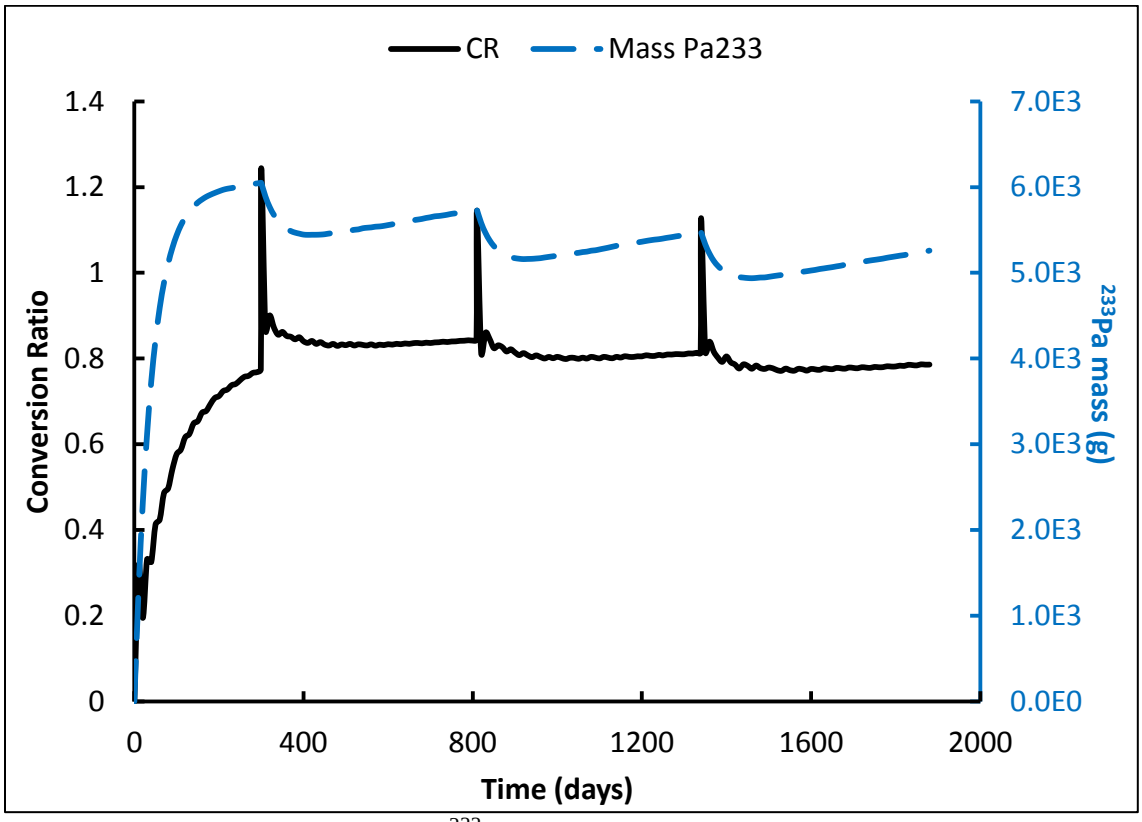

Figure 4.21. The build-up mass of ^{233}Pa vs. the CR with burnup time.

At the time of feeding and after each peak, the CR decreased a little bit because there was an increase in the consumption of ^{233}U and a decrease in the production of fissile material. The fission cross section of ^{233}U is higher than the absorption cross section of ^{232}Th at low neutron energy, as shown in Figure 4.22. So, after each feeding the atom ratio ^{233}U/^{232}Th would be increased. Therefore, more ^{233}U atoms would cause

more neutrons to be absorbed to get fission at thermal energy. Fewer neutrons would be absorbed by ^{232}Th, which would reduce the production of ^{233}Pa and would also reduce the production of fissile material. Thus, the CR would decrease. The build-up mass of ^{233}Pa increased with time to the point of the first feeding, which showed the peak of CR (as shown in Figure 4.21). At this point, the build-up mass of ^{233}Pa decreased with time and then started to increase, as explained above. The same scenario is repeated after each fed, and the average CR throughout the lifetime was about 0.78.

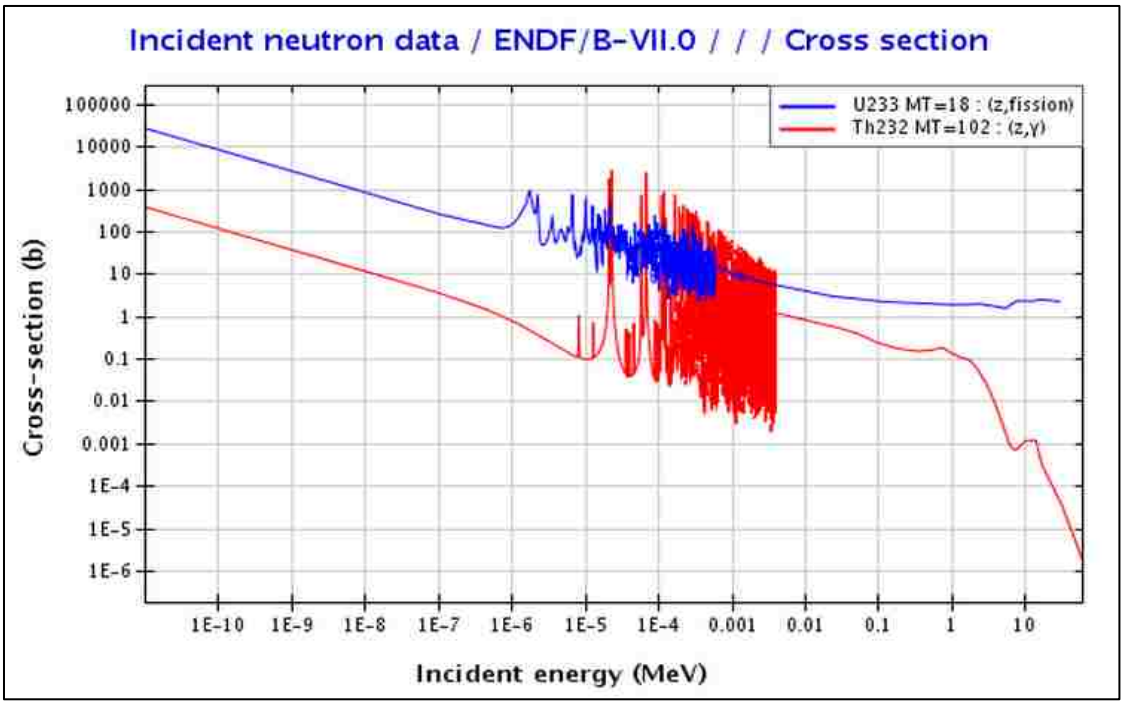

Figure 4.22. The fission cross-section of ^{233}U vs. the absorption cross-section of ^{232}Th.

4.3.7. Material Balance of Actinides, Minor Actinides (MA), and Fission Products (FP). Table 4.4 shows the material balance of actinides (such as U^{fiss}, ^{232}Th, and Pu), the MA, and the concentrations of solid FP and gas FP in the LFTR for 1880 days of operation. “Initial inventory” is the weight (in tons) of materials at the beginning

of life (t=0), and the "total net feed" is the net weight makeup (in tons) of materials during 1880 days of operation. The "total demand" is the total net of fissile and fertile material needed to operate the LFTR for 5 years, which is the sum of the "initial inventory" and the "total net feed." The "final remain" is the final weight of actinides, minor actinides, and fission products at the closing of the reactor.

Finally, the "net production" is the value that determines if there was a production or consumption of the materials by subtracting the final remain from the total demand. If the number is negative, then the material was consumed. If it is positive, then the material was produced.

Table 4.4. Material balance of LFTR after 5 years of operation.

	^{232}Th (ton)	U^{fis}+^{233}Pa (ton)	Pu (g)	MA (g)	All FP (kg)	Gas FP (kg)
Initial inventory	7.644	0.154	---	---	---	---
Total net feed	---	0.081	---	---	---	---
Total demand	7.644	0.235	---	---	---	---
Final remain	7.380	0.172	7.63	34.5	294.3	---
Net production	- 0.264	- 0.063	7.63	34.5	294.3	7.1

Almost 90% of the plutonium produced was ^{238}Pu (with a half-life 87.7 years). Table 4.5 shows the fuel salt composition at the beginning of life and at each step of refueling. During the burnup of the fuel with time, the fuel composition changed because

of the component materials that were consumed. The fuel composition of LiF-BeF_2-ThF_4-UF_4 should stay in the mixed liquid form. Otherwise, it will affect/attack the reactor vessel and graphite material. For this case, the change in the fuel salt composition during burnup time must be watched and necessary adjustment made to the fuel salt composition by periodically adding Li, F, Th, and Be. The mixture of LiF-ThF_4 should be added at the eutectic point at a ratio of 71 mol% – 29 mol% [33].

Table 4.5. Fuel salt composition at the main steps of the LFTR operation.

Burnup (days)	LiF (mol%)	BeF_2 (mol%)	ThF_4 (mol%)	UF_4 (mol%)	Other elements
0	71.76	16.0	12.0	0.24	0.0
300	71.80	16.0	11.91	0.26	0.03
810	71.81	15.96	11.78	0.28	0.17
1340	71.81	15.93	11.65	0.29	0.32
1880	71.88	15.95	11.55	0.26	0.36

4.4. CONCLUSION

The results of this study were promising and successful in demonstrating a prefatory small commercial LFTR design. The outcome of using a small core reactor with a diameter/height of 280/260 cm that would operate for more than five years at a power level of 150 MW_{th} was studied. The fuel system ^{7}LiF - BeF_2 - ThF_4 - UF_4 with a (^{233}U/^{232}Th) = 2.01 % enrichment was the candidate fuel for this reactor core. The next chapter presents a discussion of the optimization of the LFTR in order to increase the cycle lengths and study the change in the thermal/fast neutron flux inside the core.

5. AN OPTIMIZATION OF THE LFTR CORE

This chapter presents an optimization for the LFTR core, (discussed in Chapter 4) in order to increase the cycle length of burnup. To do that, the radius of the fuel rods at the outer rings of the LFTR core was increased while keeping the total mass/volume of the fuel inside the core fixed. Thus, the radius of the fuel rods at the inner rings of the core was decreased. Various scenarios with different radii were analyzed. Finally, the best configuration is illustrated in Figure 5.1. The optimized LFTR core has one outer ring, and each fuel rod has a radius of 6.8 cm. Each of the fuel rods at the inner rings has a radius of 5.57 cm. By increasing the radii of the fuel rods at the outer ring of the original LFTR core, the k_{eff} value was expected to be decreased at the edge of the core. This expectation was based on the k_{inf} vs graphite/^{233}U atom density ratio, which is illustrated in Chapter 4/ Figure 4.5. Thus, a reduction in the neutron leakage from the core and also enhance the conversion ratio were expected. On the other hand, decreasing the radii of the fuel rods at the inner rings of the original LFTR core would increase the k_{eff} values around the center of the core and increase the neutron flux. Figure 5.2 shows the time behavior of burnup at a power level of 150 MW_{th} for the optimized LFTR core compared with the original LFTR core. It shows an increase in the k_{eff} value at the beginning of life (t=0) for the optimized LFTR core (equal to 1.075) compared with the k_{eff} value of the original LFTR core (equal 1.071). The burnup calculations were performed using MCNP6, and FP gases were removed from the fuel salt every 10 days. The k_{eff} took about 340 days to drop from 1.075 to almost 1.0 for the optimized LFTR core. This showed that there was an increase in the cycle length compared with the

original LFTR core, which took 300 days for the k_{eff} to drop to almost 1.0. The burnup calculations for just the first cycle length were performed to see the improvement of the fuel cycle length for the optimized LFTR core compared with the original LFTR core. The refueling calculations for the next fuel cycle lengths were not performed, but an improvement for the next cycle lengths of the optimized LFTR core is expected.

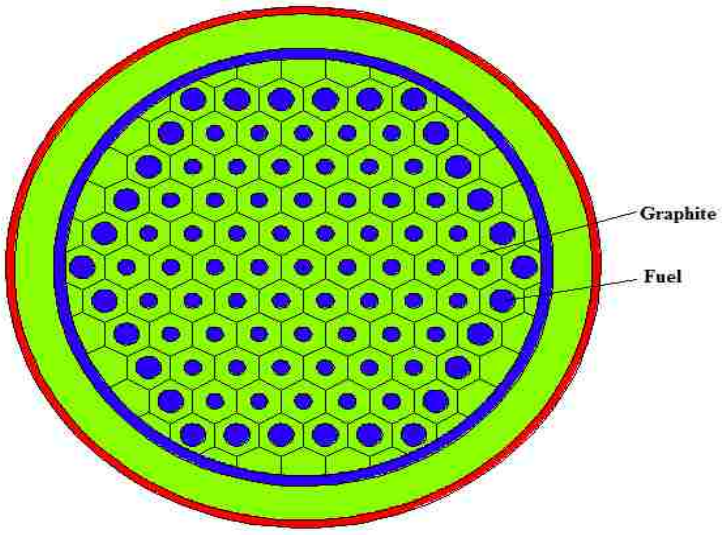

Figure 5.1. The x-y section of the optimized LFTR core.

Decreasing the radii of the fuel rods at the inner rings of the core allowed the volume of the graphite moderator to increase in each hexagonal unit cell, allowing more fast neutrons to be thermalized. Thus, an increase in the thermal neutron flux inside the core was expected. Figure 5.3 represents the radial thermal flux of the optimized LFTR core vs the original LFTR core. On the other hand, increasing the radii of the fuel rods at the outer ring of the core decreased the graphite moderator volume, which led to a decrease in the thermalized neutron flux. Figure 5.4 shows that no significant changes occurred in the radial fast neutron flux between the optimized LFTR core and the original LFTR core.

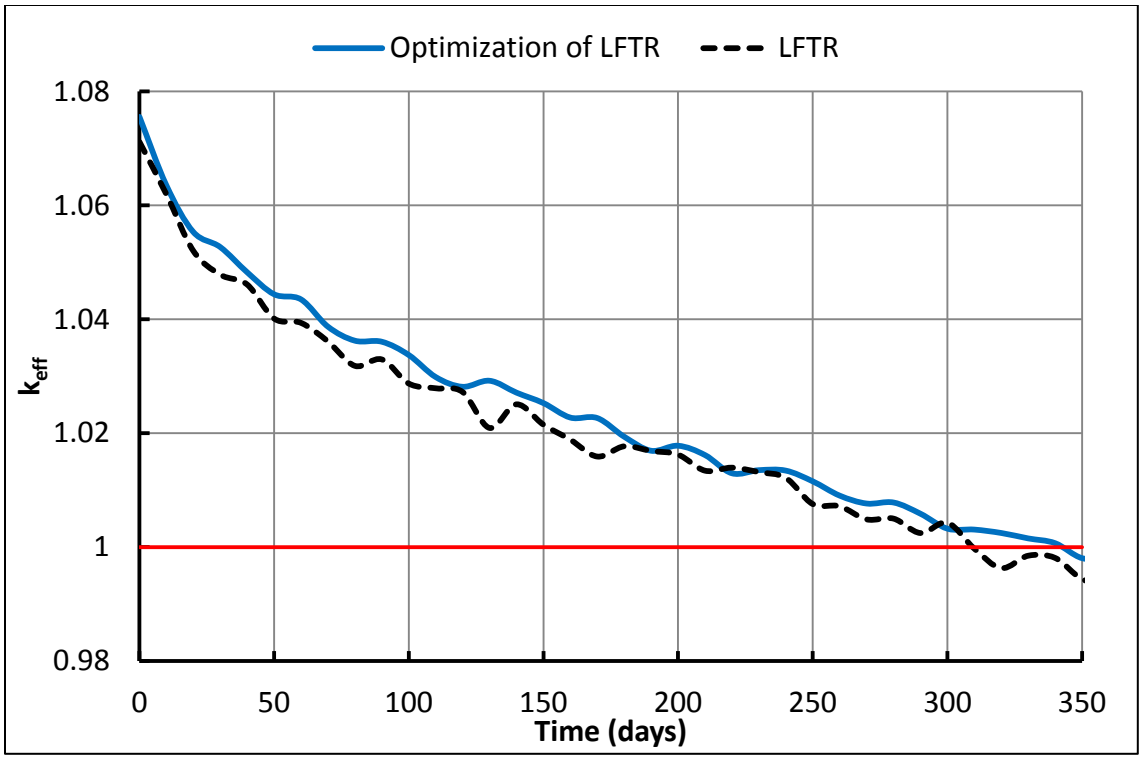

Figure 5.2. The k_{eff} of the optimized LFTR vs original LFTR core.

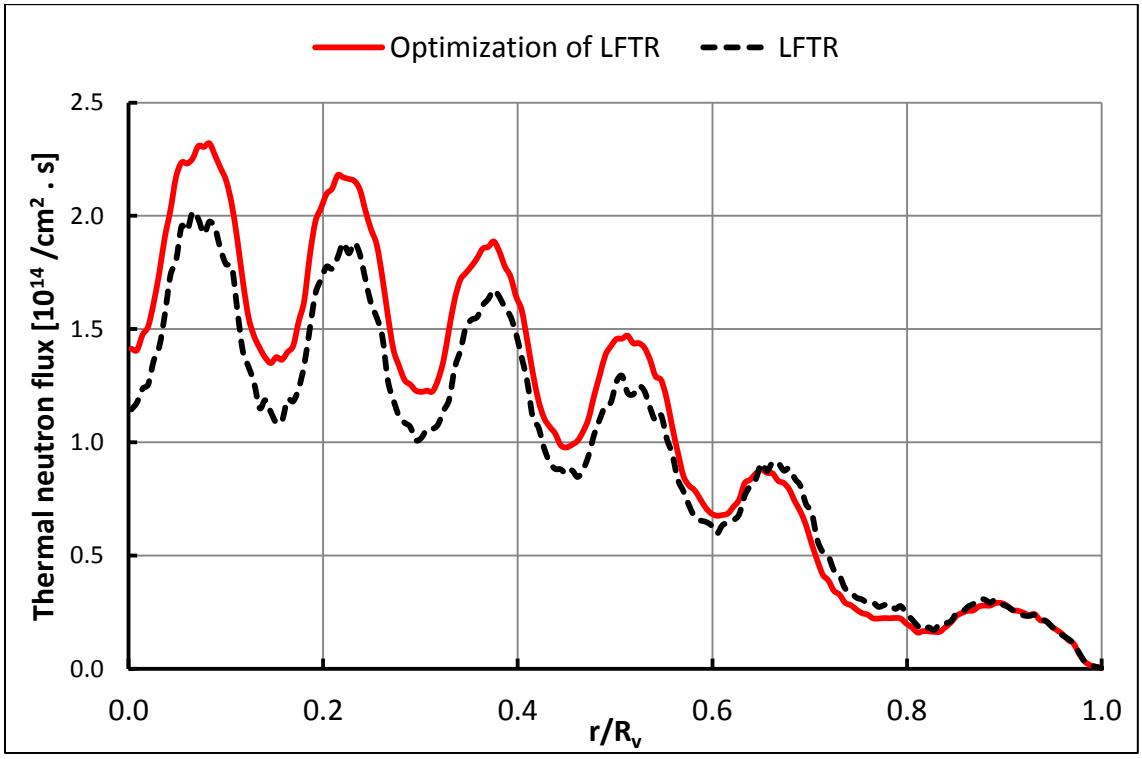

Figure 5.3. The radial thermal neutron flux of the optimized LFTR vs original LFTR.

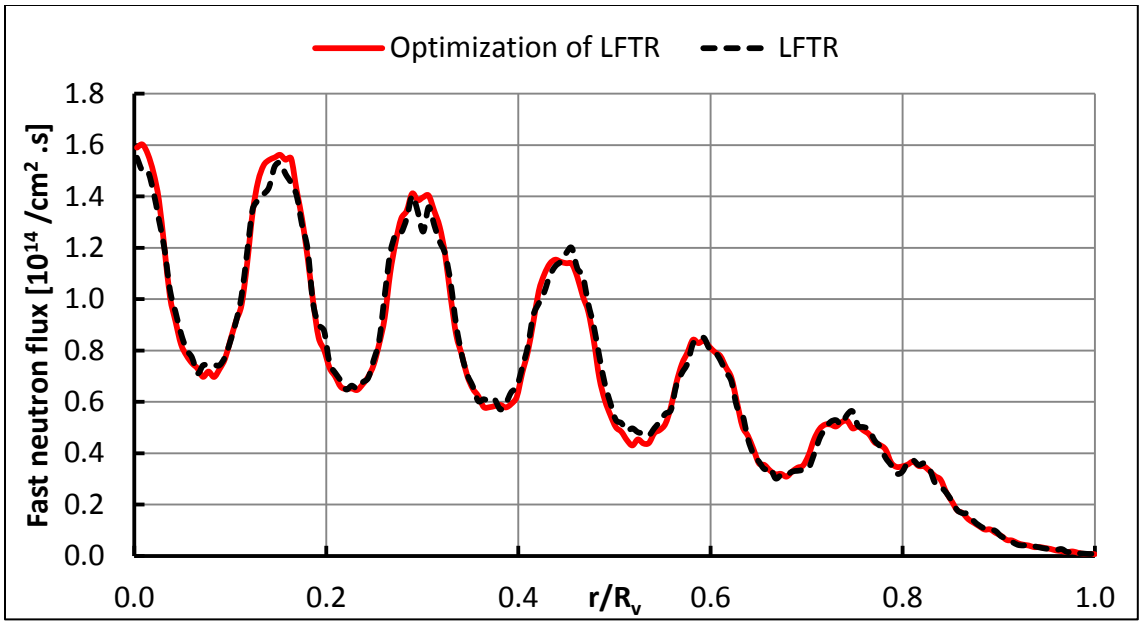

Figure 5.4. The radial fast neutron flux of the optimized LFTR vs original LFTR.

Figure 5.5 shows the radial total neutron flux of the optimized LFTR core compared with the original LFTR core. The significant change of the total flux at the center of the optimized LFTR core came from the thermal neutron flux.

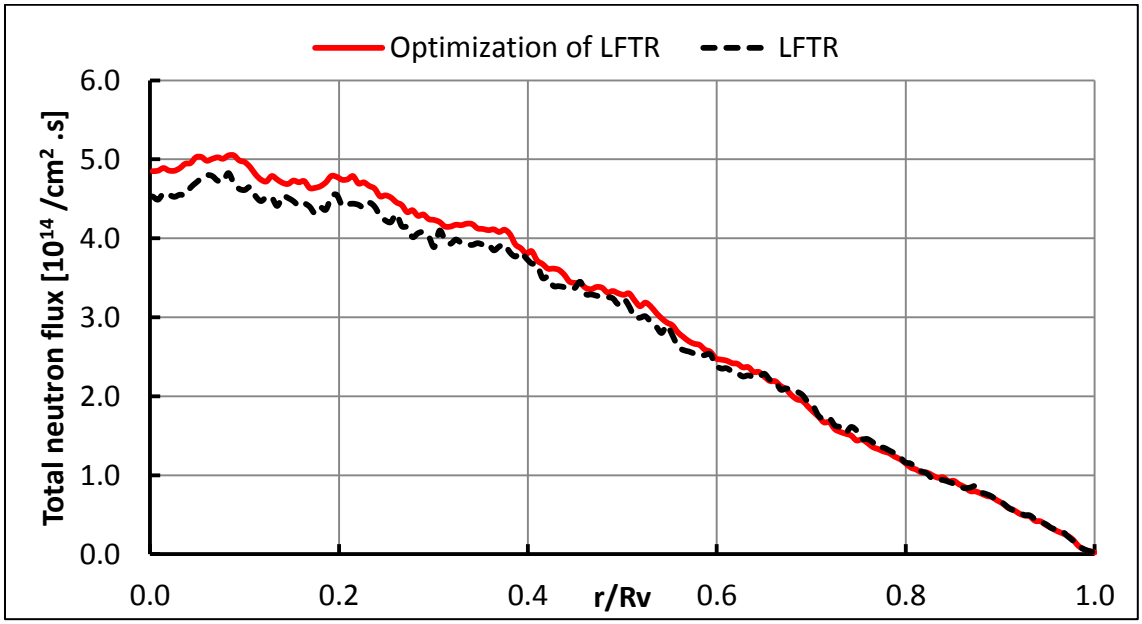

Figure 5.5. The radial total neutron flux of the optimized LFTR vs original LFTR.

5.1. CONCLUSION

An optimization was made on the LFTR core by increasing the radii of the fuel rods at the outer rings of the core while keeping the total mass/volume of the fuel inside the core fixed. After conducting many scenarios, finally, the best configuration of the optimized LFTR core was obtained. The burnup calculations of the optimized LFTR core showed an increase in the cycle length for about 40 days. Decreasing the radii of the fuel rods of the inner core increased the thermal neutron flux values (compared with the original LFTR core). There was no fundamental effect from the fast neutron flux on the change of the total neutron flux of the optimized LFTR core. The burnup calculations were only performed for the first cycle length. The continuous removal of the fission product gases from the fuel salt was performed every 10 days, and no burnup calculations were done for the next cycles of the refueling processes. An improvement for the next cycle lengths of the optimized LFTR core is expected.

SUMMARY AND CONCLUSION

In this dissertation, a complete feasibility studies of a conceptual small thermal commercial liquid fluoride thorium reactor LFTR design, has been demonstrated. The core performance and the burnup analysis were obtained using MCNP6 code. The results were promising and the main outcomes obtained are as follows:

1. The reactor can be operated for five years at a thermal power level of 150 MW_{th} together with a load factor of 100% with an initial inventory of fissile material ^{233}U of 0.154 (ton).
2. The total net feed of ^{233}U-fissile was 0.081 (ton). At the end of reactor operation, 0.172 (ton) was the final remain of fissile material.
3. The average fuel conversion ratio CR was 0.78.
4. The temperature coefficient of reactivity at the beginning of life (t=0) was -2.83×10^{-5} / *T*.
5. The reactor produced 7.63 (g) of Pu for a 5 years of operation. 89.84% of the produced Pu was ^{238}Pu (with a half-life 87.7 years).
6. The production of minor actinide (MA) was 34.5 (g) with mostly ^{237}Np and ^{238}Np, and no Am or Cm were produced during the burnup time.
7. The first cycle length of burnup was increased 40 days by optimized the reactor core.

REFERENCES

[1] R. Hargraves, R. Moir,"Liquid Fluoride Thorium Reactors: An old idea in nuclear power gets reexamined," American Scientist, Vol. 98, p. 304-313 (2010).

[2] Y. Xiao, D. Zhang, Z. Guo, Y. Wu, W. Tain, G. Su, S. Qiu, "Numerical analysis for a molten salt reactor in the presence of localized perturbations," Progress in Nuclear Energy: 60, 61-72 (2012).

[3] Nuclear Science Introduction of Thorium in the Nuclear Fuel Cycle Short- to long-term considerations OECD 2015 NEA No. 7224 NUCLEAR ENERGY AGENCY.

[4] Advanced Reactor Concepts, 2011. The U.S. Department of Energy's Office of Nuclear Energy, 15 February 2012. http://www.ne.anl.gov/activ/pdfs/2012_AdvReactor_Factsheet_Final.pdf

[5] Gen IV, 2009. GIF R&D Outlook for Generation IV Nuclear Energy Systems, 21 August 2009. https://www.gen-4.org/gif/upload/docs/application/pdf/2013-09/gif_rd_outlook_for_generation_iv_nuclear_energy_systems.pdf

[6] Hore-Lacy, I., & Association, W. (2010). Generation IV nuclear reactors. Retrieved January 11, 2010, from http://www.eoearth.org/view/article/152940

[7] W. K. Ergen et al, The Aircraft Reactor Experiment-Physics, Nuclear Science and Engineering 2, 826-840 (1957).

[8] E. S. Bettis et al, The Aircraft Reactor Experiment-Design and Construction, Nuclear Science and Engineering 2, 804-825 (1957).

[9] E.S Bettis et al, The Aircraft Reactor Experiment-Operation, Nuclear Science and Engineering 2, 841-853 (1957).

[10] Molten Salt Reactor Program Quarterly Progress Report for the period ending Jan 31, 1958 (PDF), ORNL-2474, Oak Ridge National Laboratory

[11] M.W. Rosenthal, P.R. Kasten, and R.B. Briggs. Molten-Salt Reactors - History, Status and Potential. Nuclear Applications and Technology, 8(107), 1970.

[12] Weinberg, Alvin (1997). The First Nuclear Era: The Life and Times of a Technological Fixer. Springer.ISBN 978-1-56396-358-2.

[13] Cohen, Linda R.; Noll, Roger G. (1991). The Technology pork barrel. Brookings Institution. p. 234.ISBN 0-8157-1508-0. Retrieved 28 February 2012.

[14] L. Mathieu, D. Heuer, E. Merle-Lucotte, R. Brissot, C. Le Brun, E. Liatard, J.-M. Loiseaux, O. MAplan, A. Nuttin, D. Lecarpentier, "Possible Configurations for the Thorium Molten Salt Reactor and Advantages of the Fast Nonmoderated Version", Nuclear Science and Engineering: 161, 78-89 (2009).

[15] Ingersoll, D.; Forsberg, C.; MacDonald, P. (February 2007). "Trade Studies for the Liquid-Salt-Cooled Very High-Temperature Reactor: Fiscal Year 2006 Progress Report" (PDF). ORNL/TM-2006/140 (Oak Ridge National Laboratory).

[16] Ottewitte, Eric Heinz. 1982. Configuration of a Molten Chloride Fast Reactor on a Thorium Fuel Cycle to Current Fuel Cycle Concerns. Ph.D. diss., University of California Los Angeles.

[17] P. Rubiolo, D. Heuer, E. Merle-Lucotte, M. Brovchenko, V. Ghetta, M. Allibert, A. Laureau, "Overview and Perspectives of the Molten Salt Fast Reactor (MSFR) Concept," CMSNT, Mumbai (2013).

[18] Thorium-Fuelled Molten Salt Reactors, The Weinberg Foundation, June 2013, http://www.theweinberg-foundation.org/wp-content/uploads/2013/06/Thorium-Fuelled-Molten-Salt-ReactorsWeinberg-Foundation.pdf

[19] "IAEA-TECDOC-1450 Thorium Fuel Cycle-Potential Benefits and Challenges" (PDF). International Atomic Energy Agency. May 2005. Retrieved 2009-03-23.

[20] http://www.iaea.org/OurWork/ST/NE/NEFW/Technical_Areas/NFC/advanced-fuel-cycles-crp-thorium-2011.html.

[21] International Atomic Energy Agency, IAEA-TECDOC - 1349, Potential of thorium based fuel cycles to constrain plutonium and reduce long lived waste toxicity.

[22] INST, AERE, Bangladesh 11-13, Feb. 2007, "Introduction of SRAC for Reactor Physics Analyses".

[23] "Advanced Reactors with Innovative Fuels," United Kingdom 22-24 October 2001.

[24] K. Mitachi, T. Yamamoto, R. Yoshioka, "Self-sustaining Core Design for 200 MWe Molten-Salt Reactor with Thorium-Uranium Fuel: FUJI-U3-(0)," TU2007 (International Workshop on Thorium Utilization for Sustainable Development of Nuclear energy), Tsinghua University, Beijing, China (2007).

[25] J. S. Hendricks, et al., MCNPX 2.6.0 Extensions, LANL Report LA-UR-08-2216, Los Alamos, 2008; http://mcnpx.lanl.gov/.

[26] H. Grady Hughes and Michael R. James, "MCNP6 Class." Los Alamos National Laboratory, March 7, 2014.

[27] Denise B. Pelowitz, ed., "MCNPX User's Manual, Version 2.7.0," Los Alamos National Laboratory Report, LA-CP-11-00438 (April 2011).

[28] Laurie S. Waters, editor, MCNPTM User's Manual Version 2.3.0, April 2002, LA-UR-02-2607.

[29] R.C. Robertson, et al., "Conceptual Design Study of a Single-fluid Molten-Salt Breeder Reactor", ORNL-4541, (1970).

[30] K. Okumura, K. Kaneko, K. Tsuchihashi, "The SRAC95: General Neutronic Calculation Code System," JAERI-Data/Code 96-015 (1996).

[31] T. Nakagawa, et al, "Japanese Evaluated Nuclear Data Library Version 3 Revision－2, JENDL-3.2," Journal of Nuclear Science and Technology, vol.32, p1259 (1995).

[32] W. R. Grimes, D. R. Cuneo, F. F. Blankenship, G. W. Keilholtz, H. F. Poppendick, M. T. Robinson, "Chemical aspects of molten-fluoride-salt reactor fuels," Addison-Wesley Pub. Co., 1958.

[33] C. F. Weaver, R. E. Thoma, H. Insley. H. A. Friedman, "phase equilibria in molten salt breeder reactor fuels," ORNL-2896, Des 27 1960.

[34] S. Cantor et al., "Physical properties of molten-salt reactor fuel, coolant, and flush salts," ORNL-TM-2316, Oak Ridge National Laboratory (1968), pp. 28.

[35] S. Cantor, “Reactor Chem. Div. Ann. Progr. Rept,” Dec. 31, 1965, USAEC Report ORNL-3913, pp. 27-29.

APPENDIX

SAMPLE MCNP 5, AND MCNP 6 INPUT FILES

1. MCNP6 code to verification FUJI-U3-(0) model

```
FUJI-U3-(0) model and parameters
c Cell Cards
1  1 -3.33  -71 ((-7 8 -9):-70:-80:90) u=1  imp:n=1 vol=53562.8  $ Liquid fuel channel
2  2 -1.84   71:((7:-8:9) 70 80 -90) u=1 imp:n=1 vol=92125.14   $ Graphite moderator
c 3  1 -3.33  -71 ((-7 8 -9):-70:-80:90)       u=4 imp:n=1            $
c 4  2 -1.84   (71:((7:-8:9) 70 80 -90)) #5  u=4 imp:n=1            $
c 5  6 -2.51  -77 44 -55          u=4 imp:n=1                        $ Control rod B4C
6  1 -3.33  -71 (-70:-80:90)     u=2 imp:n=1    vol=43820.52523  $ Liquid fuel channel
7  2 -1.84   71:(70 -90 80)      u=2 imp:n=1    vol=101867.4643  $ Graphite moderator
8  1 -3.33  -71                  u=3 imp:n=1    vol=65718.15991  $ Liquid fuel channel
9  2 -1.84   71                  u=3 imp:n=1    vol=79969.82967  $ Graphite moderator
10 2 -1.84  -11                  u=9 imp:n=1                        $ Graphite moderator
11 0 -101 81 -91  imp:n=1 fill=5
12 0  -1 -4 -2 -5 -3 -6 u=5 imp:n=1 lat=2 fill=-16:16 -16:16 0:0   $ Lattice
    9 9 9 9 9 9 9 9 9 9 9 9 9 9 9 9 9 9 9 9 9 9 9 9 9 9 9 9 9 9 9 9 9
    9 9 9 9 9 9 9 9 9 9 9 9 9 9 9 9 9 9 9 9 9 9 9 9 9 9 9 9 9 9 9 9 9
    9 9 9 9 9 9 9 9 9 9 9 9 9 9 9 9 9 9 9 9 3 3 3 3 3 9 9 9 9 9 9 9 9
    9 9 9 9 9 9 9 9 9 9 9 9 9 9 9 9 9 9 9 3 3 3 3 3 3 3 3 3 9 9 9 9 9
    9 9 9 9 9 9 9 9 9 9 9 9 9 9 9 9 9 3 3 3 3 3 2 2 2 3 3 3 3 3 9 9 9 9
    9 9 9 9 9 9 9 9 9 9 9 9 9 9 9 3 3 3 3 3 2 2 2 2 2 2 3 3 3 3 3 9 9 9
    9 9 9 9 9 9 9 9 9 9 9 9 9 3 3 3 2 2 2 2 2 2 2 2 2 2 3 3 3 9 9 9 9
    9 9 9 9 9 9 9 9 9 9 9 3 3 3 2 2 2 2 2 2 2 2 2 2 2 2 3 3 3 3 9 9 9
    9 9 9 9 9 9 9 9 9 9 3 3 3 2 2 2 2 2 2 2 2 2 2 2 2 2 3 3 3 9 9 9 9
    9 9 9 9 9 9 9 9 9 3 3 2 2 2 2 2 2 2 1 1 2 2 2 2 2 2 2 2 3 3 9 9 9
    9 9 9 9 9 9 9 9 3 3 2 2 2 2 2 2 2 1 1 1 1 2 2 2 2 2 2 2 2 3 3 9 9 9
    9 9 9 9 9 9 9 3 3 2 2 2 2 2 2 1 1 1 1 1 1 1 2 2 2 2 2 2 3 3 9 9 9 9
    9 9 9 9 9 9 3 3 2 2 2 2 2 1 1 1 1 1 1 1 1 1 1 2 2 2 2 3 3 9 9 9 9 9
    9 9 9 9 9 9 3 3 2 2 2 2 2 1 1 1 1 1 1 1 1 1 1 2 2 2 2 3 3 9 9 9 9 9
    9 9 9 9 9 3 3 3 2 2 2 2 1 1 1 1 1 1 1 1 1 1 1 2 2 2 2 3 3 3 9 9 9 9
    9 9 9 9 9 3 3 2 2 2 2 2 1 1 1 1 1 1 1 1 1 1 1 2 2 2 2 3 3 9 9 9 9 9
    9 9 9 9 3 3 2 2 2 2 2 2 1 1 1 1 1 1 1 1 1 1 1 2 2 2 2 3 3 9 9 9 9 9
    9 9 9 9 3 3 2 2 2 2 2 2 1 1 1 1 1 1 1 1 1 1 1 2 2 2 2 3 3 9 9 9 9 9
    9 9 9 3 3 3 2 2 2 2 2 1 1 1 1 1 1 1 1 1 1 1 1 2 2 2 2 3 3 3 9 9 9 9
    9 9 9 3 3 2 2 2 2 2 2 1 1 1 1 1 1 1 1 1 1 1 1 2 2 2 2 3 3 9 9 9 9 9
    9 9 9 3 3 2 2 2 2 2 2 1 1 1 1 1 1 1 1 1 1 1 1 2 2 2 2 3 3 9 9 9 9 9
    9 9 9 3 3 2 2 2 2 2 2 1 1 1 1 1 1 1 1 1 1 1 1 2 2 2 2 3 3 9 9 9 9 9
    9 9 3 3 2 2 2 2 2 2 2 1 1 1 1 1 1 1 1 1 1 1 1 2 2 2 2 3 3 9 9 9 9 9
    9 9 3 3 2 2 2 2 2 2 2 1 1 1 1 1 2 2 2 2 2 2 2 3 3 9 9 9 9 9 9 9 9
    9 9 3 3 2 2 2 2 2 2 2 1 1 2 2 2 2 2 2 2 2 2 3 3 9 9 9 9 9 9 9 9 9
```

```
    9 9 3 3 3 2 2 2 2 2 2 2 2 2 2 2 2 2 2 2 3 3 3 9 9 9 9 9 9 9 9 9 9
    9 9 3 3 3 3 2 2 2 2 2 2 2 2 2 2 2 2 3 3 3 3 9 9 9 9 9 9 9 9 9 9 9
    9 9 9 3 3 3 2 2 2 2 2 2 2 2 2 2 2 3 3 3 9 9 9 9 9 9 9 9 9 9 9 9 9
    9 9 9 3 3 3 3 3 2 2 2 2 2 2 3 3 3 3 3 9 9 9 9 9 9 9 9 9 9 9 9 9 9
    9 9 9 9 3 3 3 3 3 2 2 2 3 3 3 3 3 9 9 9 9 9 9 9 9 9 9 9 9 9 9 9 9
    9 9 9 9 9 3 3 3 3 3 3 3 3 3 3 9 9 9 9 9 9 9 9 9 9 9 9 9 9 9 9 9 9
    9 9 9 9 9 9 9 3 3 3 3 3 9 9 9 9 9 9 9 9 9 9 9 9 9 9 9 9 9 9 9 9 9
    9 9 9 9 9 9 9 9 9 9 9 9 9 9 9 9 9 9 9 9 9 9 9 9 9 9 9 9 9 9 9 9 9
    9 9 9 9 9 9 9 9 9 9 9 9 9 9 9 9 9 9 9 9 9 9 9 9 9 9 9 9 9 9 9 9 9
13  1 -3.33  -111 101 -91 81      imp:n=1     vol=2630088.157   $ cyl fuel path
14  1 -3.33  -111 91 -92          imp:n=1     vol=682013.985    $ Top fuel path
15  1 -3.33  -111 82 -81          imp:n=1     vol=682013.985    $ Bottom fuel path
16  2 -1.84  (111:92:-82) -112 83 -93   imp:n=1                 $ Reflector
17  3 -8.671 (112:93:-83) -113 84 -94   imp:n=1                 $ Hastelloy vessel
18  0  113:-84:94                       imp:n=0                 $ Outside world

c Surface Cards
1        px   9.5        $ 1st side of hexagonal prism
2   12   px   9.5        $ 2nd side of hexagonal prism
3   13   px   9.5        $ 3rd side of hexagonal prism
4   14   px   9.5        $ 4th side of hexagonal prism
5   15   px   9.5        $ 5th side of hexagonal prism
6   16   px   9.5        $ 6th side of hexagonal prism
7        cz   6.28       $ Cylinder in hexagonal prism core-1
70       cz   5.18       $ Cylinder in hexagonal prism core-2
71       cz   6.7        $ Cylinder in hexagonal prism core-3
8        pz  -123        $ Bottom of core-1
80       pz  -193        $ Bottom of core-2
81       pz  -233        $ Bottom of core-3
82       pz  -236.776    $ Bottom of the fuel path
83       pz  -267.0      $ Bottom of the reflector
84       pz  -272.0      $ Bottom of Hastelloy-N
9        pz   123        $ Top of core-1
90       pz   193        $ Top of core-2
91       pz   233        $ Top of core-3
92       pz   236.776    $ Top of the fuel path
93       pz   267.0      $ Top of the reflector
94       pz   272.0      $ Top of Hastelloy-N
c 10     cz   116        $ Vessel
c 100    cz   196        $ Vessel
101      cz   236        $ Vessel
111      cz   239.776    $ Fuel path
112      cz   270.0      $ Reflector
113      cz   275.0      $ Hastelloy-N
11       cz   50         $ Graphite place-holder
c 77       c/z  8 0 1
```

```
c 44      pz   92
c 55      pz   233

c Data Cards
  c Materials
burn   time=40,60,100 18r mat=1 power=337.5 pfrac=1.0,1.0,1.0 18r bopt=1.0 -14 -1
         omit=1 7 7016 8018 8019 9018 10021 10022 91230
         matvol=33595706.4
m1   92233.72c -0.008760933     $ LiF-BeF2-ThF4-UF4 fuel salt
       90232.72c -0.436163945    $ 71.76-16-12-0.24 Mol% initial composition
       3007.72c   -0.078010184   $ Enriched in Li-7
       4009.72c   -0.022586585
       9019.72c   -0.454478352
m2   6000.72c -1                $ Graphite
mt2   grph.16t
c m3   28000.72c -0.739           $ 73.9% Nickel
c     42000.72c -0.12             $ 12.0% Molybdenum
c     24000.72c -0.07             $ 7.0%  Cr
c     26000.72c -0.05             $ 5.0%  Fe
c     41093.72c -0.02             $ 2.0%  Nb
c     14000.72c -0.001            $ 0.1%  Si
m3   28058.72c -0.50308903  28060.72c -0.19378797      $ Nickel
       28061.72c -0.00842460  28062.72c -0.02685526      $ Nickel
       28064.72c -0.00684314                            $ 73.9% Nickel
       42092.72c -0.01780800  42094.72c -0.01110000      $ Molybdenum
       42095.72c -0.01910400  42096.72c -0.02001600      $ Molybdenum
       42097.72c -0.01146000  42098.72c -0.02895600      $ Molybdenum
       42100.72c -0.01155600                            $ 12.0% Molybdenum
       26054.72c -0.00292250  26056.72c -0.04587700      $ Fe
       26057.72c -0.00105950  26058.72c -0.000141        $ 5.0%  Fe
       24050.72c -0.0030415    24052.72c -0.0586523      $ Cr
       24053.72c -0.0066507   24054.72c -0.0016555       $ 7.0%  Cr
       41093.72c -0.02                                  $ 2.0%  Nb
       14028.72c -0.0009223   14029.72c -0.0000467       $ Si
       14030.72c -0.000031                              $ 0.1%  Si
c m6   5010.72c -0.6 5011.72c -0.2 6000.72c -0.2        $ B4C control rod
*TR12  0 0 0    60  30 90   150  60 90   90 90 0    1
*TR13  0 0 0   120  30 90   150 120 90   90 90 0   1
*TR14  0 0 0   180  90 90   90 180 90   90 90 0    1
*TR15  0 0 0   120 150 90  30 120 90   90 90 0    1
*TR16  0 0 0    60 150 90   30  60 90   90 90 0    1
kcode 10000 1.0 30 130
ksrc  0 0 0
F4:n 1 2 6 7 8 9                    $ Energy profile at cell 1,2,6,7,8,9
c SD4
E0 1.00000e-9 1.05925e-9 1.12202e-9 1.18850e-9 1.25893e-9 &
```

1.33352e-9 1.41254e-9 1.49624e-9 1.58489e-9 1.67880e-9 &
1.77828e-9 1.88365e-9 1.99526e-9 2.11349e-9 2.23872e-9 &
2.37137e-9 2.51189e-9 2.66073e-9 2.81838e-9 2.98538e-9 &
3.16228e-9 3.34965e-9 3.54813e-9 3.75837e-9 3.98107e-9 &
4.21697e-9 4.46684e-9 4.73151e-9 5.01187e-9 5.30884e-9 &
5.62341e-9 5.95662e-9 6.30957e-9 6.68344e-9 7.07946e-9 &
7.49894e-9 7.94328e-9 8.41395e-9 8.91251e-9 9.44061e-9 &
1.00000e-8 1.05925e-8 1.12202e-8 1.18850e-8 1.25893e-8 &
1.33352e-8 1.41254e-8 1.49624e-8 1.58489e-8 1.67880e-8 &
1.77828e-8 1.88365e-8 1.99526e-8 2.11349e-8 2.23872e-8 &
2.37137e-8 2.51189e-8 2.66073e-8 2.81838e-8 2.98538e-8 &
3.16228e-8 3.34965e-8 3.54813e-8 3.75837e-8 3.98107e-8 &
4.21697e-8 4.46684e-8 4.73151e-8 5.01187e-8 5.30884e-8 &
5.62341e-8 5.95662e-8 6.30957e-8 6.68344e-8 7.07946e-8 &
7.49894e-8 7.94328e-8 8.41395e-8 8.91251e-8 9.44061e-8 &
1.00000e-7 1.05925e-7 1.12202e-7 1.18850e-7 1.25893e-7 &
1.33352e-7 1.41254e-7 1.49624e-7 1.58489e-7 1.67880e-7 &
1.77828e-7 1.88365e-7 1.99526e-7 2.11349e-7 2.23872e-7 &
2.37137e-7 2.51189e-7 2.66073e-7 2.81838e-7 2.98538e-7 &
3.16228e-7 3.34965e-7 3.54813e-7 3.75837e-7 3.98107e-7 &
4.21697e-7 4.46684e-7 4.73151e-7 5.01187e-7 5.30884e-7 &
5.62341e-7 5.95662e-7 6.30957e-7 6.68344e-7 7.07946e-7 &
7.49894e-7 7.94328e-7 8.41395e-7 8.91251e-7 9.44061e-7 &
1.00000e-6 1.05925e-6 1.12202e-6 1.18850e-6 1.25893e-6 &
1.33352e-6 1.41254e-6 1.49624e-6 1.58489e-6 1.67880e-6 &
1.77828e-6 1.88365e-6 1.99526e-6 2.11349e-6 2.23872e-6 &
2.37137e-6 2.51189e-6 2.66073e-6 2.81838e-6 2.98538e-6 &
3.16228e-6 3.34965e-6 3.54813e-6 3.75837e-6 3.98107e-6 &
4.21697e-6 4.46684e-6 4.73151e-6 5.01187e-6 5.30884e-6 &
5.62341e-6 5.95662e-6 6.30957e-6 6.68344e-6 7.07946e-6 &
7.49894e-6 7.94328e-6 8.41395e-6 8.91251e-6 9.44061e-6 &
1.00000e-5 1.05925e-5 1.12202e-5 1.18850e-5 1.25893e-5 &
1.33352e-5 1.41254e-5 1.49624e-5 1.58489e-5 1.67880e-5 &
1.77828e-5 1.88365e-5 1.99526e-5 2.11349e-5 2.23872e-5 &
2.37137e-5 2.51189e-5 2.66073e-5 2.81838e-5 2.98538e-5 &
3.16228e-5 3.34965e-5 3.54813e-5 3.75837e-5 3.98107e-5 &
4.21697e-5 4.46684e-5 4.73151e-5 5.01187e-5 5.30884e-5 &
5.62341e-5 5.95662e-5 6.30957e-5 6.68344e-5 7.07946e-5 &
7.49894e-5 7.94328e-5 8.41395e-5 8.91251e-5 9.44061e-5 &
1.00000e-4 1.05925e-4 1.12202e-4 1.18850e-4 1.25893e-4 &
1.33352e-4 1.41254e-4 1.49624e-4 1.58489e-4 1.67880e-4 &
1.77828e-4 1.88365e-4 1.99526e-4 2.11349e-4 2.23872e-4 &
2.37137e-4 2.51189e-4 2.66073e-4 2.81838e-4 2.98538e-4 &
3.16228e-4 3.34965e-4 3.54813e-4 3.75837e-4 3.98107e-4 &
4.21697e-4 4.46684e-4 4.73151e-4 5.01187e-4 5.30884e-4 &
5.62341e-4 5.95662e-4 6.30957e-4 6.68344e-4 7.07946e-4 &

```
   7.49894e-4 7.94328e-4 8.41395e-4 8.91251e-4 9.44061e-4 &
   1.00000e-3 1.05925e-3 1.12202e-3 1.18850e-3 1.25893e-3 &
   1.33352e-3 1.41254e-3 1.49624e-3 1.58489e-3 1.67880e-3 &
   1.77828e-3 1.88365e-3 1.99526e-3 2.11349e-3 2.23872e-3 &
   2.37137e-3 2.51189e-3 2.66073e-3 2.81838e-3 2.98538e-3 &
   3.16228e-3 3.34965e-3 3.54813e-3 3.75837e-3 3.98107e-3 &
   4.21697e-3 4.46684e-3 4.73151e-3 5.01187e-3 5.30884e-3 &
   5.62341e-3 5.95662e-3 6.30957e-3 6.68344e-3 7.07946e-3 &
   7.49894e-3 7.94328e-3 8.41395e-3 8.91251e-3 9.44061e-3 &
   1.00000e-2 1.05925e-2 1.12202e-2 1.18850e-2 1.25893e-2 &
   1.33352e-2 1.41254e-2 1.49624e-2 1.58489e-2 1.67880e-2 &
   1.77828e-2 1.88365e-2 1.99526e-2 2.11349e-2 2.23872e-2 &
   2.37137e-2 2.51189e-2 2.66073e-2 2.81838e-2 2.98538e-2 &
   3.16228e-2 3.34965e-2 3.54813e-2 3.75837e-2 3.98107e-2 &
   4.21697e-2 4.46684e-2 4.73151e-2 5.01187e-2 5.30884e-2 &
   5.62341e-2 5.95662e-2 6.30957e-2 6.68344e-2 7.07946e-2 &
   7.49894e-2 7.94328e-2 8.41395e-2 8.91251e-2 9.44061e-2 &
   1.00000e-1 1.05925e-1 1.12202e-1 1.18850e-1 1.25893e-1 &
   1.33352e-1 1.41254e-1 1.49624e-1 1.58489e-1 1.67880e-1 &
   1.77828e-1 1.88365e-1 1.99526e-1 2.11349e-1 2.23872e-1 &
   2.37137e-1 2.51189e-1 2.66073e-1 2.81838e-1 2.98538e-1 &
   3.16228e-1 3.34965e-1 3.54813e-1 3.75837e-1 3.98107e-1 &
   4.21697e-1 4.46684e-1 4.73151e-1 5.01187e-1 5.30884e-1 &
   5.62341e-1 5.95662e-1 6.30957e-1 6.68344e-1 7.07946e-1 &
   7.49894e-1 7.94328e-1 8.41395e-1 8.91251e-1 9.44061e-1 &
   1.00000e+0 1.05925e+0 1.12202e+0 1.18850e+0 1.25893e+0 &
   1.33352e+0 1.41254e+0 1.49624e+0 1.58489e+0 1.67880e+0 &
   1.77828e+0 1.88365e+0 1.99526e+0 2.11349e+0 2.23872e+0 &
   2.37137e+0 2.51189e+0 2.66073e+0 2.81838e+0 2.98538e+0 &
   3.16228e+0 3.34965e+0 3.54813e+0 3.75837e+0 3.98107e+0 &
   4.21697e+0 4.46684e+0 4.73151e+0 5.01187e+0 5.30884e+0 &
   5.62341e+0 5.95662e+0 6.30957e+0 6.68344e+0 7.07946e+0 &
   7.49894e+0 7.94328e+0 8.41395e+0 8.91251e+0 9.44061e+0 &
   1.00000e+1 1.05925e+1 1.12202e+1 1.18850e+1 1.25893e+1 &
   1.33352e+1 1.41254e+1 1.49624e+1 1.58489e+1 1.67880e+1 &
   1.77828e+1 1.88365e+1 2.00000e+1
```

2. A FORTRAN program to initiate MCNP code to calculate k-inf

```
program k-inf
   implicit none
   character(70) :: fn
   integer, parameter :: outunit=44
   integer :: filenum,numfiles
   real*8, parameter::Li=7.0160040d0          ! Molar Mass (g/mol) of lithium-7
```

```
   real*8, parameter::F=18.9984032d0          ! Molar Mass (g/mol) of fluorine
   real*8, parameter::Be=9.0121821d0          ! Molar Mass (g/mol) of beryllium
   real*8, parameter::Th=232.0380504d0        ! Molar Mass (g/mol) of Th-232
   real*8, parameter::U=233.0396282d0         ! Molar Mass (g/mol) of U-233
   real*8 :: N_LiF,N_BeF2,N_ThF4,N_UF4   ! Mole fraction of LiF,BeF2,ThF4,UF4
   real*8 :: N1,N2,N3,N4                      ! Mole fraction of LiF,BeF2,ThF4,UF4
   real*8 :: V1_LiF,V1_BeF2,V1_ThF4,V1_UF4   ! Molar volume (cm3) of
!LiF,BeF2,ThF4,UF4 at T=600C respectively
!(S. Cantor et al., Physical properties of molten-salt reactor fuel, coolant, and flush
!salts,ORNL-TM-2316 , Oak Ridge National Laboratory (1968). page-28 )
   real*8 :: V2_LiF,V2_BeF2,V2_ThF4,V2_UF4   ! Molar volume (cm3) of
!LiF,BeF2,ThF4,UF4 at T=800C respectively
   real*8 :: M_LiF,M_BeF2,M_ThF4,M_UF4        ! Molar Mass (g/mol) of
!LiF,BeF2,ThF4,UF4
   real*8 :: M_Li,M_Be,M_Th,M_U         !,M_F  ! Molar Mass (g/mol) of !Li,Be,Th,U,F
   real*8 :: ma_LiF,ma_BeF2,ma_ThF4,ma_UF4  ! Molecular mass (g) of
!LiF,BeF2,ThF4,UF4
   real*8 :: ma_Li,ma_Be,ma_Th,ma_U,ma_F     ! Element mass (g) of Li,Be,Th,U,F
   real*8 :: w_Li,w_Be,w_Th,w_U,w_F           ! Weight fraction of Li,Be,Th,U,F
!respectively
   real*4 :: r,p,T,rho,temp

   V1_LiF=13.411d0
   V1_BeF2=23.6d0
   V1_ThF4=46.43d0
   V1_UF4=46.43d0

   V2_LiF=14.142d0
   V2_BeF2=24.4d0
   V2_ThF4=47.59d0
   V2_UF4=47.59d0

   M_Li=Li
   M_Be=Be
   M_Th=Th
   M_U=U
   !M_F=11*F

   M_LiF=Li+F
   M_BeF2=Be+2*F
   M_ThF4=Th+4*F
   M_UF4=U+4*F

   r=0.5d0              ! Radius of fuel channel
   p=13.0d0             ! Half of the pitch
```

```
   numfiles=(int(p)-1)*2+1   ! # of files created based on the ((integer)) value of p
!(where p !could be real #)

    print*,'Please insert the values of mole fraction of the salt composition in mol%'
    print*,""
    print*,'1- insert the mole fraction of LiF'
    read*,N_LiF
    print*,""
    print*,'2- insert the mole fraction of BeF2'
    read*,N_BeF2
    print*,""
    print*,'3- insert the mole fraction of ThF4'
    read*,N_ThF4
    print*,""
    print*,'4- insert the mole fraction of UF4'
    read*,N_UF4
    print*,""
    print*,'5- insert the temperature in Kelvin (K)'
    read*,temp

    N1=100*N_LiF
    N2=100*N_BeF2
    N3=100*N_ThF4
    N4=100*N_UF4

     T=temp-273.15              ! Temperature in Celsius (ºC)

    call density(N_LiF,N_BeF2,N_ThF4,N_UF4,&
                 V1_LiF,V1_BeF2,V1_ThF4,V1_UF4,&
                 V2_LiF,V2_BeF2,V2_ThF4,V2_UF4,&
                 M_LiF,M_BeF2,M_ThF4,M_UF4,T,rho,&
                 ma_LiF,ma_BeF2,ma_ThF4,ma_UF4,&
                 ma_Li,ma_Be,ma_Th,ma_U,ma_F,&
                 w_Li,w_Be,w_Th,w_U,w_F,&
                 M_Li,M_Be,M_Th,M_U)
    !print*,rho

    open(unit=20,file="k-inf.bat")

    do filenum=1,numfiles

      write(fn,fmt='(i0,a)') filenum, '.txt'          ! Build filename -- i.txt
      open(unit=outunit,file=fn, form='formatted')    ! Open it with a fixed unit number

   write (outunit,10)"LFTR unit cell model for infinite lattice"
   write (outunit,10)"c Cell Cards"
```

```
write (outunit,11)"10  1",-rho,"-7 8 -9                  imp:n=1  $ Liquid fuel channel"
write (outunit,10)"20  2 -1.84  -1 -2 -3 -4 -5 -6 7 8 -9  imp:n=1 $ Gr moderator"
write (outunit,10)"30  0        1:2:3:4:5:6:-8:9        imp:n=0  $ Outside world"
write (outunit,10)"
write (outunit,10)"c Surface Cards"
write (outunit,12)"*1        px",p," $ 1st side of hexagonal prism"
write (outunit,12)"*2   12  px",p,"  $ 2nd side of hexagonal prism"
write (outunit,12)"*3   13  px",p,"  $ 3rd side of hexagonal prism"
write (outunit,12)"*4   14  px",p,"  $ 4th side of hexagonal prism"
write (outunit,12)"*5   15  px",p,"  $ 5th side of hexagonal prism"
write (outunit,12)"*6   16  px",p,"  $ 6th side of hexagonal prism"
write (outunit,12)" 7         cz",r,"   $ Cylinder in hexagonal prism"
write (outunit,10)"*8         pz -130 $ Bottom of hexagonal prism"
write (outunit,10)"*9         pz  130 $ Top of hexagonal prism"
write (outunit,10)"
write (outunit,10)"c Data Cards"
write (outunit,10)"  c Materials"
write (outunit,14)"m1   92233.72c",-w_U, "  $ LiF-BeF2-ThF4-UF4 fuel salt"
write (outunit,17)" 90232.72c",-w_Th,"  $",N1,'-',N2,'-',N3,'-',N4,"Mol% Int. comp"
write (outunit,14)" 3007.72c",-w_Li,"     $ enriched in Li-7"
write (outunit,14)" 4009.72c",-w_Be,"    $ Be"
write (outunit,14)" 9019.72c",-w_F, "     $ F"
write (outunit,10)"m2    6000.72c -1       $ graphite"
write (outunit,10)"mt2   grph.16t"
write (outunit,10)"*TR12  0 0 0   60  30 90     150  60 90   90 90 0   1"
write (outunit,10)"*TR13  0 0 0   120  30 90   150 120 90  90 90 0   1"
write (outunit,10)"*TR14  0 0 0   180  90 90   90 180 90    90 90 0   1"
write (outunit,10)"*TR15  0 0 0   120 150 90  30 120 90    90 90 0   1"
write (outunit,10)"*TR16  0 0 0    60 150 90   30  60 90     90 90 0   1"
write (outunit,10)"kcode 5000 1.0 30 130"
write (outunit,10)"ksrc  0 0 0"

   write(20,13)'mcnp5  i=',filenum,'.txt','o=',filenum,'tasks 8'

   close(outunit)
  r=r+0.5d0
   end do

   close(20)

   10 format (a)
   11 format (a,1x,f6.3,1x,a)
   12 format (a,1x,f4.1,1x,a)
   13 format (a,i2,a,3x,a,i2,3x,a)
   14 format (a,1x,f12.10,1x,a)
   17 format (a,1x,f12.10,1x,a,1x,f5.2,1x,a,1x,f5.2,1x,a,1x,f5.2,1x,a,1x,f5.2,1x,a)
```

```
end program k_inf
      subroutine density(N1,N2,N3,N4,V11,V12,V13,V14,&
                  V21,V22,V23,V24,M1,M2,M3,M4,Tt,rhoo,&
                  ma11,ma22,ma33,ma44,&
                  ma1,ma2,ma3,ma4,ma5,&
                  w1,w2,w3,w4,w5,&
                  m11,m22,m33,m44)

   real*8 :: N1,N2,N3,N4          ! Mole fraction of LiF,BeF2,ThF4,UF4 RESP.
   real*8 :: V11,V12,V13,V14      ! Molar volume(cm3) of the comp. at T=600ºC
   real*8 :: V21,V22,V23,V24      ! Molar volume(cm3) of the comp. at T=800ºC
   real*8 :: M1,M2,M3,M4          ! Molar Mass (g/mol) of LiF,BeF2,ThF4,UF4 RESP.
   real*8 :: m11,m22,m33,m44      ! Molar Mass (g/mol) of Li,Be,Th,U,F respectively
   real*8 :: ma11,ma22,ma33,ma44  ! Molecular mass (g) of LiF,BeF2,ThF4,UF4
   real*8 :: ma1,ma2,ma3,ma4,ma5  ! Element mass (g) of Li,Be,Th,U,F respectively
   real*8 :: w1,w2,w3,w4,w5       ! Weight fraction of Li,Be,Th,U,F respectively
   real*8 :: rho1,rho2,a,b        ! rho1, rho2 are the densities of salt composition !at
600ºC, 800ºC resp !!! a & b are constants.
   real*8 :: sum1,sum2            ! sum1 is sum of molecular mass, sum2 is sum of !element
mass
   real*4 :: Tt,rhoo              ! rhoo is the density at the T=626.85ºC (900K)

   rho1=(N1*M1+N2*M2+N3*M3+N4*M4)/(N1*V11+N2*V12+N3*V13+N4*V14)

   rho2=(N1*M1+N2*M2+N3*M3+N4*M4)/(N1*V21+N2*V22+N3*V23+N4*V24)

   b=(rho1-rho2)/200              ! 200 is the difference between T1=600ºC & T2=800ºC
   a=rho1+b*600                   ! or a=rho2+b*800

   rhoo=a-b*Tt

   !ccccccccccccccccccccccccccccccccc

   ma11=M1*N1/100      ! Molecular_mass(g)=(Molar_Mass * Mole_fraction)/100
   ma22=M2*N2/100
   ma33=M3*N3/100
   ma44=M4*N4/100

   sum1=ma11+ma22+ma33+ma44
   !ccccccccccccccccccccccccccccccccc
   ma1=m11*ma11/M1            ! Element_mass(g)=(Molar_Mass(element)*
!Molecular_mass)/Molar_Mass(molecular)
   ma2=m22*ma22/M2
   ma3=m33*ma33/M3
   ma4=m44*ma44/M4
   ma5=sum1-(ma1+ma2+ma3+ma4)              ! This is the mass of F
```

```
   sum2=ma1+ma2+ma3+ma4+ma5

   !ccccccccccccccccccccccccccccccc

   w1=ma1/sum2
   w2=ma2/sum2
   w3=ma3/sum2
   w4=ma4/sum2
   w5=ma5/sum2

   !print*,w1,w2,w3,w4,w5,Tt
   print*,N1+N2+N3+N4,w1+w2+w3+w4+w5


   return
   end subroutine density
```

3. Sample MCNP code to calculate k-inf

```
LFTR unit cell model for infinite lattice
c Cell Cards
10  1 -3.330 -7 8 -9                    imp:n=1  $ liquid fuel channel
20  2 -1.84  -1 -2 -3 -4 -5 -6 7 8 -9   imp:n=1  $ graphite moderator
30  0        1:2:3:4:5:6:-8:9           imp:n=0  $ outside world

c Surface Cards
*1        px 14.0  $ 1st side of hexagonal prism
*2   12   px 14.0  $ 2nd side of hexagonal prism
*3   13   px 14.0  $ 3rd side of hexagonal prism
*4   14   px 14.0  $ 4th side of hexagonal prism
*5   15   px 14.0  $ 5th side of hexagonal prism
*6   16   px 14.0  $ 6th side of hexagonal prism
 7        cz   6.0   $ Cylinder in hexagonal prism
*8        pz -150   $ Bottom of hexagonal prism
*9        pz  150   $ Top of hexagonal prism

c Data Cards
  c Materials
m1   92233.72c -.0087533667    $ LiF-BeF2-ThF4-UF4 fuel salt
     90232.72c -.4357872877    $ 71.76 - 16.00 - 12.00 - 0.24 Mol% initial composition
     3007.72c   -.0787963973   $ enriched in Li-7
     4009.72c   -.0225675308   $ Be
     9019.72c   -.4540954175   $ F
m2    6000.72c -1              $ graphite
mt2   grph.16t
```

```
*TR12  0 0 0    60  30 90     150  60 90   90 90 0   1
*TR13  0 0 0   120  30 90    150 120 90   90 90 0   1
*TR14  0 0 0   180  90 90     90 180 90   90 90 0   1
*TR15  0 0 0   120 150 90    30 120 90   90 90 0   1
*TR16  0 0 0    60 150 90     30  60 90    90 90 0   1
kcode 5000 1.0 30 130
ksrc  0 0 0
```

4. Liquid Fluorite Thorium Reactor LFTR design

LFTR model and parameters

```
1  1 -3.33  -7          u=1      imp:n=1    vol=29405.30724 $ liquid fuel channel
2  2 -1.84   7          u=1      imp:n=1    vol=122807.3177 $ graphite moderator
3  2 -1.84 -11          u=9      imp:n=1    vol=152212.6250 $ graphite moderator
4  0 -10 8 -9 imp:n=1 fill=5
5  0 -1 -4 -2 -5 -3 -6 u=5 imp:n=1 lat=2 fill=-7:7 -7:7 0:0   $ lattice
    9 9 9 9 9 9 9 9 9 9 9 9 9 9
     9 9 9 9 9 9 9 9 9 9 9 9 9 9
      9 9 9 9 9 9 9 1 1 1 1 1 9 9
       9 9 9 9 9 9 1 1 1 1 1 1 9 9
        9 9 9 9 9 1 1 1 1 1 1 1 9 9
         9 9 9 9 1 1 1 1 1 1 1 1 9 9
          9 9 9 1 1 1 1 1 1 1 1 1 9 9
           9 9 1 1 1 1 1 1 1 1 1 1 9 9
            9 9 1 1 1 1 1 1 1 1 1 9 9 9
             9 9 1 1 1 1 1 1 1 1 1 9 9 9 9
              9 9 1 1 1 1 1 1 1 1 9 9 9 9 9
               9 9 1 1 1 1 1 1 1 9 9 9 9 9 9
                9 9 1 1 1 1 1 1 1 9 9 9 9 9 9 9
                 9 9 9 9 9 9 9 9 9 9 9 9 9 9 9
                  9 9 9 9 9 9 9 9 9 9 9 9 9 9 9
6   1 -3.33  -100 10 -9 8          imp:n=1    vol=1640979.507  $ cyl fuel path
7   1 -3.33  -100 9 -91            imp:n=1    vol=475206.7296  $ top fuel path
8   1 -3.33  -100 81 -8            imp:n=1    vol=475206.7296  $ bottom fuel path
9   2 -1.84  (100:91:-81) -111 82 -92   imp:n=1     vol=10452499.73  $ reflector
10  3 -8.671 (111:92:-82) -112 83 -93 imp:n=1                  $ Hastelloy vessel (N)
11  0  112:-83:93                  imp:n=0                     $ outside world
```

c Surface Cards

```
1        px   13       $ 1st side of hexagonal prism
2   22   px   13       $ 2nd side of hexagonal prism
3   33   px   13       $ 3rd side of hexagonal prism
4   44   px   13       $ 4th side of hexagonal prism
5   55   px   13       $ 5th side of hexagonal prism
6   66   px   13       $ 6th side of hexagonal prism
```

```
7       cz    6       $ Cylinder in hexagonal prism
8       pz  -130      $ Bottom of hexagonal prism
81      pz  -137      $ Bottom of fuel path
82      pz  -160      $ Bottom of reflector
83      pz  -165      $ Bottom of Hastelloy-N
9       pz   130      $ Top of hexagonal prism
91      pz   137      $ Top of fuel path
92      pz   160      $ Top of reflector
93      pz   165      $ Top of Hastelloy-N
10      cz   140      $ Core radius
100     cz   147      $ fuel
111     cz   170      $ reflector:inner reactor vessel
112     cz   175      $ Hastelloy-N
11      cz   50       $ graphite place-holder

c Data Cards
  c Materials
burn time=10 19r mat=1 power=150.0 pfrac=1.0 19r bopt=1.0 -14 -1
    omit=1 7 7016 8018 8019 9018 10021 10022 91230
    matvol=5267275.924
m1   92233.72c -.0087533667    $ LiF-BeF2-ThF4-UF4 fuel salt
       90232.72c -.4357872877    $ 71.76 - 16.00 - 12.00 - 0.24 Mol% initial comp.
       3007.72c   -.0787963973    $ enriched in Li-7
       4009.72c   -.0225675308    $ Be
       9019.72c   -.4540954175    $ F
m2    6000.72c -1                 $ graphite
mt2   grph.16t
m3   28058.72c -0.50308903  28060.72c -0.19378797      $      Nickel
       28061.72c -0.00842460  28062.72c -0.02685526      $      Nickel
       28064.72c -0.00684314                             $ 73.9% Nickel
       42092.72c -0.01780800  42094.72c -0.01110000      $      Molybdenum
       42095.72c -0.01910400  42096.72c -0.02001600      $      Molybdenum
       42097.72c -0.01146000  42098.72c -0.02895600      $      Molybdenum
       42100.72c -0.01155600                             $ 12.0% Molybdenum
       26054.72c -0.00292250  26056.72c -0.04587700      $      Fe
       26057.72c -0.00105950  26058.72c -0.000141        $ 5.0%  Fe
       24050.72c -0.0030415   24052.72c -0.0586523       $      Cr
       24053.72c -0.0066507   24054.72c -0.0016555       $ 7.0%  Cr
       41093.72c -0.02                                   $ 2.0%  Nb
       14028.72c -0.0009223   14029.72c -0.0000467       $      Si
       14030.72c -0.000031                               $ 0.1%  Si
*TR22  0 0 0   60  30 90    150  60 90    90 90 0   1
*TR33  0 0 0   120  30 90   150 120 90   90 90 0   1
*TR44  0 0 0   180  90 90   90 180 90    90 90 0   1
*TR55  0 0 0   120 150 90  30 120 90     90 90 0   1
*TR66  0 0 0   60 150 90    30  60 90     90 90 0   1
```

```
kcode 5000 1.0 30 130
ksrc  0 0 0
```

5. Continuous removal of FP gases for the first cycle without refueling

```
c Data Cards
  c Materials
burn time=10 39r mat=1 power=150.0 pfrac=1.0 39r bopt=1.0 -14 -1
    omit=1 7 7016 8018 8019 9018 10021 10022 91230
    matvol=5267275.924
    MATMOD=40 1  1 -1 13 2004 0.0
              1003 0.0 10020 0.0 36082 0.0 36083 0.0 36084 0.0 36086 0.0
             54130 0.0 54131 0.0 54132 0.0 54134 0.0 54135 0.0 54136 0.0
                       2  1 -1 13 2004 0.0
              1003 0.0 10020 0.0 36082 0.0 36083 0.0 36084 0.0 36086 0.0
             54130 0.0 54131 0.0 54132 0.0 54134 0.0 54135 0.0 54136 0.0
                       3  1 -1 13 2004 0.0
              1003 0.0 10020 0.0 36082 0.0 36083 0.0 36084 0.0 36086 0.0
             54130 0.0 54131 0.0 54132 0.0 54134 0.0 54135 0.0 54136 0.0
                       4  1 -1 13 2004 0.0
              1003 0.0 10020 0.0 36082 0.0 36083 0.0 36084 0.0 36086 0.0
             54130 0.0 54131 0.0 54132 0.0 54134 0.0 54135 0.0 54136 0.0
                       5  1 -1 13 2004 0.0
              1003 0.0 10020 0.0 36082 0.0 36083 0.0 36084 0.0 36086 0.0
             54130 0.0 54131 0.0 54132 0.0 54134 0.0 54135 0.0 54136 0.0
                       6  1 -1 13 2004 0.0
              1003 0.0 10020 0.0 36082 0.0 36083 0.0 36084 0.0 36086 0.0
             54130 0.0 54131 0.0 54132 0.0 54134 0.0 54135 0.0 54136 0.0
                       7  1 -1 13 2004 0.0
              1003 0.0 10020 0.0 36082 0.0 36083 0.0 36084 0.0 36086 0.0
             54130 0.0 54131 0.0 54132 0.0 54134 0.0 54135 0.0 54136 0.0
                       8  1 -1 13 2004 0.0
              1003 0.0 10020 0.0 36082 0.0 36083 0.0 36084 0.0 36086 0.0
             54130 0.0 54131 0.0 54132 0.0 54134 0.0 54135 0.0 54136 0.0
                       9  1 -1 13 2004 0.0
              1003 0.0 10020 0.0 36082 0.0 36083 0.0 36084 0.0 36086 0.0
             54130 0.0 54131 0.0 54132 0.0 54134 0.0 54135 0.0 54136 0.0
                       10 1 -1 13 2004 0.0
              1003 0.0 10020 0.0 36082 0.0 36083 0.0 36084 0.0 36086 0.0
             54130 0.0 54131 0.0 54132 0.0 54134 0.0 54135 0.0 54136 0.0
                       11 1 -1 13 2004 0.0
              1003 0.0 10020 0.0 36082 0.0 36083 0.0 36084 0.0 36086 0.0
             54130 0.0 54131 0.0 54132 0.0 54134 0.0 54135 0.0 54136 0.0
                       12 1 -1 13 2004 0.0
              1003 0.0 10020 0.0 36082 0.0 36083 0.0 36084 0.0 36086 0.0
```

54130 0.0 54131 0.0 54132 0.0 54134 0.0 54135 0.0 54136 0.0
13 1 -1 13 2004 0.0
1003 0.0 10020 0.0 36082 0.0 36083 0.0 36084 0.0 36086 0.0
54130 0.0 54131 0.0 54132 0.0 54134 0.0 54135 0.0 54136 0.0
14 1 -1 13 2004 0.0
1003 0.0 10020 0.0 36082 0.0 36083 0.0 36084 0.0 36086 0.0
54130 0.0 54131 0.0 54132 0.0 54134 0.0 54135 0.0 54136 0.0
15 1 -1 13 2004 0.0
1003 0.0 10020 0.0 36082 0.0 36083 0.0 36084 0.0 36086 0.0
54130 0.0 54131 0.0 54132 0.0 54134 0.0 54135 0.0 54136 0.0
16 1 -1 13 2004 0.0
1003 0.0 10020 0.0 36082 0.0 36083 0.0 36084 0.0 36086 0.0
54130 0.0 54131 0.0 54132 0.0 54134 0.0 54135 0.0 54136 0.0
17 1 -1 13 2004 0.0
1003 0.0 10020 0.0 36082 0.0 36083 0.0 36084 0.0 36086 0.0
54130 0.0 54131 0.0 54132 0.0 54134 0.0 54135 0.0 54136 0.0
18 1 -1 13 2004 0.0
1003 0.0 10020 0.0 36082 0.0 36083 0.0 36084 0.0 36086 0.0
54130 0.0 54131 0.0 54132 0.0 54134 0.0 54135 0.0 54136 0.0
19 1 -1 13 2004 0.0
1003 0.0 10020 0.0 36082 0.0 36083 0.0 36084 0.0 36086 0.0
54130 0.0 54131 0.0 54132 0.0 54134 0.0 54135 0.0 54136 0.0
20 1 -1 13 2004 0.0
1003 0.0 10020 0.0 36082 0.0 36083 0.0 36084 0.0 36086 0.0
54130 0.0 54131 0.0 54132 0.0 54134 0.0 54135 0.0 54136 0.0
21 1 -1 13 2004 0.0
1003 0.0 10020 0.0 36082 0.0 36083 0.0 36084 0.0 36086 0.0
54130 0.0 54131 0.0 54132 0.0 54134 0.0 54135 0.0 54136 0.0
22 1 -1 13 2004 0.0
1003 0.0 10020 0.0 36082 0.0 36083 0.0 36084 0.0 36086 0.0
54130 0.0 54131 0.0 54132 0.0 54134 0.0 54135 0.0 54136 0.0
23 1 -1 13 2004 0.0
1003 0.0 10020 0.0 36082 0.0 36083 0.0 36084 0.0 36086 0.0
54130 0.0 54131 0.0 54132 0.0 54134 0.0 54135 0.0 54136 0.0
24 1 -1 13 2004 0.0
1003 0.0 10020 0.0 36082 0.0 36083 0.0 36084 0.0 36086 0.0
54130 0.0 54131 0.0 54132 0.0 54134 0.0 54135 0.0 54136 0.0
25 1 -1 13 2004 0.0
1003 0.0 10020 0.0 36082 0.0 36083 0.0 36084 0.0 36086 0.0
54130 0.0 54131 0.0 54132 0.0 54134 0.0 54135 0.0 54136 0.0
26 1 -1 13 2004 0.0
1003 0.0 10020 0.0 36082 0.0 36083 0.0 36084 0.0 36086 0.0
54130 0.0 54131 0.0 54132 0.0 54134 0.0 54135 0.0 54136 0.0
27 1 -1 13 2004 0.0
1003 0.0 10020 0.0 36082 0.0 36083 0.0 36084 0.0 36086 0.0
54130 0.0 54131 0.0 54132 0.0 54134 0.0 54135 0.0 54136 0.0

```
            28 1 -1 13 2004 0.0
         1003 0.0 10020 0.0 36082 0.0 36083 0.0 36084 0.0 36086 0.0
        54130 0.0 54131 0.0 54132 0.0 54134 0.0 54135 0.0 54136 0.0
            29 1 -1 13 2004 0.0
         1003 0.0 10020 0.0 36082 0.0 36083 0.0 36084 0.0 36086 0.0
        54130 0.0 54131 0.0 54132 0.0 54134 0.0 54135 0.0 54136 0.0
            30 1 -1 13 2004 0.0
         1003 0.0 10020 0.0 36082 0.0 36083 0.0 36084 0.0 36086 0.0
        54130 0.0 54131 0.0 54132 0.0 54134 0.0 54135 0.0 54136 0.0
            31 1 -1 13 2004 0.0
         1003 0.0 10020 0.0 36082 0.0 36083 0.0 36084 0.0 36086 0.0
        54130 0.0 54131 0.0 54132 0.0 54134 0.0 54135 0.0 54136 0.0
            32 1 -1 13 2004 0.0
         1003 0.0 10020 0.0 36082 0.0 36083 0.0 36084 0.0 36086 0.0
        54130 0.0 54131 0.0 54132 0.0 54134 0.0 54135 0.0 54136 0.0
            33 1 -1 13 2004 0.0
         1003 0.0 10020 0.0 36082 0.0 36083 0.0 36084 0.0 36086 0.0
        54130 0.0 54131 0.0 54132 0.0 54134 0.0 54135 0.0 54136 0.0
            34 1 -1 13 2004 0.0
         1003 0.0 10020 0.0 36082 0.0 36083 0.0 36084 0.0 36086 0.0
        54130 0.0 54131 0.0 54132 0.0 54134 0.0 54135 0.0 54136 0.0
            35 1 -1 13 2004 0.0
         1003 0.0 10020 0.0 36082 0.0 36083 0.0 36084 0.0 36086 0.0
        54130 0.0 54131 0.0 54132 0.0 54134 0.0 54135 0.0 54136 0.0
            36 1 -1 13 2004 0.0
         1003 0.0 10020 0.0 36082 0.0 36083 0.0 36084 0.0 36086 0.0
        54130 0.0 54131 0.0 54132 0.0 54134 0.0 54135 0.0 54136 0.0
            37 1 -1 13 2004 0.0
         1003 0.0 10020 0.0 36082 0.0 36083 0.0 36084 0.0 36086 0.0
        54130 0.0 54131 0.0 54132 0.0 54134 0.0 54135 0.0 54136 0.0
            38 1 -1 13 2004 0.0
         1003 0.0 10020 0.0 36082 0.0 36083 0.0 36084 0.0 36086 0.0
        54130 0.0 54131 0.0 54132 0.0 54134 0.0 54135 0.0 54136 0.0
            39 1 -1 13 2004 0.0
         1003 0.0 10020 0.0 36082 0.0 36083 0.0 36084 0.0 36086 0.0
        54130 0.0 54131 0.0 54132 0.0 54134 0.0 54135 0.0 54136 0.0
            40 1 -1 13 2004 0.0
         1003 0.0 10020 0.0 36082 0.0 36083 0.0 36084 0.0 36086 0.0
        54130 0.0 54131 0.0 54132 0.0 54134 0.0 54135 0.0 54136 0.0
m1   92233.72c -.0087533667    $ LiF-BeF2-ThF4-UF4 fuel salt
     90232.72c -.4357872877    $ 71.76 - 16.00 - 12.00 - 0.24 Mol% initial comp.
     3007.72c   -.0787963973   $ enriched in Li-7
     4009.72c   -.0225675308   $ Be
     9019.72c   -.4540954175   $ F
```

6. Fission products as an input for the first refueling cycle

```
c Data Cards
  c Materials
burn time=10 54r mat=1 power=150.0 pfrac=1.0 54r bopt=1.0 -14 -1
    omit 1 76 6014 7016 8018 8019 9018 10021 10022 32075
            34075 34081 35080 36081 38085 39086 39087
            39092 39093 40089 40097 41091 41092 41096
            41097 41098 41099 42091 42093 42101 43097
            43098 44097 45104 45106 45107 45108 45109
            45110 45111 46103 46109 46111 46112 47106
            47108 47110 48107 48109 48115 49114 49116
            49117 49118 49119 49121 50121 51122 52121
            52127 52129 53128 53132 53133 53134 54127
            60149 61145 61146 62145 62146 64150 64151
            64159 66157 66159 88227 89228
    matvol=5267275.924
c ----------------------------------------
m1 90229.72c -2.5502E-08
    90230.72c  -1.4776E-08
c   90231.72c   -1.2617E-08
    90232.72c  -4.3274E-01
    90233.72c  -2.0147E-07
    91231.72c  -1.9994E-06
    91232.72c  -5.0650E-09
    91233.72c  -3.4462E-04
    92232.72c  -4.0750E-07
    92233.72c  -9.4670E-03
    92234.72c  -3.3687E-04
    92235.72c  -1.6963E-05
    92236.72c  -3.4655E-07
    3006.72c    -2.0500E-07
    3007.72c    -7.8837E-02
    4009.72c    -2.2545E-02
    7015.72c    -2.6766E-08
    8016.72c    -2.0899E-06
    8017.72c    -2.0278E-09
    9019.72c    -4.5448E-01
    33075.72c  -6.6987E-08
    35081.72c  -3.3835E-06
    37085.72c  -1.5961E-05
    37087.72c  -3.9753E-05
    39089.72c  -4.8941E-05
    40090.72c  -6.9835E-07
    40091.72c  -4.8685E-05
    40092.72c  -6.6303E-05
```

40093.72c -7.3708E-05
40094.72c -7.3139E-05
40096.72c -6.2088E-05
42095.72c -3.7447E-05
43099.72c -5.1710E-05
44101.72c -3.6017E-05
44103.72c -3.4598E-06
45103.72c -1.3779E-05
46104.72c -1.0766E-06
46105.72c -5.3008E-06
46106.72c -1.1176E-06
46108.72c -9.2676E-07
46110.72c -4.8913E-07
47109.72c -4.5888E-07
48110.72c -4.4572E-08
48111.72c -2.6430E-07
48112.72c -1.7197E-07
48113.72c -6.3968E-09
50120.72c -3.0161E-07
53127.72c -7.0803E-06
53129.72c -2.1759E-05
53135.72c -1.0202E-07
55133.72c -8.4474E-05
55134.72c -2.2431E-06
55135.72c -2.9443E-05
55136.72c -1.4559E-07
55137.72c -1.0452E-04
56138.72c -9.2733E-05
59141.72c -8.5385E-05
60143.72c -8.3733E-05
60145.72c -5.5862E-05
60147.72c -1.5271E-06
60148.72c -2.2375E-05
61147.72c -2.1406E-05
61148.72c -8.7265E-08
61149.72c -1.6302E-07
62147.72c -2.3047E-06
62149.72c -3.8791E-07
62150.72c -1.3420E-05
62151.72c -1.5682E-06
62152.72c -6.6759E-06
63151.72c -1.9179E-09
64152.72c -1.1711E-09
64154.72c -4.9562E-09
64155.72c -8.7835E-10
64156.72c -5.6335E-07

```
    64157.72c  -2.8464E-09
    64158.72c  -1.6621E-07
    64160.72c  -5.7588E-09
```

7. Fission products as an input for the 2nd refueling cycle

```
c Data Cards
  c Materials
burn time=10 64r mat=1 power=150.0 pfrac=1.0 64r bopt=1.0 -14 -1
    omit 1 96 6014 7016 8018 8019 9018 10021 10022 32075
            34075 34081 35080 36081 38085 39086 39087
            39092 39093 40089 40097 41091 41092 41096
            41097 41098 41099 42091 42093 42101 43097
            43098 44097 45104 45106 45107 45108 45109
            45110 45111 46103 46109 46111 46112 47106
            47108 47110 48107 48109 48115 49114 49116
            49117 49118 49119 49121 50121 51122 52121
            52127 52129 53128 53132 53133 53134 54127
            60149 61145 61146 62145 62146 64150 64151
            64159 66157 66159 88227 89228 30069 31070
            32071 33072 33073 36079 40088 41100 46113
            46114 49122 49123 54125 56131 58137 67163
            67164 68163 68165 92229
    matvol=5267275.924
c ------------------------------------
m1 90228.72c -1.2269E-08
    90229.72c -6.0804E-08
    90230.72c -4.8820E-08
c   90231.72c -1.2548E-08
    90232.72c -4.2791E-01
    90233.72c -1.9095E-07
    91231.72c -4.0771E-06
    91232.72c -9.7833E-09
    91233.72c -3.2615E-04
    92232.72c -2.1358E-06
    92233.72c -1.0119E-02
    92234.72c -8.4182E-04
    92235.72c -9.1747E-05
    92236.72c -4.9144E-06
    92237.72c -6.1715E-09
    92238.72c -1.0705E-09
    93237.72c -1.1871E-07
    94238.72c -1.0944E-08
    3006.72c   -4.0794E-07
    3007.72c   -7.8847E-02
```

4009.72c -2.2513E-02
7015.72c -7.1668E-08
8016.72c -5.6027E-06
8017.72c -5.4599E-09
9019.72c -4.5468E-01
31071.72c -2.2155E-09
32072.72c -5.8074E-09
32073.72c -1.5585E-08
32074.72c -3.8940E-08
32076.72c -2.0255E-07
33075.72c -1.7872E-07
34076.72c -2.2354E-09
34077.72c -3.7632E-07
34078.72c -8.0200E-07
34079.72c -2.1313E-06
34080.72c -3.6665E-06
34082.72c -9.3283E-06
35081.72c -9.0553E-06
37085.72c -4.3092E-05
37086.72c -6.4900E-09
37087.72c -1.0705E-04
38086.72c -8.3101E-08
38087.72c -6.6379E-10
38088.72c -9.1633E-05
39089.72c -1.4231E-04
39090.72c -3.1210E-08
39091.72c -1.8839E-05
40090.72c -2.7774E-06
40091.72c -1.4351E-04
40092.72c -1.7883E-04
40093.72c -1.9840E-04
40094.72c -1.9766E-04
40095.72c -2.1051E-05
40096.72c -1.6740E-04
41095.72c -1.1416E-05
42095.72c -1.1922E-04
42096.72c -2.5181E-06
42097.72c -1.0290E-04
42098.72c -9.8174E-05
42099.72c -7.3375E-07
42100.72c -8.6173E-05
43099.72c -1.3435E-04
44099.72c -3.2967E-09
44100.72c -7.7186E-06
44101.72c -9.6013E-05
44102.72c -4.9127E-05

44103.72c -3.5009E-06
44104.72c -1.9754E-05
45103.72c -3.7273E-05
45105.72c -4.0038E-08
46104.72c -8.7367E-06
46105.72c -1.4248E-05
46106.72c -3.7649E-06
46107.72c -2.3389E-06
46108.72c -2.4413E-06
46110.72c -1.3179E-06
47109.72c -1.1359E-06
48110.72c -2.8622E-07
48111.72c -7.1725E-07
48112.72c -4.6863E-07
48113.72c -6.7061E-09
48114.72c -5.9951E-07
48116.72c -3.0482E-07
49115.72c -2.0124E-07
50115.72c -1.5471E-08
50116.72c -1.1126E-07
50117.72c -3.1807E-07
50119.72c -4.3035E-07
50120.72c -8.1281E-07
50122.72c -9.6525E-07
51121.72c -4.8388E-07
51123.72c -1.3111E-06
52122.72c -1.1274E-08
52124.72c -1.0705E-08
52125.72c -4.0624E-07
52126.72c -5.0293E-08
52128.72c -2.0551E-05
52130.72c -5.2352E-05
53127.72c -1.9140E-05
53129.72c -5.8302E-05
53130.72c -2.2058E-09
53131.72c -2.0659E-06
53135.72c -1.0233E-07
54129.72c -1.2917E-09
55133.72c -2.1921E-04
55134.72c -1.3128E-05
55135.72c -8.3443E-05
55136.72c -1.7906E-07
55137.72c -2.7723E-04
56134.72c -3.2899E-06
56135.72c -7.7356E-09
56136.72c -4.3359E-06

56137.72c -6.2568E-06
56138.72c -2.5016E-04
57139.72c -1.6780E-04
58140.72c -1.6808E-04
58141.72c -1.5852E-05
58142.72c -1.8230E-04
59141.72c -2.3958E-04
60142.72c -1.8736E-06
60143.72c -2.0670E-04
60144.72c -9.1804E-05
60145.72c -1.4476E-04
60146.72c -8.1566E-05
60147.72c -1.5335E-06
60148.72c -6.0179E-05
60150.72c -1.4686E-05
61147.72c -4.1676E-05
61148.72c -1.5574E-07
61149.72c -1.8537E-07
62147.72c -1.3105E-05
62148.72c -1.0341E-05
62149.72c -4.8911E-07
62150.72c -3.8764E-05
62151.72c -2.2746E-06
62152.72c -1.6421E-05
62153.72c -8.1907E-08
62154.72c -1.4487E-06
63151.72c -3.1790E-09
63152.72c -2.9469E-09
63153.72c -9.1975E-06
63154.72c -1.0682E-06
63155.72c -3.7125E-07
64152.72c -4.6693E-09
64154.72c -4.9212E-08
64155.72c -4.1215E-09
64156.72c -2.0738E-06
64157.72c -4.1886E-09
64158.72c -4.8484E-07
64160.72c -1.5522E-08
65159.72c -2.9697E-08
66160.72c -8.6855E-10
66161.72c -2.9811E-09
66162.72c -1.0619E-09

8. Fission products as an input for the 3rd refueling cycle

```
c Data Cards
  c Materials
burn time=10 62r mat=1 power=150.0 pfrac=1.0 62r bopt=1.0 -14 -1
    omit 1 99 6014 7016 8018 8019 9018 10021 10022 32075
            34075 34081 35080 36081 38085 39086 39087
            39092 39093 40089 40097 41091 41092 41096
            41097 41098 41099 42091 42093 42101 43097
            43098 44097 45104 45106 45107 45108 45109
            45110 45111 46103 46109 46111 46112 47106
            47108 47110 48107 48109 48115 49114 49116
            49117 49118 49119 49121 50121 51122 52121
            52127 52129 53128 53132 53133 53134 54127
            60149 61145 61146 62145 62146 64150 64151
            64159 66157 66159 88227 89228 30069 31070
            32071 33072 33073 36079 40088 41100 46113
            46114 49122 49123 54125 56131 58137 67163
            67164 68163 68165 92229 30070 49124 67166
    matvol=5267275.924
c -----------------------------------------
m1 90228.72c -3.8469E-08
    90229.72c  -9.2452E-08
    90230.72c  -9.0521E-08
c   90231.72c  -1.2283E-08
    90232.72c  -4.2307E-01
    90233.72c  -1.8184E-07
    91231.72c  -5.2995E-06
    91232.72c  -1.2124E-08
    91233.72c  -3.1075E-04
    92232.72c  -4.4079E-06
    92233.72c  -1.0671E-02
    92234.72c  -1.2931E-03
    92235.72c  -1.9229E-04
    92236.72c  -1.6929E-05
    92237.72c  -2.0591E-08
    92238.72c  -5.0281E-09
    93237.72c  -6.7010E-07
    93238.72c  -1.1818E-09
    94238.72c  -9.8187E-08
    94239.72c  -6.9509E-09
    94240.72c  -1.3993E-09
    3006.72c    -5.2734E-07
    3007.72c    -7.8843E-02
    4009.72c    -2.2471E-02
    7015.72c    -1.1801E-07
```

```
      8016.72c    -9.2395E-06
      8017.72c    -9.0123E-09
      9019.72c    -4.5481E-01
c     30070.72c   -5.4182E-10
      31071.72c   -4.4965E-09
      32072.72c   -1.1840E-08
      32073.72c   -3.1251E-08
      32074.72c   -7.9447E-08
      32076.72c   -4.1126E-07
      33075.72c   -2.9184E-07
      34076.72c   -6.3717E-09
      34077.72c   -7.5245E-07
      34078.72c   -1.6406E-06
      34079.72c   -4.2347E-06
      34080.72c   -7.5472E-06
      34082.72c   -1.8956E-05
      35081.72c   -1.4845E-05
      37085.72c   -7.1042E-05
      37086.72c   -1.0211E-08
      37087.72c   -1.7650E-04
      38086.72c   -2.4181E-07
      38087.72c   -1.5889E-09
      38088.72c   -1.8632E-04
      39089.72c   -2.3936E-04
      39090.72c   -3.2988E-08
      39091.72c   -1.8842E-05
      40090.72c   -5.1320E-06
      40091.72c   -2.6100E-04
      40092.72c   -2.9553E-04
      40093.72c   -3.2699E-04
      40094.72c   -3.2716E-04
      40095.72c   -2.1108E-05
      40096.72c   -2.7645E-04
      41095.72c   -1.1505E-05
      42095.72c   -2.3397E-04
      42096.72c   -8.5921E-06
      42097.72c   -2.0921E-04
      42098.72c   -2.0041E-04
      42099.72c   -7.3484E-07
      42100.72c   -1.7565E-04
      43099.72c   -2.1489E-04
      44099.72c   -7.0077E-09
      44100.72c   -2.1915E-05
      44101.72c   -1.5702E-04
      44102.72c   -1.0182E-04
      44103.72c   -3.5345E-06
```

44104.72c -4.0343E-05
45103.72c -5.6334E-05
45105.72c -4.0592E-08
46104.72c -2.2255E-05
46105.72c -2.3465E-05
46106.72c -6.8373E-06
46107.72c -4.7100E-06
46108.72c -3.9837E-06
46110.72c -2.1739E-06
47109.72c -1.7548E-06
48110.72c -6.9679E-07
48111.72c -1.1863E-06
48112.72c -7.8198E-07
48113.72c -7.2008E-09
48114.72c -1.2198E-06
48116.72c -6.2070E-07
49115.72c -2.8922E-07
50115.72c -3.0961E-08
50116.72c -3.4953E-07
50117.72c -6.4682E-07
50118.72c -3.7145E-07
50119.72c -8.7397E-07
50120.72c -1.3419E-06
50122.72c -1.9609E-06
50123.72c -1.0137E-07
50124.72c -1.8388E-06
51121.72c -9.6313E-07
51123.72c -2.6384E-06
52122.72c -4.2801E-08
52124.72c -4.4664E-08
52125.72c -8.3820E-07
52126.72c -1.0529E-07
52128.72c -4.1774E-05
52130.72c -1.0654E-04
53127.72c -3.1126E-05
53129.72c -9.5121E-05
53130.72c -3.3443E-09
53131.72c -2.0586E-06
53135.72c -1.0228E-07
55133.72c -3.4709E-04
55134.72c -2.8479E-05
55135.72c -1.4316E-04
55136.72c -2.1318E-07
55137.72c -4.5022E-04
56134.72c -1.3175E-05
56135.72c -5.5482E-08

56136.72c -9.7335E-06
56137.72c -1.8513E-05
56138.72c -4.1342E-04
57138.72c -6.4001E-10
57139.72c -3.4033E-04
58140.72c -3.4374E-04
58141.72c -1.5821E-05
58142.72c -3.7089E-04
59141.72c -4.1376E-04
60142.72c -5.6788E-06
60143.72c -3.1120E-04
60144.72c -2.1165E-04
60145.72c -2.3073E-04
60146.72c -1.7258E-04
60147.72c -1.5395E-06
60148.72c -9.9209E-05
60150.72c -2.9865E-05
61147.72c -5.1501E-05
61148.72c -1.7996E-07
61149.72c -1.9535E-07
62147.72c -2.7400E-05
62148.72c -2.6554E-05
62149.72c -5.6101E-07
62150.72c -6.4796E-05
62151.72c -2.9945E-06
62152.72c -2.3936E-05
62153.72c -1.0909E-07
62154.72c -2.9655E-06
63151.72c -4.4971E-09
63152.72c -4.3000E-09
63153.72c -2.0046E-05
63154.72c -2.8173E-06
63155.72c -9.3190E-07
64152.72c -8.4274E-09
64153.72c -6.9793E-10
64154.72c -2.6089E-07
64155.72c -1.2431E-08
64156.72c -6.8657E-06
64157.72c -7.6437E-09
64158.72c -9.6654E-07
64160.72c -2.5640E-08
65159.72c -6.2411E-08
66160.72c -3.6680E-09
66161.72c -5.3552E-09
66162.72c -2.7287E-09
66163.72c -1.1681E-09

9. Axial and radial fluxes

```
c ---------------------------------------------------------------------
FMESH4:n GEOM=rec ORIGIN=0 -1 -1 &                $ Radial flux
IMESH=175 IINTS=175 &                             $
JMESH=1 JINTS=1 &                                 $
KMESH=1 KINTS=1 &                                 $
emesh=1e-6 5.2e-2 20 eints=1 1 1                  $
c ---------------------------------------------------------------------
FMESH14:n GEOM=rec ORIGIN=0 -1 -166 &             $ x-z flux1
IMESH=176 IINTS=175 &                             $
JMESH=1 JINTS=1 &                                 $
KMESH=166 KINTS=332 &                             $
emesh=5e-7 20 eints=1 1                           $
c ---------------------------------------------------------------------
FMESH24:n GEOM=rec ORIGIN=0 -1 -165 &             $ x-z flux2
IMESH=175 IINTS=174 &                             $
JMESH=1 JINTS=1 &                                 $
KMESH=165 KINTS=330 &                             $
emesh=5e-7 20 eints=1 1                           $
c ---------------------------------------------------------------------
FMESH34:n GEOM=rec ORIGIN=-178 -178 -165 &        $ Matlab flux1
IMESH=178 IINTS=178 &                             $
JMESH=178 JINTS=178 &                             $
KMESH=165 KINTS=1 &                               $
emesh=1e-6 5.2e-2 20 eints=1 1 1                  $
c ---------------------------------------------------------------------
FMESH44:n GEOM=rec ORIGIN=-179 -179 -165 &        $ Matlab flux2
IMESH=179 IINTS=179 &                             $
JMESH=179 JINTS=179 &                             $
KMESH=165 KINTS=1 &                               $
emesh=1e-6 5.2e-2 20 eints=1 1 1                  $
c ---------------------------------------------------------------------
FMESH54:n GEOM=rec ORIGIN=-180 -180 -165 &        $ Matlab flux3
IMESH=180 IINTS=180 &                             $
JMESH=180 JINTS=180 &                             $
KMESH=165 KINTS=1 &                               $
emesh=1e-6 5.2e-2 20 eints=1 1 1                  $
c ---------------------------------------------------------------------
FMESH64:n GEOM=rec ORIGIN=-181 -181 -165 &        $ Matlab flux4
IMESH=181 IINTS=181 &                             $
JMESH=181 JINTS=181 &                             $
KMESH=165 KINTS=1 &                               $
emesh=1e-6 5.2e-2 20 eints=1 1 1                  $
```

VITA

Safwan Qasim Mohammad Jaradat was born in Irbid, Jordan. He received his Bachelor of Science in Physics from Jordan University of Science and Technology, Irbid, Jordan in June 2005. He received his M.S in Physics from Jordan University of Science and Technology in January 2011. After that, he joined at Missouri University of Science and Technology for pursuing his PhD in 2011 and received his PhD in Nuclear Engineering from Missouri University of Science and Technology in December 2015.